The role of photosynthetic rates in daily and yearly wetland CO_2 and CH_4 fluxes

By

Jess Turner

A dissertation submitted in partial fulfillment of

the requirements for the degree of

Doctor of Philosophy

(Freshwater and Marine Science)

at the

UNIVERSITY OF WISCONSIN-MADISON

2023

Date of final oral examination: 3/1/2023

The dissertation is approved by the following members of the Final Oral Committee:

Ankur R. Desai, Professor, Department of Atmospheric and Oceanic Sciences
Kimberly P. Wickland, Research Ecologist, United States Geological Survey
Paul C. Stoy, Associate Professor, Biological Systems Engineering
Chris Kucharik, Professor, Department of Agronomy
Emily H. Stanley, Professor, Center for Limnology

Acknowledgements

From the year that I began college, I was fortunate to have collegiate mentors who gave me the confidence to pursue engineering and the sciences, never give up, and eventually apply and get accepted to graduate school. Dr. Letitia Thomas, Dr. Nancy Campos, Dr. Kendra Cadogan, and many more strong, intelligent women including from years prior to the start of my undergraduate career, sacrificed the many hours needed to look over my application essays, write recommendation letters, and provide the constructive criticism necessary for me to improve as a scientist, colleague, and individual.

My family members ensured that my writing made sense to those outside of my hyper-specific field, checked in on my physical and mental health, and were there for me whether I succeeded or failed. Similarly, I must thank the anonymous readers who have read my work online, cited it, commented on it, or shared it with others, for their silent support. Their readership assured me that my research was reaching people outside of my small, academic circle and potentially inspiring the greater public which I strive to serve.

Of course, I also owe my development into a scientist to my main advisor, Dr. Ankur Desai, who shaped and refined my ambiguous, big ideas into specific, manageable hypotheses through his direction. I am equally thankful to my lab members, committee members, and all other scientists who have collaborated with me on various projects throughout my Ph.D. I am grateful to my fiancé, Terrell Richardson, for being there throughout my Ph.D. journey. My dog, Asha, and cat, Haku, were also great comrades as they made working from home and on the computer more interesting than it would have been without them.

This work was financially supported through several small research grants and by my advisor. The CO2-LAMPs and the Smart Rock sensor built during the CUAHSI workshop were funded through multiple sources; the Anna Grant Birge Memorial Award from the Center for Limnology at UW-Madison, the Graduate Summer Research Award from the UW-Madison Department of Integrative Biology, the Student Research Grants Competition funded by UW-Madison, project funds from the Ecometeorology lab run by Dr. Ankur Desai at UW-Madison, and a PeatNEEDs microgrant from the Peatland Early Career Action Network. Small research grant funding covered the cost of transportation to the field sites, sensors, the Smart Rock sensor-building workshop by CUAHSI, flights, lodging, and incidentals. I was also personally funded by the National Science Foundation Graduate Research Fellowship Program and by a research assistantship from the North Temperate Lakes Long Term Ecological Research program. I appreciate help from the administrative teams in the Department of Integrative Biology, Department of Atmospheric and Oceanic Sciences, and Center for Limnology, for helping me manage the grants and travel funds necessary for me to carry out my research. Thank you, all.

Contents

1 Introduction

1.1 Where wetland carbon begins

Hours to millennia can pass in the time between when a carbon dioxide molecule (CO_2) enters through a leaf during photosynthesis, and when it is respired out through roots after cycling through the Calvin and Krebs Cycles or being locked away in woody plant tissues. The process has multiple names used by different fields, referred to as a pulse or short-term carbon (C) cycling response, C residence time, or lag time. Regardless of what it is called, the movement of C through plants and entire ecosystems is crucial to understanding the C cycle and modeling our future climate. C is typically traced as it moves through an ecosystem using C isotopes, but in the next few chapters, I explore whether this can also be done *post hoc* by looking for correlations among different variables throughout study periods ranging from a few days to an entire year using statistical testing, spectral and signal analysis. Spontaneous events like floods or typhoons also present great serendipitous opportunities to observe the duration of natural C pulses (Hikino et al., 2022). This is especially evident in the following chapter, which highlights a particularly wet year where wetland gross primary productivity (GPP) and resulting methane (CH_4) fluxes were captured and compared.

C residence time should not be confused with turnover time, which is the time it takes for C to cycle entirely through part or all of an ecosystem, either being broken down or transforming into something else. CO_2 turnover times in forest ecosystems are much slower than C pulse-response times. For instance, the turnover time in temperate forests has been

estimated at 2-5 years for leaf litter, 5-10 for root litter, 40-100+ for low-density humus, and 100+ years for mineral-derived C (Gaudinski et al., 2000). Fresh plant litter decomposes the fastest compared to poorly defined intermediate carbon pools and stabilized soil organic matter, the latter of which can take thousands of years to move through the entire ecosystem (Mcleod et al., 2011; Macreadie et al., 2021). In comparison, the C pulse-response of trees measured as the lag time between tree uptake of $^{13}CO_2$ and corresponding soil CO_2 emission has been measured at 0.5 to 4 days or more, and changes with the season (Epron et al., 2011). Studies of C residence times in plants, soils, and ecosystems are abundant and have contributed greatly to scientific understanding of terrestrial C cycling. However, wetlands present a special challenge due to complex interactions between their terrestrial and aquatic components, and multiple, counteracting drivers of CO_2 and CH_4 emissions.

In many ways, wetlands are just as unique as all other ecosystems. Like oceans, deserts, or tropical rainforests, they can be identified by their plants and animals, hydrology, or unique soil microbial communities. But unlike other ecosystems, wetlands differ in their complexity. C sequestration in wetlands is not as simple as in forests, where a consistent level of C is converted to woody biomass over time and can be roughly estimated from stand age. Wetlands are also a far cry from deserts, which are essentially dormant until monsoon rains cause large releases of gas and provide much-needed water for plants and animals (Sponseller, 2007). The fact that wetlands are both terrestrial and aquatic is part of what complicates the physical, biological, and chemical relationships within. This work aims to join the growing body of scientific literature on wetland C fluxes by analyzing direct observations of half-hourly

resolution fluxes of CO_2 and CH_4 and detecting environmental drivers despite complex or nonlinear relationships between variables.

1.2 Where wetland carbon ends

A delay between canopy photosynthesis and soil respiration has been documented in numerous studies of different ecosystem types (Högberg et al., 2001; Baldocchi et al., 2006; Stoy et al., 2007; Moyano et al., 2008; Vargas et al., 2011; Kuzyakov and Cheng, 2004; Detto et al., 2012; Han et al., 2014; Hafner et al., 2012). Studies have also shown that the amount of time it takes for CO_2 to cycle through a plant or ecosystem is controlled by hydrologic state within a growing season, or from one season to another (Tangen & Bansal, 2019; Turner et al., 2021). In fact, it is widely known that half of all CO_2 consumed by plants will ultimately be released back into the atmosphere. It is much more difficult to pinpoint exactly how long after a CO_2 molecule enters an ecosystem, that that CO_2 molecule will be released.

Tallgrass prairie responds to water level manipulation as early as one day after treatment with an increase of soil CO_2 emissions (Liu et al., 2002). Soil CO_2 emissions in the Sonoran Desert also demonstrate a strong response to water, releasing a pulse of CO_2 after artificial rainfall and returning to background levels within two days (Sponseller, 2007). Wastewater treatment wetlands have a similar response time, removing selected nutrients from water most efficiently with a hydraulic residence time of three days in cattail (Sirianuntapiboon et al., 2006) and four days in a mix of *Phragmites australis, Typha latifolia,* and more (Toet et al., 2005). Plant growth happens more quickly than nutrient removal, with cattail growing fastest when hydraulic retention time is less than one day.

In a global analysis of C turnover times, Carvalhais *et al* (2014) determined a model-derived overall mean global C turnover time of approximately 23 years. Wetlands had an estimated difference of 0.6 % from the mean global C turnover rate. Estimated global C turnover time increased to approximately 43 years in a later study which implemented new observation-based datasets of soil organic C stocks, but only considered terrestrial ecosystem C (Fan et al., 2020). Another study found that saltwater prompted CO_2 production in a freshwater wetland in the short term (2 weeks), while limiting CH_4 (Chambers et al., 2011). Wetland C cycling is clearly dependent on multiple factors and can vary depending on the type of C and timescale being investigated. Physical and biological storage of C throughout the wetland C cycle, and probabilities of chemical reaction as time goes on, make it less likely that wetland C follows a predictable pathway. For instance, C pulses in wetlands could be the result of changing deep soil or porewater CO_2 stocks (Campeau et al., 2021). This supports the idea of wetlands as corridors through which C will "spiral", or exchange with biotic and abiotic components of terrestrial and aquatic environments while also moving downstream (Harvey & Gooseff, 2015).

Eventually, wetland C will join aboveground and belowground global wetland C stocks, estimated to be 520–710 petagrams of C (PgC) in 2022, or 1792-1882 PgC when including permafrost C (Poulter et al., 2022). Although this amount of C pales in comparison to C storage in the oceans (38,858 PgC), wetlands store nearly as much C as the atmosphere (829 PgC), despite only covering an estimated 5-6% of global land area (Janse et al., 2019). Protecting wetland C stocks and maximizing burial rates while also reducing emissions is especially important considering fossil fuel emissions, estimated at 9.5 ± GtC yr^{-1}, are more than an order

or magnitude greater than the highest estimates of global wetland C burial (0.07-0.19 GtC yr^{-1}) (Ciais et al., 2013; Friedlingstein et al., 2022). Estimates of global C stocks are made using field sampling, remote sensing, and ecosystem modeling, and continue to change as the extent of tropical wetlands is better defined. Wetland C that becomes part of long-term soil storage must evade transformation through reactions such as combustion due to lower water table levels, drainage, degradation, peat harvest, and conversion to plantations for crops such as oil palm (Gaveau et al., 2014).

1.3 How CO_2 and CH_4 fluxes are influenced by photosynthesizing plants

Net ecosystem exchange of CO_2 inherently provides information on photosynthesis, partitioning into CO_2 uptake by plants (GPP) and CO_2 respired by autotrophs and heterotrophs (ecosystem respiration, Reco) via the hyperbolic light-response curve (Falge et al., 2001; Lasslop et al., 2010). Yet, how exactly plants factor into CH_4 emissions is not fully understood, leading to large variability in process-based methane model outputs (Tang et al., 2010). Comparisons of wetland lateral CO_2 export and photosynthetic rates are uncommon, with lateral flux studies tending to focus more on hydrological effects (Knox et al., 2018; Shahan, 2022). Lateral CO_2 export or wetland CH_4 flux cannot be simply estimated from photosynthesis, though scientists are getting closer to finding a solution. A recent study quantified CH_4 emissions according to leaf area and conductance of cattail, lotus, and water lily (Villa et al., 2020). Including such information as land surface model parameters could eventually improve estimates of local and global wetland CH_4 emissions.

This dissertation explores the influence of plants on lateral and vertical components of CO_2 and CH_4 fluxes. Chapter two compares wetland photosynthetic CO_2 uptake, or gross primary productivity (GPP) to CH_4 fluxes in two riverine fen wetlands during a year with historically high precipitation and the following, drier year. This research highlights the influence of photosynthesizing plants on the size of the wetland C sink, and how they can prompt CH_4 fluxes in other parts of the ecosystem, namely soil emissions from methanogens.

The third chapter tests a new, low-cost sensing platform called the CO2-LAMP for measuring dissolved CO_2 in wetland surface waters. Dissolved CO_2 concentrations were combined with tide gage data to estimate lateral flux of dissolved CO_2, a component of DIC. Granger causality was calculated among tidal variables to identify environmental drivers of dissolved CO_2. This methodology was tested and found to be successful in a challenging tidal salt marsh environment, which supported the investigation of lateral C fluxes in chapter four.

The fourth chapter builds on concepts introduced in earlier chapters, such as signal analysis of ecosystem data and the connection between above-ground and below-ground processes in wetlands, to investigate a potential physical connection between GPP and dissolved CO_2 in wetland surface and porewater. Direct measurements of dissolved CO_2, some of which were collected using the CO2-LAMP platform discussed in the previous chapter, were incorporated with CO_2 exchange rates to explore lateral and vertical CO_2 fluxes across different wetland types. Chapter four focuses mostly on variability in lateral flux across daily and yearly timescales to provide better understanding of a relatively understudied aspect of the wetland C balance: CO_2 partial pressure (P_{CO2}).

1.4 Transformation of CO_2

P_{CO2} can be used to calculate dissolved CO_2 in water using Henry's law and is one form of dissolved inorganic carbon (DIC). DIC includes CO_2, bicarbonate (HCO_3^-), carbonate (CO_3^{2-}), and carbonic acid (H_2CO_3), which almost immediately dissociates to form HCO_3^-. Although wetlands are the ecosystem of discussion in this dissertation, the abundance of research on freshwater and saltwater ecosystems such as rivers, streams, and tidal creeks, offers insight into less researched and less well understood aspects of wetland biogeochemistry. Dissolved inorganic carbon is the most abundant C phase in many rivers, and streams and tidal creeks and mostly comes from groundwater and porewater exchange, as well as soil respiration produced by roots and microbes as they decompose organic matter (OM) in headwater streams.

The speciation of DIC depends on, and can be roughly estimated by, pH and temperature. However, estimating P_{CO2} from titration alkalinity, temperature, and DIC is likely to produce errors in carbonate systems due to the influence of alkalinity on the carbonate equilibrium (Van Dam et al., 2019). Weathering of C-containing rocks, which uses respired CO_2 and produces HCO_3^-, is common in streams of the arctic, subarctic, and circumboreal regions, especially during low flow. Springs and wetlands can enhance weathering due to groundwater and soil water abundance, as well as a high ratio of streambed to catchment area, and therefore more groundwater contact, in headwater streams. In marsh ecosystems, pathways of anaerobic organic matter degradation such as sulfate reduction are a significant contributor to the total DIC and alkalinity pool (Wang et al 2016).

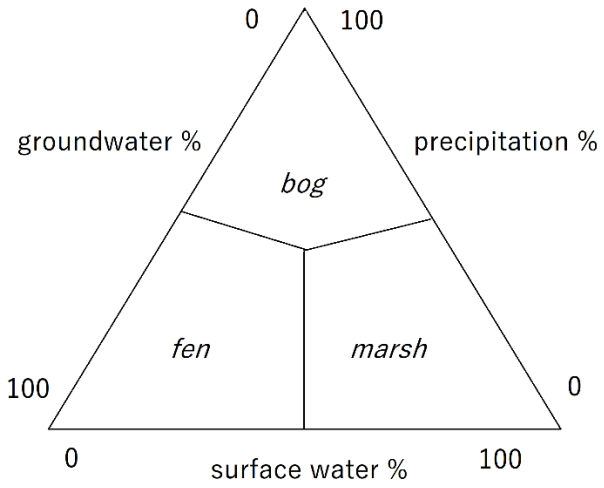

Figure 1.1. Wetland water source pyramid.

Carbon dioxide emitted from headwater streams can be produced or consumed in-stream (i.e., aquatic metabolism) or be terrestrially derived, such as from runoff or groundwater. The three main wetland water sources are exemplified above (Fig 1.1). In coastal wetlands, CO_2 from respiration processes in marsh sediments can be laterally exported to adjacent water bodies or offshore through porewater exchange driven by tidal pumping (Santos et al 2021). P_{CO2} is therefore an important component of lateral C flux from wetlands. Groundwater is a key contributor, with CO_2 concentrations as high as four times that of stream water in certain cases (Lupon et al., 2019). Dissolved inorganic carbon in small headwater streams tends to be dominated by allochthonous sources, with approximately 72% of CO_2 emissions from streams and rivers in the United States being terrestrially derived or produced as internal abiotic CO_2 (Hotchkiss et al., 2015). Small headwater streams tend to contribute larger amounts of CO_2 to the atmosphere than large-catchment rivers, largely due to

weathering of carbonate and silicate rocks, which produces bicarbonate in freshwater streams. Carbon dioxide will stay in the form of bicarbonate in environments with pH 4.3 to 8.3, such as the ocean, which prevents CO_2 from easily reentering the atmosphere. Bicarbonate then turns into carbonate by losing a hydrogen atom when the pH surpasses 8.3.

Scientific studies make a distinction between porewater and surface water CO_2, as the concentration of CO_2 in soil porewater is much greater than at the water surface (Rosentreter, 2022). Porewater is believed to contribute to the high DIC outwelling from mangroves and tidal marshes (Maher et al., 2018; Wang et al. 2016; Tamborski et al. 2021). Wetland porewater is richer in both new and old soil C respiration products, such as CH_4, and it mixes with surface waters during flushing events (e.g., snowmelt, tidal exchange). Soil porewater is more influenced by weathering than surface water and is typically measured with gas chromatography (Itoh et al., 2008; Thompson et al., 2009; Holmes et al., 2015).

1.5 Measuring lateral fluxes to improve wetland C sink estimations

Wetlands are gaining international interest because their protection and restoration can provide countries with sought-after carbon credits under the Paris Agreement. Although the maximum climate mitigation potential of wetland restoration is significantly less than that of forest reforestation (<50 vs. 300 Tg CO_2 equivalents yr^{-1}), wetlands have a higher C production density than forests (Fargione et al., 2018). Wetlands can sequester C faster than mature forests and do so in a smaller land area, while also being less susceptible to fire (Gallagher et al., 2022; Duarte et al., 2013; Mcleod et al., 2011). Restoration and conservation of blue carbon ecosystems alone, of which mangrove forests and tidal marshes are a part, could offset around three percent of global CO_2 emissions (Macreadie et al., 2021).

On the regional level, wetlands are also attractive investments for private companies looking to offset their C footprint. Measuring lateral C loss and CH_4 emissions, which reduce the net C sink of wetlands, is an important step in reducing uncertainty in wetland C mitigation potentials. Integrating multi-scale observations to produce representative grids of C balance is one way to monitor and verify nature-based climate solutions, or NbCS (Novick et al., 2022). In wetlands, this would equate to the combination of flux tower data with remote sensing, tree inventory, soil cores, and static chambers to observe C across space and time, resulting in a half-hourly, 10 m resolution, robust observation method which will be more accessible to those outside of the scientific realm (e.g., landowners) and market relevant. In fact, measurements of lateral C exports from runoff, including simultaneous measurements of both C concentration and water flow, have the potential to reveal biases in the type of data used in NbCS assessments, be used in comparison with other C market models, or be used to test new ways of quantifying and monitoring the impact of NbCS.

Measuring lateral C import and export can also help parse gas emissions due to anthropogenic or upstream inputs, such as nitrogen fertilizers which can contribute to wetland N_2O emissions downstream, and lead to more accurate estimates of wetland C sinks (Malerba et al., 2022). Clarifying the causes of greenhouse gas emissions from wetlands can also help promote healthy wetlands. For example, removing anoxic sediments would reduce CH_4 produced by the decomposition of wetland OM, but it would also restrict the soil carbon sequestration which is offsetting those CH_4 emissions.

Dissolved inorganic carbon, which includes dissolved CO_2, can have a much larger diel range than DOC in tidal wetlands, leading to much higher potential lateral losses (Board et al.,

2020). As dissolved CO_2 is exported from tidal wetlands into the more acidic ocean environment, it becomes part of the marine biological C pump and can be stored in the ocean for millennia (Maher et al., 2018). Measuring dissolved CO_2 quantities and tracing it through wetland ecosystems will eventually allow scientists to determine the amount leaving wetlands and the fraction that is partitioning into long-term storage pools downstream and improve wetland C sink estimations.

1.6 Research scope and limitations

This work will evaluate the role of photosynthetic rates on daily and yearly wetland CO_2 and CH_4 fluxes using eddy covariance and chamber-based estimates of net ecosystem exchange of CO_2 and CH_4, gross primary productivity of CO_2, and dissolved CO_2 in surface and porewater. This work will not delve into wetland soil C profiles; gases other than CH_4 or CO_2; DOC; global wetland areal coverage; ecosystem modeling; the myriad co-benefits of wetland protection and restoration; or the global wetland C sink. Research shows that net ecosystem exchange is a better method of measuring C sequestration than organic carbon accumulation at different soil depths within the soil profile (Gallagher et al., 2022). Although N_2O flux measurement using the eddy covariance technique is becoming more common, fluxes are considerably lower than that of CO_2 and are frequently at or below the detection limit of fast-response analyzers. Nevertheless, a standard for instrumentation selection and data processing of N_2O flux measurements was published at the end of 2018 (Nemitz et al., 2018). Dissolved CO_2 (a component of DIC) is the focus of the following chapters, rather than DOC, due to its relevance to photosynthesis and the stronger likelihood of CO_2 evasion and its important role in the wetland C sink (Cao et al., 2016). Global wetland extent, ecosystem modeling, co-benefits, and

global wetland C sink quantification are essential, related aspects to this research but are deserving of separate discussion.

1.7 References

Knox, S. H., Windham-Myers, L., Anderson, F., Sturtevant, C., & Bergamaschi, B. (2018). Direct and indirect effects of tides on ecosystem-scale CO2 exchange in a brackish tidal marsh in Northern California. *Journal of Geophysical Research: Biogeosciences*, 123(3), 787-806.

Cao, X., Wu, P., Han, Z., Tu, H., & Zhang, S. (2016). Factors controlling the isotope composition of dissolved inorganic carbon in a karst-dominated wetland catchment, Guizhou Province, Southwest China. *Environmental Earth Sciences*, *75*, 1-14.

Carvalhais, N., Forkel, M., Khomik, M., Bellarby, J., Jung, M., Migliavacca, M., ... & Reichstein, M. (2014). Global covariation of carbon turnover times with climate in terrestrial ecosystems. *Nature*, *514*(7521), 213-217.

Chambers, L. G., Reddy, K. R., & Osborne, T. Z. (2011). Short-term response of carbon cycling to salinity pulses in a freshwater wetland. *Soil Science Society of America Journal*, 75(5), 2000-2007.

Ciais, P., Sabine, C., Bala, G., Bopp, L., Brovkin, V., Canadell, J., ... & Thornton, P. (2014). Carbon and other biogeochemical cycles. In Climate change 2013: the physical science basis. Contribution of Working Group I to the Fifth Assessment Report of the Intergovernmental Panel on Climate Change (pp. 465-570). Cambridge University Press.

Detto, M., Molini, A., Katul, G., Stoy, P., Palmroth, S., & Baldocchi, D. (2012). Causality and persistence in ecological systems: a nonparametric spectral Granger causality approach. *The American Naturalist*, *179*(4), 524-535.

Epron, D., Ngao, J., Dannoura, M., Bakker, M. R., Zeller, B., Bazot, S., ... & Loustau, D. (2011). Seasonal variations of belowground carbon transfer assessed by in situ 13 CO 2 pulse labelling of trees. *Biogeosciences*, 8(5), 1153-1168.

Falge, E, Baldocchi, D, Olson, R et al. (2001) Gap filling strategies for defensible annual sums of net ecosystem exchange. *Agricultural and Forest Meteorology*, 107, 43–69.

Fan, N., Koirala, S., Reichstein, M., Thurner, M., Avitabile, V., Santoro, M., ... & Carvalhais, N. (2020). Apparent ecosystem carbon turnover time: uncertainties and robust features. *Earth System Science Data*, 12(4), 2517-2536.

Fargione, J. E., Bassett, S., Boucher, T., Bridgham, S. D., Conant, R. T., Cook-Patton, S. C., ... & Griscom, B. W. (2018). Natural climate solutions for the United States. *Science Advances*, *4*(11), eaat1869.

Friedlingstein, P., Jones, M. W., O'Sullivan, M., Andrew, R. M., Bakker, D. C., Hauck, J., ... & Zeng, J. (2022). Global carbon budget 2021. *Earth System Science Data*, 14(4), 1917-2005.

Gallagher, J. B., Zhang, K., & Chuan, C. H. (2022). A Re-evaluation of Wetland Carbon Sink Mitigation Concepts and Measurements: A Diagenetic Solution. *Wetlands*, 42(3), 1-15.

Gaudinski, J. B., Trumbore, S. E., Davidson, E. A., & Zheng, S. (2000). Soil carbon cycling in a temperate forest: radiocarbon-based estimates of residence times, sequestration rates and partitioning of fluxes. *Biogeochemistry*, 51(1), 33-69.

Gualtieri, C., Angeloudis, A., Bombardelli, F., Jha, S., & Stoesser, T. (2017). On the values for the turbulent Schmidt number in environmental flows. *Fluids*, 2(2), 17.

Hafner, S., Unteregelsbacher, S., Seeber, E., Lena, B., Xu, X., Li, X., ... & Kuzyakov, Y. (2012). Effect of grazing on carbon stocks and assimilate partitioning in a Tibetan montane pasture revealed by 13 CO2 pulse labeling. *Global Change Biology*, *18*(2), 528-538.

Harvey, J., & Gooseff, M. (2015). River corridor science: Hydrologic exchange and ecological consequences from bedforms to basins. *Water Resources Research*, 51(9), 6893-6922.

Hikino, K., Danzberger, J., Riedel, V. P., Rehschuh, R., Ruehr, N. K., Hesse, B. D., ... & Grams, T. E. (2022). High resilience of carbon transport in long-term drought-stressed mature Norway spruce trees within 2 weeks after drought release. *Global Change Biology*, *28*(6), 2095-2110.

Hotchkiss, E. R., Hall Jr, R. O., Sponseller, R. A., Butman, D., Klaminder, J., Laudon, H., ... & Karlsson, J. J. N. G. (2015). Sources of and processes controlling CO 2 emissions change with the size of streams and rivers. *Nature Geoscience*, 8(9), 696-699.

Janse, J. H., Van Dam, A. A., Hes, E. M., de Klein, J. J., Finlayson, C. M., Janssen, A. B., ... & Verhoeven, J. T. (2019). Towards a global model for wetlands ecosystem services. *Current Opinion in Environmental Sustainability*, 36, 11-19.

Lasslop, G., Reichstein, M., Papale, D., Richardson, A. D., Arneth, A., Barr, A., ... & Wohlfahrt, G. (2010). Separation of net ecosystem exchange into assimilation and respiration using a light response curve approach: critical issues and global evaluation. *Global change biology*, *16*(1), 187-208.

Liu, X., Wan, S., Su, B., Hui, D., & Luo, Y. (2002). Response of soil CO2 efflux to water manipulation in a tallgrass prairie ecosystem. *Plant and soil*, 240(2), 213-223.

Lupon, A., Denfeld, B. A., Laudon, H., Leach, J., Karlsson, J., & Sponseller, R. A. (2019). Groundwater inflows control patterns and sources of greenhouse gas emissions from streams. *Limnology and Oceanography*, 64(4), 1545-1557.

Macreadie, P. I., Costa, M. D., Atwood, T. B., Friess, D. A., Kelleway, J. J., Kennedy, H., ... & Duarte, C. M. (2021). Blue carbon as a natural climate solution. *Nature Reviews Earth & Environment*, 2(12), 826-839.

Maher, D. T., Call, M., Santos, I. R., & Sanders, C. J. (2018). Beyond burial: Lateral exchange is a significant atmospheric carbon sink in mangrove forests. *Biology Letters*, 14(7), 20180200. https://doi.org/10.1098/rsbl.2018.0200

Malerba, M. E., Friess, D. A., Peacock, M., Grinham, A., Taillardat, P., Rosentreter, J. A., ... & Macreadie, P. I. (2022). Methane and nitrous oxide emissions complicate the climate benefits of teal and blue carbon wetlands. *One Earth*, 5(12), 1336-1341.

Mcleod, E., Chmura, G. L., Bouillon, S., Salm, R., Björk, M., Duarte, C. M., ... & Silliman, B. R. (2011). A blueprint for blue carbon: toward an improved understanding of the role of vegetated coastal habitats in sequestering CO2. *Frontiers in Ecology and the Environment*, 9(10), 552-560.

Nemitz, E., Mammarella, I., Ibrom, A., Aurela, M., Burba, G. G., Dengel, S., ... & Zahniser, M. (2018). Standardisation of eddy-covariance flux measurements of methane and nitrous oxide. *International agrophysics*.

Novick, K. A., Metzger, S., Anderegg, W. R., Barnes, M., Cala, D. S., Guan, K., ... & Wiesner, S. (2022). Informing Nature-based Climate Solutions for the United States with the best-available science. *Global change biology*.

Shahan, J. A. (2022). IMPROVING UNDERSTANDING OF ATMOSPHERIC AND HYDROLOGIC CARBON FLUXES IN A RESTORED TIDAL WETLAND (Doctoral dissertation, California State University, East Bay).

Sponseller, R. A. (2007). Precipitation pulses and soil CO2 flux in a Sonoran Desert ecosystem. *Global Change Biology*, 13(2), 426-436.

Stoy, P. C., Palmroth, S., Oishi, A. C., Siqueira, M. B., JUANG, J. Y., Novick, K. A., ... & Oren, R. A. M. (2007). Are ecosystem carbon inputs and outputs coupled at short time scales? A case study from adjacent pine and hardwood forests using impulse–response analysis. *Plant, Cell & Environment*, *30*(6), 700-710.

Tang, J., Zhuang, Q., Shannon, R. D., & White, J. R. (2010). Quantifying wetland methane emissions with process-based models of different complexities. *Biogeosciences*, 7(11), 3817-3837.

Toet, S., Van Logtestijn, R. S., Kampf, R., Schreijer, M., & Verhoeven, J. T. (2005). The effect of hydraulic retention time on the removal of pollutants from sewage treatment plant effluent in a surface-flow wetland system. *Wetlands*, 25(2), 375-391.

Villa, J. A., Ju, Y., Stephen, T., Rey-Sanchez, C., Wrighton, K. C., & Bohrer, G. (2020). Plant-mediated methane transport in emergent and floating-leaved species of a temperate freshwater mineral-soil wetland. *Limnology and Oceanography*, 65(7), 1635-1650.

2 Lagged Wetland CH_4 Flux Response in a Historically Wet Year

This chapter has been previously published as Turner, J., Desai, A. R., Thom, J., & Wickland, K. P. (2021). Lagged wetland CH4 flux response in a historically wet year. *Journal of Geophysical Research: Biogeosciences*, *126*(11), e2021JG006458.

2.1 Abstract

While a stimulating effect of plant primary productivity on soil carbon dioxide (CO_2) emissions has been well documented, links between gross primary productivity (GPP) and wetland methane (CH_4) emissions are less well investigated. Determination of the influence of primary productivity on wetland CH_4 emissions (FCH_4) is complicated by confounding influences of water table level and temperature on CH_4 production, which also vary seasonally. Here, we evaluate the link between preceding GPP and subsequent FCH_4 at two fens in Wisconsin using eddy covariance flux towers, Lost Creek (US-Los) and Allequash Creek (US-ALQ). Both wetlands are mosaics of forested and shrub wetlands, with US-Los being larger in scale and having a more open canopy. Co-located sites with multi-year observations of flux, hydrology, and meteorology provide an opportunity to measure and compare lag effects on FCH_4 without interference due to differing climate. Daily average FCH_4 from US-Los reached a maximum of 47.7 ηmol CH_4 $m^{-2}{\cdot}s^{-1}$ during the study period, while US-ALQ was more than double at 117.9 ηmol CH_4 $m^{-2}{\cdot}s^{-1}$. The lagged influence of GPP on temperature-normalized FCH_4 (T_{air}-FCH_4) was weaker and more delayed in a year with anomalously high precipitation than a following drier year at both sites. FCH_4 at US-ALQ was lower coincident with higher stream discharge in the wet year (2019), potentially due to soil gas flushing during high precipitation events and lower

water temperatures. Better understanding of the lagged influence of GPP on FCH_4 due to this study has implications for climate modeling and more accurate carbon budgeting.

2.2 Plain Language Summary

Research on what controls wetland methane emissions is continually advancing, and while this is beneficial for predicting future climate scenarios, there is still a need to understand how changes in plant productivity will influence wetland methane emissions. In this study, we investigated the strength and lag time of the relationship between gross primary productivity due to photosynthesizing plants and wetland methane flux in two closely situated sites. We also looked at how hydrology might change that relationship. We found the total amount of methane emitted in an extremely wet year was less than what was emitted in the following drier year at both wetlands potentially because of less carbon provided to the soil by photosynthesizing plants. The difference in methane emissions from one year to the next could be influenced by wetland hydrology, water temperature, or other conditions that impact methane-producing bacteria. Results from this study will help scientists better predict methane emissions following high precipitation years which may become more common in a changing climate.

2.3 Introduction

By the year 2100, mean global annual CH_4 flux (FCH_4) from natural wetlands is projected to increase from 172 Tg CH_4 yr^{-1} to anywhere between 222 and 338 Tg CH_4 yr^{-1} depending on the climate scenario (Zhang et al., 2017). Under the best climate scenario of strong climate mitigation (RCP 2.6), wetland methane (CH_4) emissions are projected to decline in the 2050s

after peaking at ~225 Tg CH_4 yr^{-1}. Radiative forcing feedback from wetland CH_4 could account for a large portion of the total radiative forcing change from CH_4, accounting for 0.04 ± 0.002 Wm^{-2}, and global mean temperature would increase slightly as a result (Zhang et al., 2017). Ecosystem-scale controls over microbial activity and resulting wetland CH_4 emissions are difficult to include in climate projection models despite their importance as a major climate feedback. Specifically, there is a need to understand and include the impact of shifting spatial patterns of vascular plants on CH_4 transport from soil into atmosphere, and biogeographical distribution of methanogen communities and their metabolic processes, which could be leading to current underestimation of CH_4 emissions with certain models. A better understanding of the relationship between gross primary productivity (GPP) and FCH_4 in fen wetlands is crucial to understanding the potential impacts of a longer growing season, higher GPP, and the shifting distribution of terrestrial ecosystems due to a changing climate (Zhang et al., 2017). In this study, we take a close look at the lagged effect of GPP on FCH_4 from two closely located north temperate fen wetlands.

Global syntheses of eddy covariance flux data and improved earth system models have contributed to a better understanding of FCH_4 drivers and variability across sites (Knox et al., 2019; Delwiche et al., 2021; Knox et al., 2021), but there is room to improve understanding even further through regional site comparisons. Driver analysis on this small-scale has the potential to explain variability in FCH_4 in locations undergoing the same synoptic meteorology on the scale of hundreds to thousands of kilometers (e.g., low pressure systems), some overlapping mesoscale meteorology at the scale of a few to hundreds of kilometers (e.g.,

thunderstorms), but separate microclimates under the scale of a kilometer (e.g., structure and function of vegetation and its influence on local climate variables).

Some prior studies have found no significant relationship between GPP and FCH_4 (Sturtevant and Oechel, 2013; Davidson et al., 2016). However, certain physical mechanisms should cause GPP and FCH_4 to be linked in wetland ecosystems, either synchronously or lagged. GPP can influence FCH_4 directly through plant-mediated transport of gas from porewater to the atmosphere (Dannenberg and Conrad, 1999; Dorodnikov et al., 2011) or indirectly through plant C fixation to soil methanogens during photosynthesis (Hatala et al., 2012). Aerenchymatous wetland plants transport dissolved CH_4 from porewater, through roots, into the root cortex, and then out through leaf sheath micropores in the lower part of the shoot (Nouchi et al., 1990; Henneberg et al., 2012). Root area is therefore an important determinant of plant-mediated CH_4 transport and will increase CH_4 production in anoxic conditions. Ecosystem-scale FCH_4 is more difficult to predict given that flux varies among plants of the same genus (Ding et al., 2005). CH_4 oxidation rate will also peak at different times of the season depending on plant type (Welsch and Yavitt, 2007).

The lag time between plant C assimilation and soil CO_2 efflux (i.e., microbial decomposition & root respiration) takes less than one day for grasses and up to 5 days for mature trees (Kuzyakov and Gavrichkova, 2010). Due to plant metabolism, one would expect, in anoxic soil conditions, a similar lagged influence of GPP on soil FCH_4, which has been detected and discussed in some studies (Mitra et al., 2020; Bridgham et al., 2013; Updegraff et al., 2001) but not others (Villa et al., 2019) or may disappear after temperature-normalization (Rinne et al., 2018; Chen et al., 2020). Methane emission can be stimulated by plant shoot clipping (which

results in the growth of new roots) in as few as three days, although the short duration of mesocosm experiments limits measurement of maximum total lag time (Rietl et al., 2017). Another experiment found a six-day lag between soaking a rice field and a rise in CH_4 emissions and a clear change in the magnitude of the FCH_4 diel cycle depending on plant growth phase (Centeno et al., 2017).

In this study we compare FCH_4 and related environmental variables of two co-located fen wetlands in Wisconsin to answer two questions: (1) What is the influence of plant C fixation on FCH_4 as measured by the lagged effect of GPP at two north temperate fen wetlands when removing the known influence of air temperature (T_{air})? (2) How do factors relating to wetland hydrology as indicated by wetland stream discharge, stream temperature (T_{stream}), and water table depth (WTD), mediate the GPP-FCH_4 relationship at both sites? We hypothesize GPP will have a strong but short-term lagged influence on temperature-normalized FCH_4 (T_{air}-FCH_4) at both sites because of allocation of recently fixed C to roots, followed by methanogenesis. Removing the influence of T_{air} will be critical to the interpretation of results. We expect wetland stream discharge to correspond with increasing FCH_4, assuming it is indicative of a higher WTD. Finally, FCH_4 should be similar but not identical at the two sites in this study given that they are co-located fens with mixed vegetative cover but possess unique physical and hydrological features, discussed below.

2.4 Methods

2.4.1 Site descriptions

Our study focuses on two sites in northern Wisconsin that are located approximately 29 km apart: US-Los and US-ALQ. US-Los (46.082777, -89.978611) is larger in scale (flux footprint radius 1,033 m), features more open canopy vegetation, and is dominated by broad-leaved deciduous shrub vegetation (20% of flux footprint). US-ALQ (46.030759, -89.606730) is smaller in scale (flux footprint radius 238 m), features more sheltered canopies, and is dominated by broad-leaved deciduous or evergreen shrub vegetation (30% of flux footprint). Both sites are mixed sedge meadow, forest, and shrub wetland. Both sites are fen wetlands, as they are surface water and groundwater sourced and have peat soil, and each is bisected by a headwater stream (Lost Creek at US-Los; Allequash Creek at US-ALQ). Detailed site descriptions are available for US-Los in Sulman et al. (2009) and for US-ALQ in Anderson and Lowry (2007). It should be noted that Allequash Creek (flowing through US-ALQ) is a groundwater-fed stream (Pint et al., 2003) and thus flows year-round.

2.4.2 Flux data

CH_4 and CO_2 eddy covariance flux data for US-ALQ (doi:10.3389/fenvs.2019.00179) and US-Los (doi:10.17190/AMF/1246071) are available on Ameriflux (Olson, B. 2020; Desai, A. 2020; https://ameriflux.lbl.gov/). All data analyzed in this study were collected during January 1, 2019 through Dec 31, 2020. Instrumentation at both sites included a sonic anemometer (Campbell Scientific, Inc., Logan, 188 UT, CSAT-3), open path infrared gas analyzer, and methane flux sensor (LI-COR, Lincoln, NE, LI7700). There was a different radiation sensor at US-Los (Kipp & Zonen 197 North America, Sterling, USA, Kipp-Zonen CNR4) than US-ALQ (Apogee Instruments Inc., Logan, UT, SN-500). There was also a different air temperature and relative humidity sensor at US-Los (Campbell Scientific, Inc., Logan, UT, CS215) than at US-ALQ (Campbell

Scientific, Inc., Logan, UT, Vaisala HMP45C 190 platinum-resistance thermometer). A quantum photosynthetically active radiation (PAR) sensor was installed only at US-Los (LI-COR, Lincoln, NE, LI-190). More information on flux tower height, footprint, and instrumentation for both sites can be found in Turner et al. (2019).

Typical in eddy covariance studies, there were portions of data missing from the continuous record that required gap-filling. There were more missing half-hourly FCH_4 data at US-ALQ than US-Los (49% vs. 34%). Fewer data were missing during the typical CO_2 uptake period from April to October (US-ALQ 44%, US-Los 23%) than during the rest of the year for both sites (US-ALQ 57%, US-Los 48%). There were more data gaps in 2019 (US-ALQ 63%, US-Los 45%) than 2020 (US-ALQ 36%, US-Los 22%). FCH_4 was gap-filled with the machine learning random forest algorithm using the "randomForest" R package (Liaw and Wiener, 2001) and gap-filling script (Kim, 2020; Kim et al., 2020). This approach was selected because it outperforms marginal distribution sampling, artificial neural networks, and support vector machine for gap-filling of eddy covariance FCH_4 data.

Net ecosystem exchange of CO_2 (NEE) was gap-filled and partitioned into GPP and ecosystem respiration (R_{eco}) using the Desai-Cook flux partitioning model (Cook et al., 2004; Desai et al., 2007), which utilizes a non-linear regression of daytime R_{eco} to PAR and is comparable to many other regressions based on moving window flux partitioning algorithms. R_{eco} in the model is calculated from a non-linear regression of nighttime NEE to T_{air}. Once again, there were more data gaps in 2019 (US-ALQ 37%, US-Los 49%) than in 2020 (US-ALQ 29%, US-Los 33%), for NEE. Fewer data were missing during the CO_2 uptake period from April to October (US-ALQ 29%, US-Los 34%) than during the rest of the year (US-ALQ 38%, US-Los 51%). No

missing data remained after gap-filling NEE for US-ALQ during either year. No missing data remained after gap-filling NEE for US-Los in 2019, but a small amount of missing data remained after gap-filling in 2020 (US-Los 94%).

2.4.3 Meteorological and hydrological data

Daily total precipitation data were from Lakeland Field Station at Lakeland Airport in Woodruff, WI (45.927222, -89.730836), located 26.1 km away from US-Los and 15.4 km from US-ALQ (NOAA, 2021). Rhinelander, WI, a city located 56 km from the study sites, received nearly 110 cm of total precipitation in 2019, making it the wettest year on record from 1908 to 2020 (Rhinelander Weather Recs., 2021). The average annual precipitation for Rhinelander during that time was 80 ± 15 cm (standard deviation). Meanwhile, the city received only 90 cm of precipitation in 2020. Stream temperature and temperature data for US-ALQ were from the National Water Information System (USGS, 2020a; https://waterdata.usgs.gov/nwis). US-ALQ lacked water table depth data during the time of study. WTD was used in place of stream discharge to understand the impact of hydrology on FCH_4 at US-Los. The water level sensor used to measure WTD was a Campbell Scientific CS451.

2.4.4 GPP-FCH_4 Lag analysis

Lag analysis involved multiple steps. First, we utilized a built-in function in MATLAB that performed a circular shift of the data ("xcorr") to estimate the direction of the strongest lag correlation based on cross correlation of the two variables of interest. Lag analysis was then performed in the direction of the strongest lag correlation as in Rinne et al. (2018). The driver variable was lagged with respect to the response variable one step at a time. Rows with missing

driver variable data were removed. Correlation and significance between variables were measured at each step. Variables analyzed for lags included GPP & FCH_4, GPP & T_{air}-FCH_4, WTD & FCH_4, WTD & T_{air}-FCH_4, and WTD & GPP. The lag was not measured past 200 days. MATLAB scripts for creating the lag analysis plots and all other plots used in this study are available online (turner-j, 2020). All lag analysis was performed with daily average data.

2.4.5 Temperature normalization of FCH_4

Covariates must be taken into careful consideration when analyzing data for FCH_4 drivers that are interrelated. One such covariate that has a noticeable impact on FCH_4 is temperature, but whether it is the soil, air, or water temperature which dominantly influences FCH_4 varies among sites (Rey-Sanchez et al., 2018; Chu et al., 2014). Removing the influence of temperature on FCH_4 before performing lag analysis with GPP should be done to eliminate any trends solely due to temperature as a driving force (Chen et al., 2020). We removed the influence of T_{air} on FCH_4 by fitting observed FCH_4 to an exponential model with T_{air} as a predictor. Non-linear regression was used to find the coefficients β_1 and β_2 in Equation 2.1 below. Observed FCH_4 from both years was then divided by predicted FCH_4 based on observed T_{air} as in Equation 2.2 below. T_{air} dependence of FCH_4 was therefore modeled and removed using the following equations:

Equation 2.1: $$F = \beta_1 \times \exp(\beta_2 \cdot T)$$

Equation 2.2: $$T_{air}FCH_4 = \frac{daily\ average\ FCH_4}{F}$$

2.5 Results

2.5.1 Meteorology and stream discharge

The two study sites, US-ALQ and US-Los, had equal means of daily average incoming radiation ($p = 0.054$) and linearly correlated but unequal means of air temperature ($r = 1$, $p << 0.01$) and vapor pressure deficit ($r = 0.97$, $p << 0.01$). Resulting differences in the variables we compare and analyze in this study at each site could therefore be due to the impacts of mesoscale or microscale meteorology; differences in magnitude of stream discharge, air temperature, or vapor pressure deficit; or abiotic or biotic site characteristics other than those previously mentioned.

The water table at US-Los was closer to the surface in 2019 than 2020 (-0.26 vs. -0.29 m below surface). Additionally, stream discharge at US-ALQ was linearly related to WTD at US-Los ($r = 0.45$, $p = << 0.01$) and was slightly higher in 2019 (0.15 m^3s^{-1}) than 2020 (0.16 m^3s^{-1}).). There was a low covariance (cov = 0.0045) and a significant, positive two-day lagged effect of precipitation at Lakeland Airport on WTD at US-Los ($r = 0.11$). Precipitation covaried with stream discharge at US-ALQ (cov = 0.01). Precipitation also covaried with T_{stream} at US-ALQ (cov = 0.56) and T_{air} at US-Los (cov = 0.81) and US-ALQ (cov = 0.91).

2.5.2 CH_4 and CO_2 fluxes in wet (2019) and dry (2020) years

FCH_4 gap-filling performance was higher with US-ALQ than US-Los ($R^2 = 0.85$ vs. 0.70). No FCH_4 data were missing at either site after gap-filling (Fig 2.1). US-ALQ emitted more than double the daily average FCH_4 as US-Los during the entire study period (approx. 19.6 versus 6.7 ηmol m^{-2} s^{-1}). Daily average FCH_4 reached a maximum of 47.7 ηmol CH_4 m^{-2} s^{-1} at US-Los and

117.9 ηmol CH_4 m^{-2} s^{-1} at US-ALQ. More carbon as CH_4 ($C\text{-}CH_4$) was emitted and less carbon as CO_2 ($C\text{-}CO_2$) was taken up annually at US-ALQ than US-Los in both years (Table 2.1). Both sites exhibited lower daily mean FCH_4 in the historically wet year of 2019 (5.5 ηmol CH_4 $m^{-2}s^{-1}$ US-Los; 13.5 ηmol CH_4 $m^{-2}s^{-1}$ US-ALQ) than in 2020 (7.8 ηmol CH_4 $m^{-2}s^{-1}$ US-Los; 25.8 ηmol CH_4 $m^{-2}s^{-1}$ US-ALQ). Cumulative annual $C\text{-}CH_4$ emission at both sites was only a fraction of $C\text{-}CO_2$ uptake. US-ALQ had the highest cumulative annual FCH_4 in comparison to FCO_2, at 10.31% in 2020. US-Los had the lowest cumulative annual FCH_4 in comparison to FCO_2, at approximately 1% in 2019.

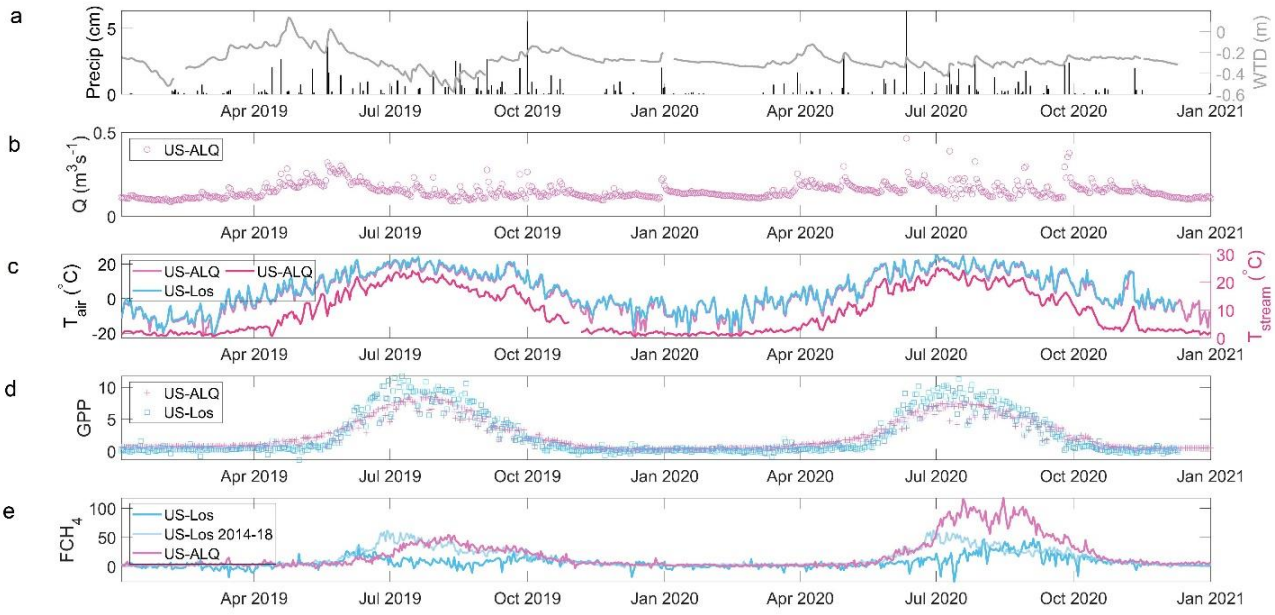

Figure 2.1. (A) Bar plot of precipitation at Lakeland Airport and timeseries of water table depth (WTD) at US-Los, (B) stream discharge (Q) at US-ALQ, (C) air temperature in degrees C at both sites and stream water temperature at US-ALQ, (D) GPP at both sites in µmol CO_2 $m^{-2}s^{-1}$, and (E) FCH_4 at both sites in ηmol CH_4 $m^{-2}s^{-1}$ and historic average FCH_4 at US-Los from 2014 to 2018.

Table 2.1. Cumulative annual FCH_4 and FCO_2 as C from US-ALQ and US-Los in 2019 and 2020.

	FCH_4 (g C-CH_4 m^{-2} yr^{-1})		FCO_2 (g C-CO_2 m^{-2} yr^{-1})	
	2019	2020	2019	2020
US-ALQ	5.08 ± 0.10	9.79 ± 0.21	-78.36 ± 2.59	-94.92 ± 2.52
US-Los	2.08 ± 0.04	2.98 ± 0.06	-202.61 ± 5.79	-148.73 ± 4.69

Note: Values are shown with standard error of the mean. Negative values indicate a C sink from the atmosphere. Positive values indicate a C source to the atmosphere.

2.5.3 GPP-FCH_4 relationship

FCH_4 preceded GPP by approximately 20 days at US-Los in 2019 (Fig 2.2A). Removing the influence of air temperature ("normalized" in Figs 2.2, 2.3) resulted in a stronger lagged correlation where FCH_4 followed GPP starting after 40 days in 2019, and the strength of the correlation continued to grow up until at least 100 days (Fig 2.2B). The lag relationships between FCH_4 and GPP, as well as T_{air}-FCH_4 and GPP, were both weakly correlated in 2019 ($r < 0.4$). The lagged influence of GPP on FCH_4 at US-Los peaked at 40 days in 2020 (Fig 2.2C). The lagged influence of GPP on T_{air}-FCH_4 at US-Los was shorter than that of FCH_4 in 2020, with a broad peak lasting 40-60 days ($r = 0.65$).

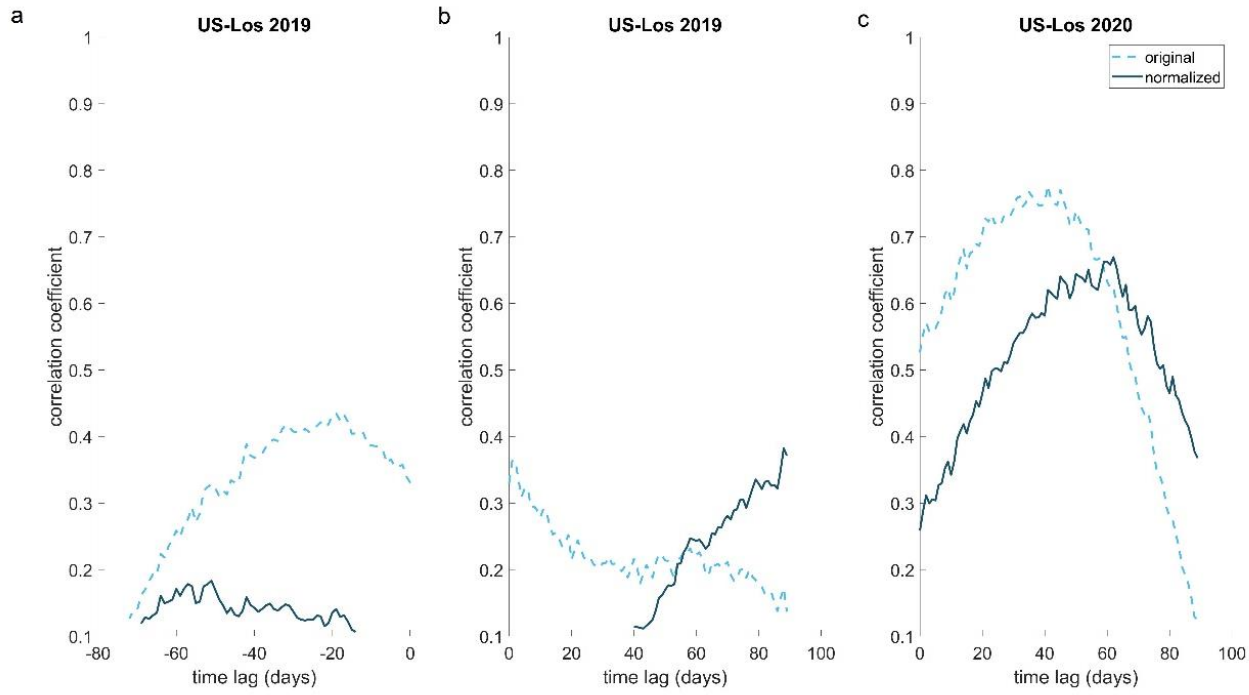

Figure 2.2. Lagged influence of GPP on FCH_4 and temperature-normalized FCH_4 at US-Los. (A) FCH_4 preceding GPP in 2019. (B) FCH_4 following GPP in 2019. (C) FCH_4 following GPP in 2020. Positive values indicate FCH_4 follows GPP. Only significant ($p < 0.05$), positive lags ($r > 0$) shown.

GPP preceded FCH_4 by approximately 20 days at US-ALQ in 2019 (Fig 2.3A). Removing the influence of air temperature on FCH_4 revealed that the strongest correlation between GPP and T_{air}-FCH_4 occurred around 60 days and plateaued until at least 100 days, meaning that GPP was not correlated with FCH_4 for at least 2 months ($r = 0.52$). The lag relationship was slightly shorter in 2020, with GPP leading FCH_4 by roughly 20 days and GPP leading T_{air}-FCH_4 by approximately 35-50 days ($r = 0.78$, Fig 2.3B). The lagged influence of GPP on T_{air}-FCH_4 was shorter, stronger, and more closely related to that of GPP and FCH_4 in 2020 than 2019 for both sites.

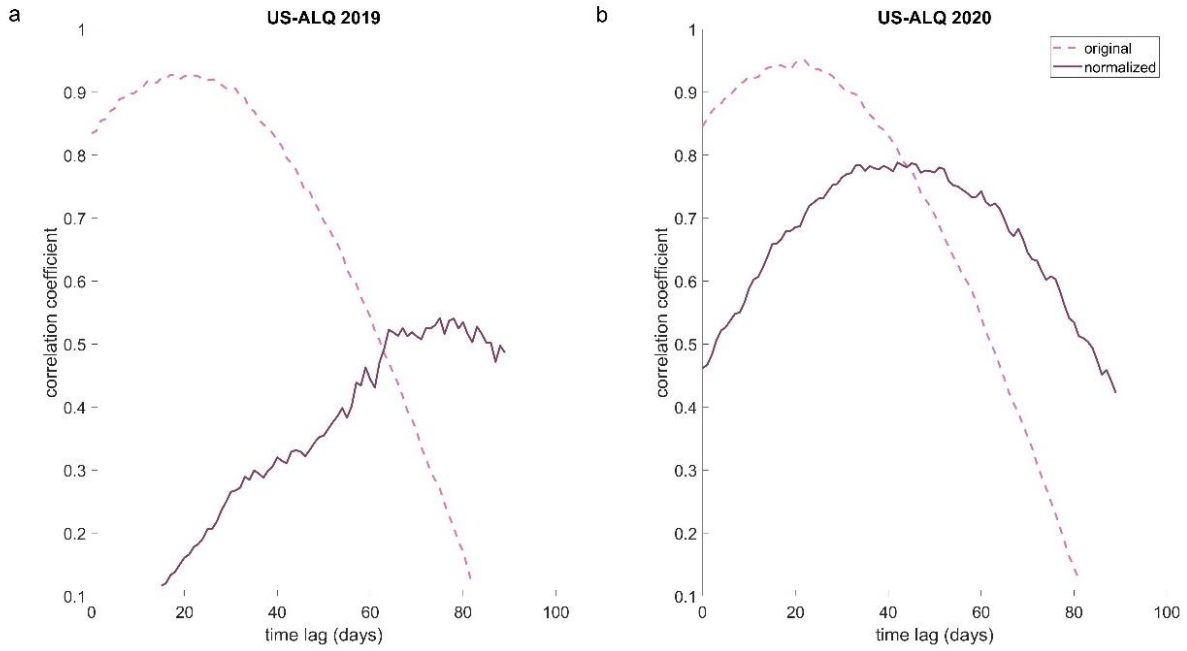

Figure 2.3. Lagged influence of GPP on FCH_4 and temperature-normalized FCH_4 at US-ALQ in 2019 and 2020. Only significant ($p < 0.05$), positive lags ($r > 0$) shown.

2.5.4 Influences of hydrology

FCH_4 at both sites was correlated with T_{air}, but the relationship was stronger at US-ALQ ($R^2 = 0.53$) than US-Los ($R^2 = 0.25$) (Figs 2.4A & 2.5A). The relationship between WTD and T_{air}-FCH_4 at US-Los was not linear in either year (Fig 3.4B & C). There was a significant inverse relationship between discharge and T_{air}-FCH_4 at US-ALQ during 2019 ($R^2 = 0.73$) (Fig 2.5B). However, there was no significant relationship between discharge and T_{air}-FCH_4 at US-ALQ in 2020 (Fig 2.5C).

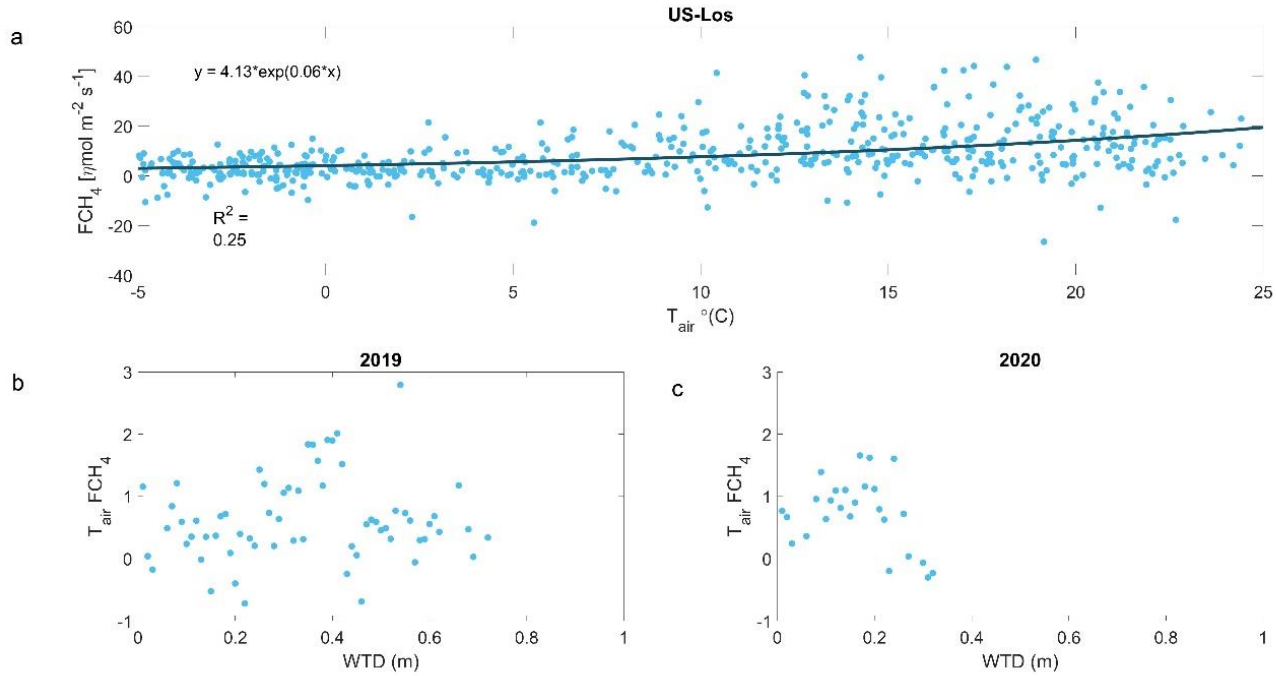

Figure 2.4. (A) Air temperature sensitivity of FCH_4 in both years combined, and (B) WTD versus temperature-normalized FCH_4 using daily average data at US-Los during 2019 and (C) 2020. R^2 displayed on the first subplot is the coefficient of determination between the best fit of the relevant model (second order polynomial) and observations. Best fit lines show significant relationships ($p < 0.05$). T_{air}- FCH_4 was bin averaged according to discharge rounded to the nearest 0.01 m.

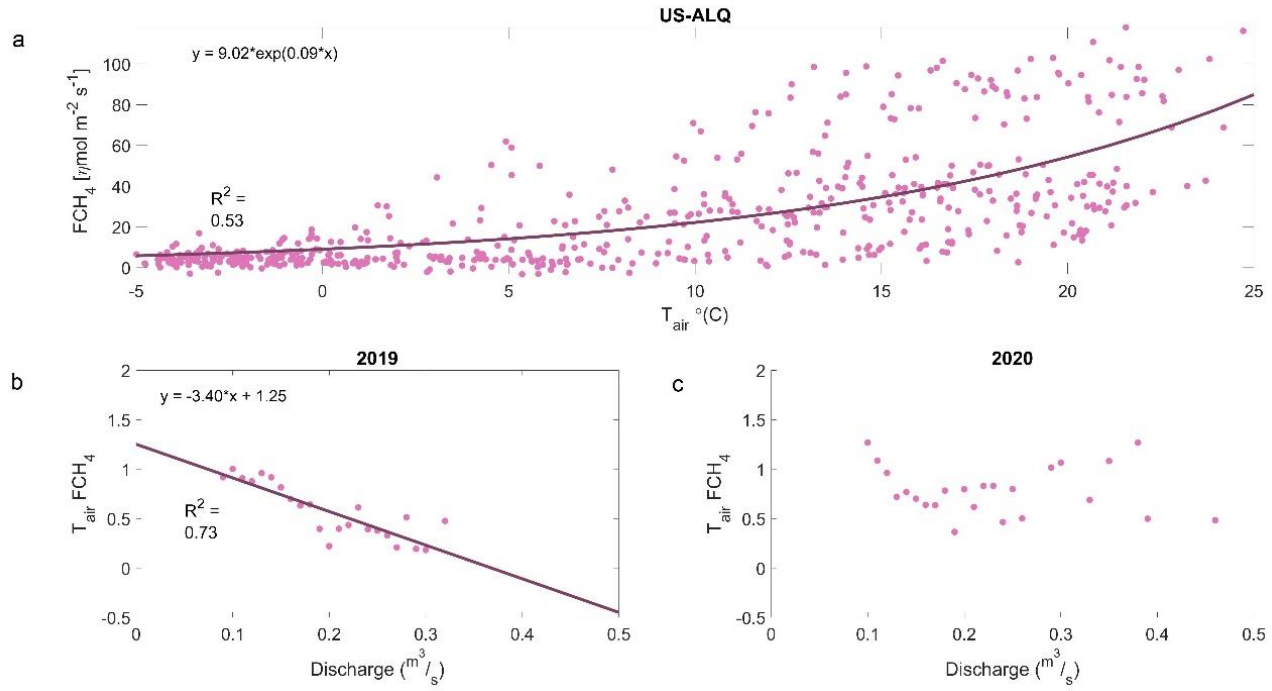

Figure 2.5. (A) Air temperature sensitivity of FCH_4 in both years and (B) Discharge versus T_{air}-FCH_4 using daily average data at US-ALQ during 2019 and (C) 2020. R^2 displayed on each plot is the coefficient of determination between the best fit of the relevant model (first or second order polynomial) and observations. Best fit lines show significant relationships ($p < 0.05$). T_{air}-FCH_4 was bin averaged according to discharge rounded to the nearest 0.01 m^3s^{-1}.

There was a significant lagged influence of WTD on FCH_4 at US-Los in 2019 (Fig 2.6A). Removing the influence of T_{air} did not greatly change the relationship (Fig 2.6B). The lagged effect of WTD on T_{air}-FCH_4 lasted 5-52 days with a peak at 24 days and a correlation coefficient of 0.27. No significant, positive correlation was detected between WTD and FCH_4 or T_{air}-FCH_4 at US-Los during 2020 (data not shown).

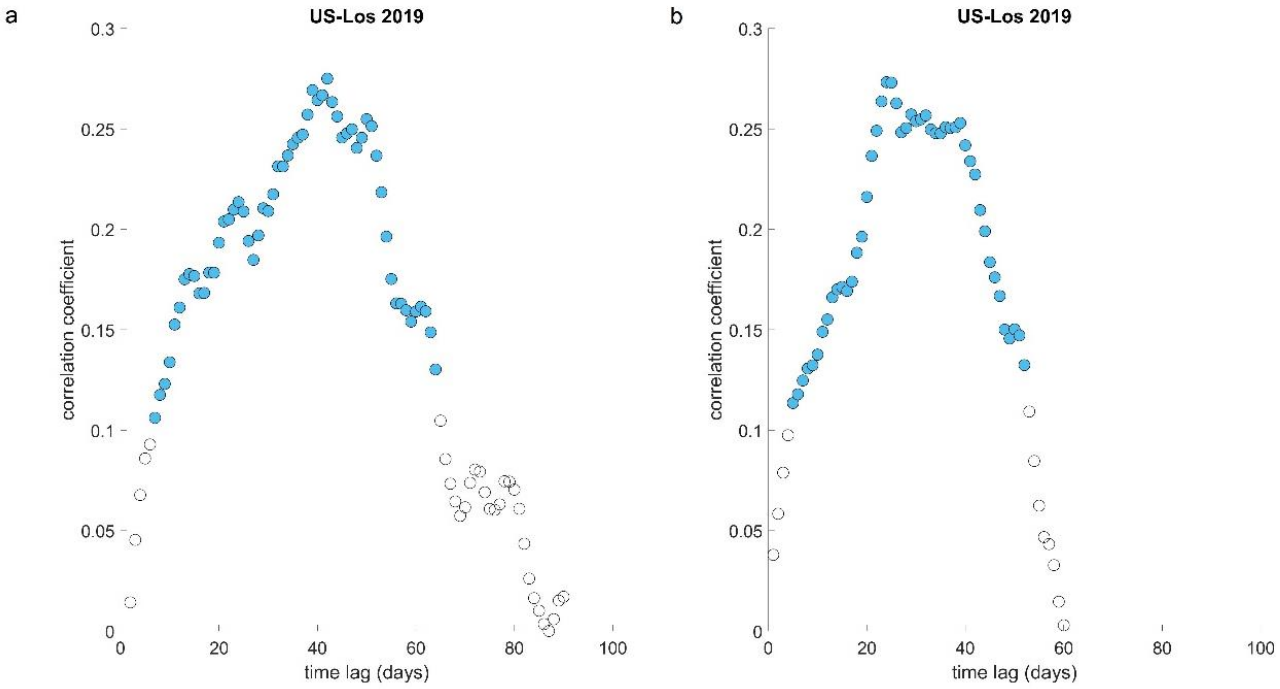

Figure 2.6. Lagged effects of water table depth (WTD) on (A) FCH_4 and (B) T_{air}-FCH_4 at US-Los in 2019. Filled blue circles represent significant ($p < 0.05$), positive ($r > 0$) lag correlations. Empty circles are not significant and/or do not represent positive correlations.

WTD variability at US-Los was lower in 2020 (var = 0.002) than 2019 (var = 0.016). Discharge variance was consistently low at US-ALQ, remaining at 0.002 in both years. Discharge was also low but typical for the stream, ranging from 0.086-0.32 m^3s^{-1} in 2019 and from 0.10-0.46 m^3s^{-1} in 2020 at US-ALQ. There was also a significant, positive ($p< 0.05$, $r>0$) lagged effect of WTD on GPP at US-Los with a very long duration of 43-140 days with a peak at 92 days ($r = 0.81$) in 2019 (Fig 2.7A). The lag effect was similar in 2020 but did not begin until around 60 days and had a lower peak correlation ($r = 0.42$, Fig 2.7B).

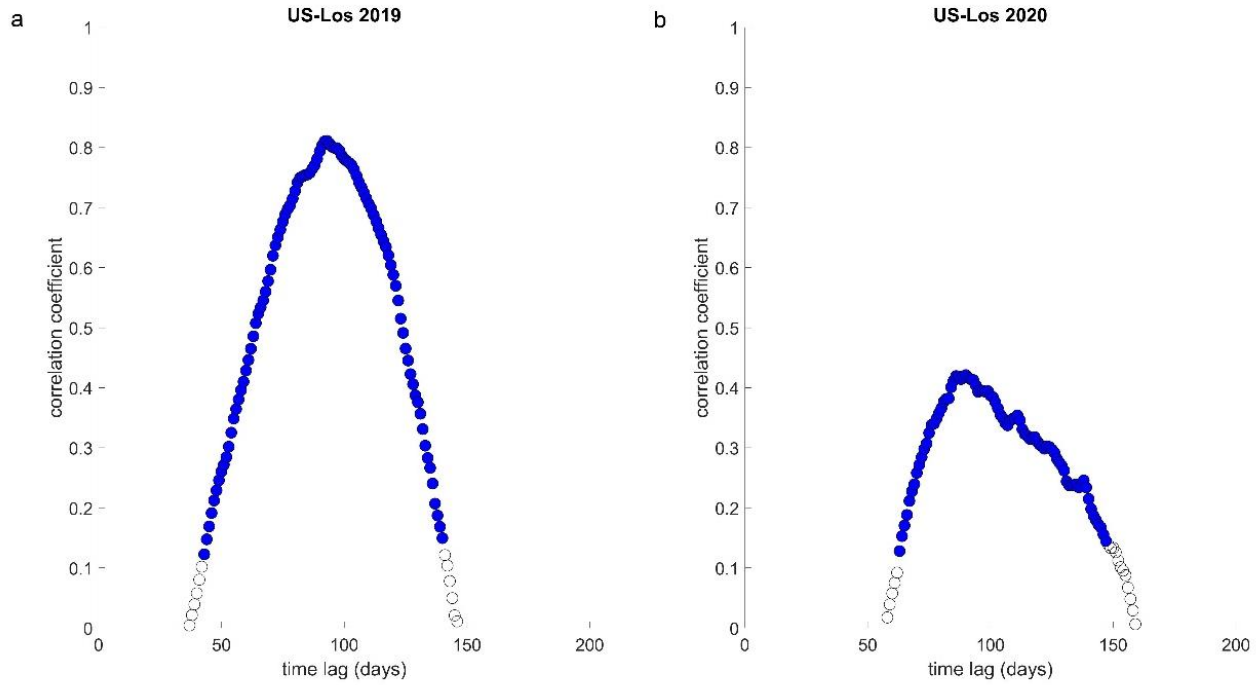

Figure 2.7. Lagged effects of water table depth (WTD) on GPP in (A) 2019 and (B) 2020 at US-Los. Filled blue circles represent significant ($p < 0.05$), positive ($r > 0$) lag correlations. Empty circles are not significant and/or do not represent positive correlations.

Higher T_{stream} was significantly positively correlated ($r = 0.15$, $p = 0.003$) with higher T_{air}-FCH_4 at US-ALQ from April to October but negatively correlated with T_{air}-FCH_4 during the rest of the year ($r = -0.28$, $p = 0$) during both years combined (Fig 2.8 A & B). However, the linear model demonstrated a poor fit to the data in both cases ($R^2 < 0.1$). Stream temperature did not surpass 5 °C during months outside April to October. Average yearly water temperature in the creek was slightly lower in 2019 than 2020 (9.3 vs. 9.6 °C).

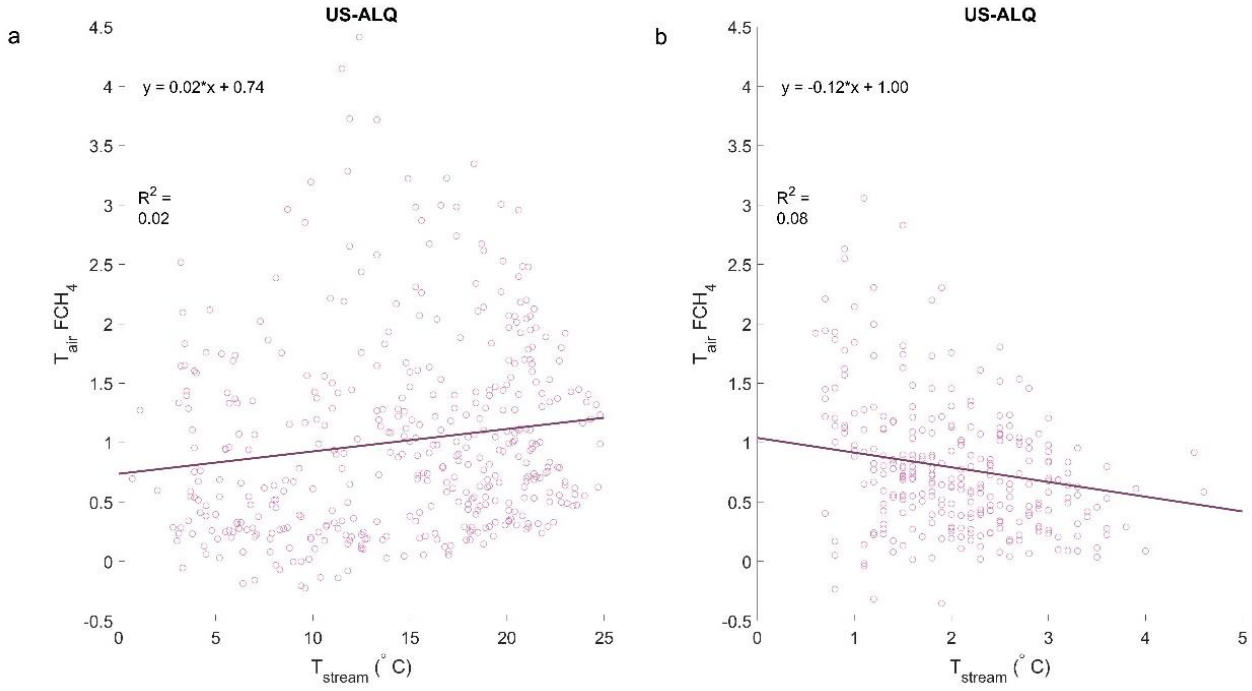

Figure 2.8. The influence of T_{stream} on T_{air}-FCH_4 at US-ALQ during (A) April to October and (B) all other months for both years combined. Solid lines represent the first-order linear regression. R^2 is the coefficient of determination between the linear regression and observations.

2.6 Discussion

2.6.1 CH_4 limitations in a historically wet year

Daily average FCH_4 for both sites was on the lower end of what is expected for wetlands in general (Nicolini et al., 2013), but cumulative annual FCH_4 aligned well within the wetland type of fens (Knox et al., 2019). Daily average FCH_4 and cumulative annual FCH_4 for both sites were lower in the historically wet year than in the following dry year (Table 2.1, Figure 2.1E). This is a noteworthy finding given that an earlier study in the same region, but from a landscape-level tall tower, concluded a dry year with a longer growing season and warmer conditions cut FCH_4 by 28% (Desai et al., 2015). These decreases in FCH_4 in unusually wet and

dry years suggest environmental extremes could reduce cumulative annual FCH_4 at these sites. The results of this study also strengthen the idea of a critical inundation level past which wetland CH_4 emissions begin to decline due to a number of possible reasons (e.g., lower light attenuation, diluted organic substrate, etc.) (Calabrese et al., 2021). However, more hydrological data from both sites is needed.

2.6.2 GPP-FCH_4 lagged relationship

At both sites, the lag between GPP and FCH_4 was weaker and took longer in 2019 than in 2020. The GPP-FCH_4 lag relationship observed at both sites during the study is supported by Delwiche et al. (2021), which found a lag relationship between FCH_4 and GPP in 83% of global freshwater wetlands, and the 20.7-day lag observed in Knox et al. (2021). T_{air} normalization of FCH_4 was critical for observation of the severe shifts in the lag effect in this study during a historically wet year, as normalization shifted the GPP-FCH_4 relationship at US-ALQ backwards by roughly twenty days in 2019. The lag correlation between GPP and subsequent T_{air}-FCH_4 observed at both sites in 2019 superseded the amount of time needed for photosynthesis, soil C fixation, and root growth, indicating the influence of another factor not considered in this study or a process that needs to be further explored.

The extremely long lagged influences of GPP on T_{air}-FCH_4 at both sites, and WTD on GPP at US-Los in comparison with the much shorter lag between WTD and FCH_4, indicate that root respiration was not a strong driver of FCH_4 in the beginning of 2019. One possible explanation is substrate limitation for methanogenesis caused by a lack of recently fixed labile C or older, more recalcitrant soil organic carbon (Oikawa et al., 2017).

In a year characterized by historical levels of precipitation, WTD fluctuated from approximately 0.2 m to -0.6 m from May to August of 2019 at US-Los. This brings into question the potential of plant stress to limit GPP, as high water level fluctuations will increase plant biomass allocation to roots rather than shoots and can have a negative impact on propagation (Wei et al., 2019) and photosynthetic potential (Ballantyne et al., 2014). Additionally, in flood years following droughts, maximum growing season GPP could decline due to plant stress or change in vegetation composition (Olefeldt et al., 2017), and the expected consequential increase in FCH_4 would not occur. Plant stress response and the resulting impact on gas flux is an area worthy of further research especially as extreme precipitation becomes more common.

2.6.3 WTD

Pugh et al. (2018) investigated WTD and monthly average FCH_4 at US-Los and found no correlation when accounting for T_{air}, but our analysis of daily average fluxes in a historically wet year revealed a lag effect of the two variables that lasted 5-52 days but reached peak correlation at 24 days. Peak lag correlation of WTD and FCH_4 in 2019 aligned well with other sites from the FLUXNET-CH4 database, which averaged approximately 18.3 days (Knox et al., 2021). The response of GPP did not follow until nearly 40 days later at US-Los in 2019, a year that was characterized by historic precipitation.

High water table level will reduce seedling establishment, growth, and survival in wetlands if it occurs during seedling establishment or for a prolonged period of time (Zacks et al., 2019). Although some plants are more resilient to flooded conditions, permanently flooded conditions cause oxygen deprivation and higher CO_2 storage in plant tissues and at the cellular

level (Pedersen et al., 2017). A shallower water table (i.e., closer to the surface) should increase FCH_4 by increasing GPP of hydric vegetation (Gomez-Casanovas et al., 2020; Musarika et al., 2017). Other studies disagree, demonstrating that a deeper water table (i.e., farther below the surface) will increase GPP in the absence of moisture stress by improving the availability of O_2 for photosynthesis in roots (Ballantyne et al., 2014).

Analysis of twenty-three sites from the FLUXNET-FCH4 database has shown that T_{air} controls FCH_4 at sites with lower WTD variability, but WTD controls FCH_4 at sites with lower T_{air} variability (Knox et al., 2019; Delwiche et al., 2021). The lack of correlation between lagged WTD and FCH_4 at US-Los in 2020, a year with more WTD variability, supports this. However, the positive relationship between WTD variability and FCH_4 appears to be species-specific (Radu and Duval, 2018).

2.6.4 Study limitations

Among the variables considered in this study, there are expected covariate relationships between precipitation, T_{air}, T_{stream}, WTD, and stream discharge, and seasonal cycles for each. WTD and temperature may alter the GPP-FCH_4 relationship because their covariance can appear like a cause and effect (direct relationship) when it is instead evidence of an indirect relationship. For example, the negative relationship between T_{stream} and T_{air}-FCH_4 outside of the months April-October (Fig 2.8 B) demonstrated how shifting seasonal patterns may mask the relationship of GPP and FCH_4.

The interactions of precipitation and T_{air} are evidenced in Dinsmore et al. (2013), where essentially all interannual variability in the export of dissolved organic carbon from a peatland

catchment was explained by interactions between the two variables. Additionally, interannual variability of total aquatic carbon (POC, DOC, DIC) concentration in a stream draining a peatland was strongly connected to GPP, but the main source of evaded CO_2 (unclear whether from stream or wetland) was suspected to be deep within the soil profile and disconnected from surface processes to some extent. This supports the idea that terrestrially-derived CO_2 in groundwater is a dominant source (other than soil) of total dissolved gas flux from riverine and wetland ecosystems (Olde, 2017). Other studies have aligned with a deep soil source (below 20 cm) of CH_4 as well (Peng et al., 2017). Flow regime and soil water content also has a clear impact on instream and riparian GPP within a forested biome (Dodd, 2018). Stream discharge and WTD should therefore be carefully considered in comparative FCH_4 driver analysis due to their interactions.

Although data were gap-filled, the fraction of missing or low-quality data that was removed was typical of eddy covariance flux data. Gap filling did not appreciably change conclusions. Where results did change as a result of gap-filling, it was the product of unequal sample sizes across years.

2.6.5 Future work

Further research at US-ALQ and US-Los could help pinpoint the magnitude and extent of FCH_4 from wetlands and wetland streams and quantify the variability in wetland FCH_4 in closely located sites due to random effects, such as differing microbial communities and their resulting rates of methanogenesis. Stream discharge and T_{stream} are tied to wetland FCH_4 but have strong spatial variability. Taking more frequent measurements of these variables and sampling

different locations within the wetland and within the water column or peat profile may reveal relationships that were previously masked by spatial or temporal variability.

2.7 Conclusions

Here, we presented FCH_4 and corresponding hydrological measurements from two wetland sites to determine (1) the importance of plant C fixation measured by the lagged effect of GPP on FCH_4 and (2) how factors relating to wetland hydrology (i.e., stream discharge, T_{stream}, and WTD) mediate the GPP-FCH_4 relationship. This study showed that two closely located wetlands can produce vastly different FCH_4 and demonstrate different seasonal cycles of FCH_4 because of different plant and microbial communities and responses, especially during a year with extreme precipitation. During a year with historically high precipitation, there was lower cumulative annual and daily average FCH_4 from the wetlands compared to the following drier year. Both wetlands displayed a longer lagged effect of GPP on FCH_4 during the wet year. US-ALQ demonstrated a decrease in T_{air}-FCH_4 with increasing stream discharge in 2019 and not in 2020, but US-Los exhibited no significant linear trend between WTD and T_{air}-FCH_4 in either year unless a lag was introduced. Lag analysis showed that FCH_4 response to WTD preceded GPP response to WTD at US-Los. A potential explanation is microbial respiration was more reliant on preexisting soil organic matter as a C source earlier in the season but was sourced by recently fixed plant C later in the season.

To answer to the second question of our study, we considered indicators of wetland hydrology and analyzed their relationship with FCH_4. As previously mentioned, there was a shorter lagged response of FCH_4 to WTD than GPP to WTD at US-Los. However, there was no

relationship between FCH_4 and WTD in 2020. The analysis of stream discharge or WTD alone can potentially mask the influence of groundwater flow or precipitation on T_{water} and resulting daily average FCH_4. It was important to consider the influence of T_{stream} during the on-season and off-season separately, and to remove the influence of T_{air} on FCH_4 when looking at the impact of stream discharge. Questions remain on whether larger fluctuations in WTD caused or indicated conditions that could have caused plant or microbial stress and lowered FCH_4 during 2019 at US-Los in comparison to US-ALQ, which emitted more CH_4 and displayed a stronger seasonal cycle. Additional work of linking lags between productivity and FCH_4 along with accounting for temperature and discharge effects will help clarify and constrain the role of wetland biogeochemistry in a changing (e.g., wetter or drier) climate.

2.8 Acknowledgements and Data

We thank our reviewers and Dr. Gavin McNicol for their valuable comments on our manuscript, and Dr. Jaclyn Matthes and Dr. Janne Rinne for providing more information on their related studies. This material is based upon work supported by the National Science Foundation Graduate Research Fellowship Program under Grant No. DGE-1747503. Any opinions, findings, and conclusions or recommendations expressed in this material are those of the author(s) and do not necessarily reflect the views of the National Science Foundation. Any use of trade, firm, or product names is for descriptive purposes only and does not imply endorsement by the U.S. Government. We also acknowledge the North Temperate Lakes LTER program (NSF DEB654 1440297, NTL LTER), United States Geological Survey (Water, Energy, and Biogeochemical Budgets Program; LandCarbon Program; Water Mission Area), and the Department of Energy Ameriflux Network Management Program. Datasets for this research are

available in these in-text data citation references: (Olson, B., 2020; Desai, A. 2020). The authors do not declare any conflicts of interest.

2.9 References

Anderson, M., and Lowry, C. (2007). Transient Functioning of a Groundwater Wetland Complex, 662 Allequash Basin, Wisconsin. PDF File. www.wri.wisc.edu/wp-content/uploads/FinalWR05R007.pdf

Ballantyne, D. M., Hribljan, J. A., Pypker, T. G., & Chimner, R. A. (2014). Long-term water table manipulations alter peatland gaseous carbon fluxes in Northern Michigan. *Wetlands ecology and management*, *22*(1), 35-47.

Bridgham, S. D., Cadillo-Quiroz, H., Keller, J. K., & Zhuang, Q. (2013). Methane emissions from wetlands: biogeochemical, microbial, and modeling perspectives from local to global scales. *Global change biology*, *19*(5), 1325-1346. DOI: 10.1111/gcb.12131

Calabrese, S., Garcia, A., Wilmoth, J. L., Zhang, X., & Porporato, A. (2021). Critical inundation level for methane emissions from wetlands. *Environmental Research Letters*. https://iopscience.iop.org/article/10.1088/1748-9326/abedea/meta

Centeno, C. A. R., Alberto, M. C. R., Wassmann, R., & Sander, B. O. (2017). Assessing diel variation of CH4 flux from rice paddies through temperature patterns. *Atmospheric environment*, *167*, 23-39. https://doi.org/10.1016/j.atmosenv.2017.08.007

Chen, W., Wang, B., Zhang, F., Li, Z., Wang, J., Yu, G., et al. (2020). Hysteretic relationship between plant productivity and methane uptake in an alpine meadow. *Agricultural and Forest Meteorology*, *288*, 107982. https://www.sciencedirect.com/science/article/pii/S0168192320300848

Chu, H., Chen, J., Gottgens, J. F., Ouyang, Z., John, R., Czajkowski, K., & Becker, R. (2014). Net ecosystem methane and carbon dioxide exchanges in a Lake Erie coastal marsh and a nearby cropland. *Journal of Geophysical Research: Biogeosciences*, *119*(5), 722-740. https://doi.org/10.1002/2013JG002520

Cook, B. D., Davis, K. J., Wang, W., Desai, A., Berger, B. W., Teclaw, R. M., ... & Heilman, W. (2004). Carbon exchange and venting anomalies in an upland deciduous forest in northern Wisconsin, USA. *Agricultural and Forest Meteorology*, *126*(3-4), 271-295. https://doi.org/10.1016/j.agrformet.2004.06.008

Dannenberg, S., & Conrad, R. (1999). Effect of rice plants on methane production and rhizospheric metabolism in paddy soil. *Biogeochemistry*, *45*(1), 53-71. https://link.springer.com/article/10.1007/BF00992873

Davidson, S. J., Sloan, V. L., Phoenix, G. K., Wagner, R., Fisher, J. P., Oechel, W. C., & Zona, D. (2016). Vegetation type dominates the spatial variability in CH 4 emissions across multiple arctic tundra landscapes. *Ecosystems*, *19*(6), 1116-1132. https://link.springer.com/article/10.1007/s10021-016-9991-0

Delwiche, K. B., Knox, S. H., Malhotra, A., Fluet-Chouinard, E., McNicol, G., Feron, S., ... & Jackson, R. B. (2021). FLUXNET-CH4: A global, multi-ecosystem dataset and analysis of methane seasonality from

freshwater wetlands. *Earth System Science Data Discussions*, 1-111. https://doi.org/10.5194/essd-2020-307

Desai, A. R., Xu, K., Tian, H., Weishampel, P., Thom, J., Baumann, D., ... & Kolka, R. (2015). Landscape-level terrestrial methane flux observed from a very tall tower. *Agricultural and Forest Meteorology*, *201*, 61-75. https://doi.org/10.1016/j.agrformet.2014.10.017

Desai, A.R. (2001-). AmeriFlux US-Los Lost Creek, Dataset. https://doi.org/10.17190/AMF/1246071

Desai, A., Noormets, A., Bolstad, P., Chen, J., Cook, B., Curtis, P., Davis, K., Euskirchen, E., Gough, C., Martin, J., Ricciuto, D., Schmid, H., Su, H-B., Tang, J., Vogel, C., and Wang, W. (2007). Influence of vegetation type, stand age and climate on carbon dioxide fluxes across the Upper Midwest, USA: implications for regional scaling of carbon flux. https://www.researchgate.net/publication/228990606_Influence_of_vegetation_type_stand_age_and_climate_on_carbon_dioxide_fluxes_across_the_Upper_Midwest_USA_implications_for_regional_scaling_of_carbon_flux

Ding, W., Cai, Z., & Tsuruta, H. (2005). Plant species effects on methane emissions from freshwater marshes. *Atmospheric Environment*, *39*(18), 3199-3207. https://doi.org/10.1016/j.atmosenv.2005.02.022

Dinsmore, K.J., Billett, M.F. and Dyson, K.E. (2013). Temperature and precipitation drive temporal variability in aquatic carbon and GHG concentrations and fluxes in a peatland catchment. *Glob Change Biol,* 19: 2133-2148. https://doi.org/10.1111/gcb.12209

Dodd, A. (2018). Flow Regime Influences on Stream and Riparian Soil Carbon Dynamics in the Ozark Highlands and Boston Mountains of Arkansas. https://scholarworks.uark.edu/cgi/viewcontent.cgi?article=4460&context=etd

Dorodnikov, M., Knorr, K. H., Kuzyakov, Y., & Wilmking, M. (2011). Plant-mediated CH 4 transport and contribution of photosynthates to methanogenesis at a boreal mire: a 14 C pulse-labeling study. *Biogeosciences*, *8*(8), 2365-2375. https://doi.org/10.5194/bg-8-2365-2011

Gomez-Casanovas, N., DeLucia, N. J., DeLucia, E. H., Blanc-Betes, E., Boughton, E. H., Sparks, J., & Bernacchi, C. J. (2020). Seasonal controls of CO2 and CH4 dynamics in a temporarily flooded subtropical wetland. *Journal of Geophysical Research: Biogeosciences*, *125*(3), e2019JG005257. https://doi.org/10.1029/2019JG005257

Hatala, J. A., Detto, M., & Baldocchi, D. D. (2012). Gross ecosystem photosynthesis causes a diurnal pattern in methane emission from rice. *Geophysical Research Letters*, *39*(6). https://doi.org/10.1029/2012GL051303

Henneberg, A., Sorrell, B. K., & Brix, H. (2012). Internal methane transport through J uncus effusus: experimental manipulation of morphological barriers to test above-and below-ground diffusion limitation. *New Phytologist*, *196*(3), 799-806. https://doi.org/10.1111/j.1469-8137.2012.04303.x

Kim, Y., Johnson, M. S., Knox, S. H., Black, T. A., Dalmagro, H. J., Kang, M., ... & Baldocchi, D. (2020). Gap-filling approaches for eddy covariance methane fluxes: A comparison of three machine learning algorithms and a traditional method with principal component analysis. *Global Change Biology*, *26*(3), 1499-1518. https://doi.org/10.1111/gcb.14845

Kim, Y. (2020). Repository EC_FCH4_gapfilling, script rf_run_for_public. https://github.com/yeonukkim/EC_FCH4_gapfilling/blob/master/rf_run_for_public.R

Knox, S.H., Jackson, R.B., Poulter, B., McNicol, G. Fluet-Chouinard, E., Zhang, Z., Hugelius, G., et al. (2019). "FLUXNET-CH4 Synthesis Activity: Objectives, Observations, and Future Directions." *Bulletin of the American Meteorological Society* 100 (12): 2607–32. https://doi.org/10.1175/BAMS-D-18-0268.1

Knox, S. H., Bansal, S., McNicol, G., Schafer, K., Sturtevant, C., Ueyama, M., ... & Jackson, R. B. (2021). Identifying dominant environmental predictors of freshwater wetland methane fluxes across diurnal to seasonal time scales. *Global change biology*.

Kuzyakov, Y., & Gavrichkova, O. (2010). Time lag between photosynthesis and carbon dioxide efflux from soil: a review of mechanisms and controls. *Global Change Biology*, *16*(12), 3386-3406. https://doi.org/10.1111/j.1365-2486.2010.02179.x

Liaw, A., & Wiener, M. (2002). Classification and regression by randomForest. *R News*, **2**(3), 18– 22. https://www.researchgate.net/publication/228451484_Classification_and_Regression_by_RandomForest

Mitra, B., Minick, K., Miao, G., Domec, J. C., Prajapati, P., McNulty, S. G., ... & Noormets, A. (2020). Spectral evidence for substrate availability rather than environmental control of methane emissions from a coastal forested wetland. *Agricultural and Forest Meteorology*, *291*, 108062. https://doi.org/10.1016/j.agrformet.2020.108062

Musarika, S., Atherton, C. E., Gomersall, T., Wells, M. J., Kaduk, J., Cumming, A. M. J., ... & Zona, D. (2017). Effect of water table management and elevated CO2 on radish productivity and on CH4 and CO2 fluxes from peatlands converted to agriculture. *Science of the Total Environment*, *584*, 665-672. https://doi.org/10.1016/j.scitotenv.2017.01.094

Nicolini, G., Castaldi, S., Fratini, G., & Valentini, R. (2013). A literature overview of micrometeorological CH4 and N2O flux measurements in terrestrial ecosystems. *Atmospheric Environment*, *81*, 311-319. https://doi.org/10.1016/j.atmosenv.2013.09.030

Nouchi, I., Mariko, S., & Aoki, K. (1990). Mechanism of Methane Transport from the Rhizosphere to the Atmosphere through Rice Plants. *Plant physiology*, *94*(1), 59–66. https://doi.org/10.1104/pp.94.1.59

Oikawa, P. Y., Jenerette, G. D., Knox, S. H., Sturtevant, C., Verfaillie, J., Dronova, I., ... & Baldocchi, D. D. (2017). Evaluation of a hierarchy of models reveals importance of substrate limitation for predicting carbon dioxide and methane exchange in restored wetlands. *Journal of Geophysical Research: Biogeosciences*, *122*(1), 145-167. https://doi.org/10.1002/2016JG003438

Olde, L. (2017). *How Do Rates of Carbon Metabolism Vary over a Geological Gradient, and How does this Contribute to Riverine Greenhouse Gas Emissions?* (Doctoral dissertation, Queen Mary University of London). https://qmro.qmul.ac.uk/xmlui/bitstream/handle/123456789/25933/Olde_L_PhD_Final_310717.pdf?sequence=1&isAllowed=y

Olefeldt, D., Euskirchen, E. S., Harden, J., Kane, E., McGuire, A. D., Waldrop, M. P., & Turetsky, M. R. (2017). A decade of boreal rich fen greenhouse gas fluxes in response to natural and experimental water table variability. *Global change biology*, *23*(6), 2428-2440. https://doi.org/10.1111/gcb.13612

Olson, B. (2015-). AmeriFlux US-ALQ Allequash Creek Site, Dataset. https://doi.org/10.17190/AMF/1480323

Peng, H., Guo, Q., Hong, B., Ding, H., Xu, C., & Yao, H. (2017). Seasonal and diurnal methane emissions from a wetland meadow on the Eastern Qinghai-Tibetan Plateau: effects of soil temperature, water table level and gross primary productivity (GPP). In *EGU General Assembly Conference Abstracts* (p. 8004). https://ui.adsabs.harvard.edu/abs/2017EGUGA..19.8004P/abstract

Pint, C. D., Hunt, R. J., & Anderson, M. P. (2003). Flowpath delineation and ground water age, Allequash Basin, Wisconsin. *Groundwater*, *41*(7), 895-902. https://doi.org/10.1111/j.1745-6584.2003.tb02432.x

Pugh, C. A., Reed, D. E., Desai, A. R., & Sulman, B. N. (2018). Wetland flux controls: how does interacting water table levels and temperature influence carbon dioxide and methane fluxes in northern Wisconsin? *Biogeochemistry*, *137*(1), 15-25. https://link.springer.com/article/10.1007/s10533-017-0414-x

Radu, D. D., & Duval, T. P. (2018). Impact of rainfall regime on methane flux from a cool temperate fen depends on vegetation cover. *Ecological Engineering*, *114*, 76-87. https://doi.org/10.1016/j.ecoleng.2017.06.047

Rey-Sanchez, A. C., Morin, T. H., Stefanik, K. C., Wrighton, K., & Bohrer, G. (2018). Determining total emissions and environmental drivers of methane flux in a Lake Erie estuarine marsh. *Ecological Engineering*, *114*, 7-15. https://doi.org/10.1016/j.ecoleng.2017.06.042

Rhinelander Weather Records. (2021). Retrieved from https://www.weather.gov/media/grb/climate/books/Rhinelander%20Record%20Books2.pdf

Rietl, A. J., Nyman, J. A., Lindau, C. W., & Jackson, C. R. (2017). Wetland methane emissions altered by vegetation disturbance: An interaction between stem clipping and nutrient enrichment. *Aquatic Botany*, *136*, 205-211. https://doi.org/10.1016/j.aquabot.2016.10.008

Rinne, J., Tuittila, E.-S., Peltola, O., Li, X., Raivonen, M., Alekseychik, P., et al. (2018). Temporal variation of ecosystem scale methane emission from a boreal fen in relation to temperature, water table position, and carbon dioxide fluxes. *Global Biogeochemical Cycles*, 32, 1087– 1106. https://doi.org/10.1029/2017GB005747

Sulman, B.N., Desai, A., Cook, B.D., Saliendra, N.Z., and Mackay, D.S. (2009). Contrasting carbon 820 dioxide fluxes between a drying shrub wetland in northern Wisconsin, USA, and nearby forests. 821 *Biogeosciences*. 6, 1115–1126. doi:10.5194/bg-6-1115-2009

Turner, J., Desai, A. R., Thom, J., Wickland, K. P., & Olson, B. (2019). Wind sheltering impacts on land-atmosphere fluxes over fens. *Frontiers in Environmental Science*, *7*, 179. https://doi.org/10.3389/fenvs.2019.00179

turner-j. (2021). turner-j/Methane-Flux-Plots: Methane Flux Lag Response Analysis (Version v0.1). Zenodo. http://doi.org/10.5281/zenodo.4617037

United States Geological Survey (USGS). (2020a). National Water Information System, “USGS 05357205 ALLEQUASH CREEK NEAR SAYNER, WI" [Data file]. Retrieved from https://maps.waterdata.usgs.gov/mapper

Updegraff, K., Bridgham, S.D., Pastor, J., Weishampel, P., Harth, C. (2001). Response of CO_2 and CH_4 emissions in peatlands to warming and water-table manipulation. *Ecological Applications*, **11**, 311– 326. https://doi.org/10.1890/1051-0761(2001)011[0311:ROCACE]2.0.CO;2

Villa, J. A., Ju, Y., Vines, C., Rey-Sanchez, C., Morin, T. H., Wrighton, K. C., & Bohrer, G. (2019). Relationships between methane and carbon dioxide fluxes in a temperate cattail-dominated freshwater wetland. *Journal of Geophysical Research: Biogeosciences*, *124*(7), 2076-2089. https://doi.org/10.1029/2019JG005167

Wei, G. W., Chen, Y., Sun, X. S., Chen, Y. H., Luo, F. L., & Yu, F. H. (2019). Growth responses of eight wetland species to water level fluctuation with different ranges and frequencies. *PloS one*, *14*(7), e0220231. https://doi.org/10.1371/journal.pone.0220231

Welsch, M. and Yavitt, J.B. (2007), Microbial CO_2 production, CH_4 dynamics and nitrogen in a wetland soil (New York State, USA) associated with three plant species (*Typha*, *Lythrum*, *Phalaris*). European Journal of Soil Science, 58: 1493-1505. https://doi.org/10.1111/j.1365-2389.2007.00955.x

Zacks, G., Greet, J., Walsh, C. J., & Raulings, E. (2019). The flooding tolerance of two critical habitat-forming wetland shrubs, Leptospermum lanigerum and Melaleuca squarrosa, at different life history stages. *Australian Journal of Botany*, *66*(7), 500-510. https://doi.org/10.1071/BT18039

Zhang, Z., Zimmermann, N.E., Stenke, A., Li, X., Hodson, E.L., Zhu, G., Huang, C., and Poulter, B. (2017). Emerging role of wetland methane emissions in driving 21st century climate change. *Proceedings of the National Academy of Sciences.* 201618765; DOI:10.1073/pnas.1618765114

3 Tidal influence on dissolved CO_2 at Sapelo Island, Georgia, USA

This chapter has been previously published as Turner, J., Desai, A. R., Blackstock, J. M., & Smith, D. (2022). Tidal influence on dissolved CO2 at Sapelo Island, Georgia, USA. *Environmental Research: Ecology*, *2*(1), 015002.

3.1 Abstract

Measuring carbon (C) loss through different pathways is essential for understanding the net ecosystem exchange of carbon dioxide (CO_2) in tidal wetlands, especially in a reality where wetland mitigation and protecting coastlines from rapid sea-level rise is a growing priority. Tracking C loss can help reveal where an ecosystem is storing the most C, but it can also help scientists understand near- and long-term impacts of wetland restoration on climate. A recently developed dissolved CO_2 (P_{CO2}) platform was tested in a subtropical salt marsh with an apparatus that raised and lowered sensor housing with the tide. Additional low-cost water quality sensors were installed nearby for measuring turbidity and salinity. Here, we evaluated how well this floating sensor platform along with twenty-eight days of biogeochemical data from a tidal salt marsh could detect C import and export from tidal effects. This work provides a pathway to low-cost, routine in-situ C exchange measurements which serve the needs of environmental managers, researchers, and others interested in better estimating wetland C storage and transport.

3.2 Introduction

Nearly three quarters of all inorganic and organic C sequestrated and exported from terrestrial inland waterways and wetlands is evaded to the atmosphere as CO_2 before the time it reaches the ocean (Ward et al., 2017). For much of this C transport, mangroves and tidal marshes represent the last stop on this journey for potential organic C sequestration while also being the first natural defense against sea level rise due to soil accretion, soil expansion, and the presence of coastal vegetation (Mudd et al., 2010; Macreadie et al., 2019). Tidal wetland C gains are expected in future climate scenarios in the US, Australia, Brazil, and China, while losses are expected in Indonesia and Mexico due to changes in wetland area (Wang et al., 2021). Coastal ecosystems play an important role in the C cycle despite their small surface area, transforming and storing significant amounts of C in marine sediment (Kirwan & Megonigal, 2013). However, environmental and human-caused stressors are projected to cause disappearance of these ecosystems and jeopardize their role as C sinks in the global C cycle (Lovelock & Reef, 2020).

In coastal ecosystems, the routine action of the tide plays a role in nearly every aspect of biogeochemistry and biogeochemical cycles (Tobias & Neubauer, 2019). One useful integrated indicator of coastal marsh biogeochemistry is P_{CO2}. Tides bring in cold water from the ocean, which increases the solubility of CO_2 and has a general positive influence on P_{CO2} concentration. Tidal inundation can temporarily lower productivity in salt marsh vegetation (Sutter et al., 2014; Mendelssohn & Morris, 2000) and increase CO_2 production by increasing organic C mineralization (Chambers, Reddy, and Osborne, 2011). Although a positive relationship between P_{CO2} and tide height has been noted in some coastal ecosystems (Mayen,

2020), the inverse relationship has also been noted (Dai et al., 2009). Turbidity caused by an abundance of inorganic particulate material may increase the partial pressure of dissolved CO_2 (P_{CO2}) by restricting light attenuation and therefore photosynthesis (Chanda et al., 2020; Kuwae et al., 2018). In Trifunovic et al. (2020), turbidity had a strong correlation with modeled CO_2 and CH_4 emissions from a salt marsh tidal creek when plants reached maturity, which authors suspected was due to the linkage between turbidity and pulses in water level rise. Tide velocity and turbulence were also more important in regulating diel creek CO_2 efflux than variability in water temperature.

Salinity can lower P_{CO2} due to a reduction in CO_2 solubility (Weiss et al., 1982) or by increasing gross primary productivity and resulting aquatic CO_2 consumption during dry season (Liu and Lai, 2019). However, in freshwater wetlands and during wet season in subtropical mangroves, gross primary productivity has been demonstrated to decrease with salinization, thereby increasing P_{CO2} (Liu and Lai, 2019; Chamberlain et al., 2020). Gross primary productivity may also regulate short-term soil CO_2 respiration in coastal wetlands (Han et al., 2014), which would lead to increased P_{CO2}. Salinity alone is not a good predictor of C within tidal marsh soils or biomass (Kolka et al., 2021).

High frequency P_{CO2} observations may hold more clues about coastal wetland biogeochemistry and implications for environmental management and climate modeling. Limiting factors from earlier studies are sample size and frequency of C cycle observations for reliable extrapolation and generalization of process understanding. Spatially and temporally frequent measurements of C on the coasts are needed to better understand the global C cycle, design relevant climate policies, and predict the impacts of climate change (Friedlingstein et al.,

2020). Measurements of P_{CO2} can be made using non-dispersive infrared gas analyzers (NDIR), electrodes, fluorescence, or spectrophotometry, and are often accompanied by measurements of water flow, atmospheric CO_2 concentration, water temperature, and salinity. P_{CO2} can be used to estimate C lost by wind-driven evasion at the water surface, or tidal CO_2 export (Raymond et al., 2000). Many P_{CO2} datasets are typically limited in terms of being either low-frequency, or high-frequency and using cost-prohibitive equipment that require expert users for analysis and maintenance. Affordable yet frequent direct observations of P_{CO2} in coastal ecosystems combined with other measurements such as eddy covariance flux, soil accretion, or lateral flow would improve estimates of whole-ecosystem gas fluxes (Song et al., 2020).

Previous studies on biogeochemistry at Sapelo Island, Georgia, USA have deployed different methods of measuring P_{CO2}. One study calculated P_{CO2} from temperature, salinity, dissolved inorganic carbon (DIC), and pH using carbonate equilibrium constants (Wang & Cai, 2004). Estimating P_{CO2} this way can lead to large error for systems other than oceans (Golub et al., 2017). Another study continuously measured P_{CO2} with a differential NDIR gas analyzer during a series of cruises around the island (Jiang et al., 2008). Seasonal metabolic cycles have previously been found to dominate P_{CO2} variability in Sapelo Sound at the northern tip of the island, with the lowest concentrations occurring in winter. Jiang et al. (2008) and Wang & Cai (2004) sampled Barn Creek and Doboy Sound, which are rivers surrounding the island, rather than in the marsh. In those studies, surface water P_{CO2} was lowest near the ocean, with increasing values towards the innermost areas of the estuaries. Higher CO_2 degassing, estimated from P_{CO2}, was observed at the river-dominated estuary in comparison to the marine-dominated estuary. Both studies highlighted the salt marshes of Sapelo Island as

significant sources of dissolved organic and inorganic carbon (Wang & Cai, 2004; Jiang et al., 2008). There was also a clear seasonal progression of P_{CO2} and total dissolved inorganic C.

Tidal direction can also play a role in coastal wetland biogeochemistry. Numerous studies have observed higher P_{CO2} concentrations during low tide (ebb) and lower P_{CO2} concentrations during high tide (flood) at a variety of coastal locations (Jiang et al., 2008; Zablocki et al., 2011; Taillardat et al., 2018; Trifunovic et al., 2020). At Sapelo Island, ebb velocities are higher than flood velocities, and have been estimated along the Duplin River using an unmanned aerial vehicle and fluorescent dye tracing (Pinton et al., 2020). Ebb velocity was greater than flood velocity by approximately 0.25 $m \cdot s^{-1}$, or 27%, during spring tide, a period which features the greatest ranges in tide heights. This feature is known as flood-ebb tidal asymmetry and can be partially caused by nonlinear tidal interactions in shallow water and is common in marsh creeks (Fagherazzi et al., 2013; Zhang et al., 2018).

We seek to evaluate how well the CO2-LAMP, a low-cost alternative P_{CO2} platform, can easily be implemented in coastal and other wetlands with frequently changing water levels. We hypothesize that (1) CO2-LAMP P_{CO2} measurements will confirm previous studies at this site showing marsh surface water is a lateral C source and (2) P_{CO2} measurements will reflect mechanisms noted in the literature and discussed above, including positive correlations with turbidity and salinity, and a weak inverse correlation with water temperature. We expect water flowing out of the marsh (ebb tide) will feature higher P_{CO2} concentrations than incoming water (flood tide), resulting in net C export in agreeance with previous research findings at this site and others (Wang & Cai, 2004; Jiang, Cai, and Wang, 2008; Call et al., 2019). Moon phase and

tide height will likely be the strongest drivers of P_{CO2} compared to other factors, such as turbidity and salinity.

Direct measurements of P_{CO2} in the marsh, presented here, are incredibly important for measuring P_{CO2} spatial variability, providing insights into C dynamics and potential mechanisms, and supporting prior studies on the marsh as an important C source. This study fills this knowledge gap with the use of a low-cost sensor platform. Measurements from the marsh may potentially influence what drives P_{CO2} of connected water bodies, thus informing previous measurements outside of the marsh. Being able to observe and evaluate these hypotheses will also allow us to evaluate the reliability of further deployment of this and similar low-cost P_{CO2} measurement platforms in more locations for longer periods to uphold tidal wetland and blue carbon mitigation initiatives (Lovelock & Reef, 2020).

3.3 Data and methodology

3.3.1 Study site

The study took place July 21st-August 17th in a Sapelo Island marsh located at 31.44 lat, -81.28 long. Sapelo Island (31.48 lat, 81.24 long) is a long-term ecological research site and barrier island off the coast of Georgia, USA, in the humid subtropical climate (Fig 3.1). There is a history of interdisciplinary scientific collaboration between researchers at Sapelo Island, Georgia and University of Wisconsin-Madison on biogeochemistry studies dating back more than fifty years (Ragotzkie & Bryson, 1955; Jones, 1980). Research on marine and estuarine ecosystems at Sapelo Island by students at UW-Madison continues as part of a fall course offered by the Department of Integrative Biology (Kara & Shade, 2009). Salt marsh is a common habitat around the island, but this study specifically focused on the location denoted by the blue star on the map below (Fig

3.1). Vegetation in the marsh is predominantly *Spartina alterniflora* and can reach as high as 2 meters (Pinton et al., 2020). *Salicornia virginica*, *Batis maritima*, and *Juncus roemarianus* can be found in smaller numbers where elevation and salinity are adequate (Sanders, 2019).

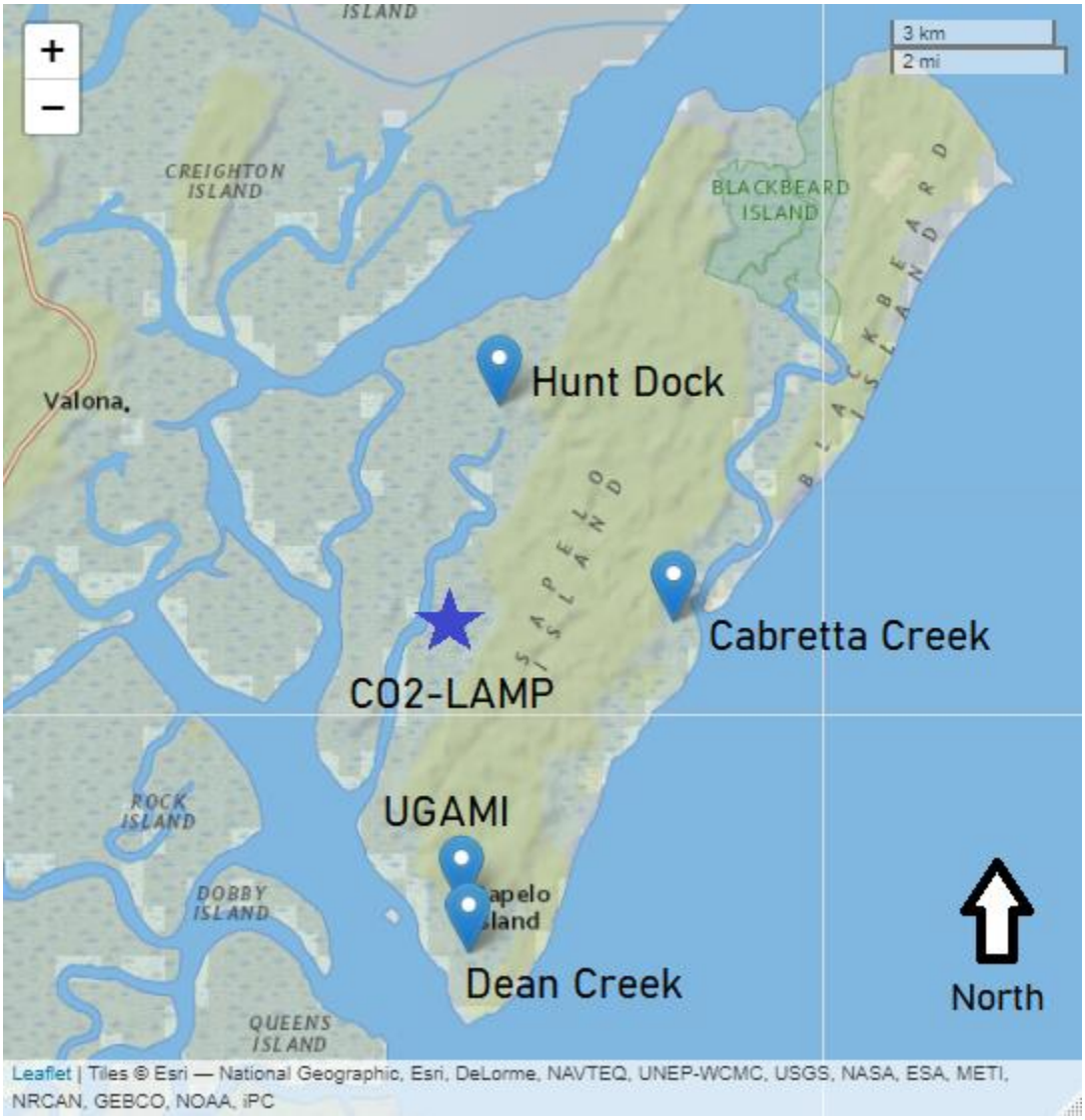

Figure 3.1. Map of instrument locations on Sapelo Island, created using "leaflet" package in R (Chang et al., 2022). Background from Esri. UGAMI stands for University of Georgia Marine Institute. The star denotes the floating pCO_2 sensor platform. Sapelo Island is located at 31.48 lat, 81.24 long.

3.3.2 Tide data

Sapelo Island hydrography is characterized by a strong tide (Ragotzkie & Reid, 1955), which varied as much as 3.23 meters during the study period at Hunt Dock. Tide height, water temperature, salinity, and turbidity were recorded by NOAA tide gages in 15-minute intervals at three different locations: Hunt Dock, Cabretta Creek, and Dean Creek (Fig 3.1; NOAA Tides & Currents, 2021; NOAA NERRS, 2022). 15-minute tide height, water temperature, salinity, and turbidity, and 1-hour moon phase data were linearly interpolated to match exactly the P_{CO2} timestamps for the purpose of statistical testing. After interpolation, all data had a resolution of approximately 1 hr. Tides lasted an average of 12 hours, 25 minutes, and 15 seconds from high tide to high tide during the study period. Water temperature ranged from 27.2 to 33.4°C at Hunt Dock during the study period. Geocentric moon phase data at hourly intervals in 2021 was retrieved from NASA Scientific Visualization Studio (Wright, n.d.).

3.3.3 Flux data

Atmospheric CO_2 concentration (ppm) was from the Georgia Coastal Ecosystems LTER Flux Tower (US-GCE) at 31.44 lat, -81.28 long. US-GCE is owned and maintained by the University of Georgia Marine Institute (UGAMI), located 5.5 km from US-GCE, at 31.40 lat, -81.28 long. It is a 10 m tall triangle tower installed on an elevated dock platform. CO_2 is measured by an enclosed CO_2 gas analyzer (CSAT LI7200) at 10 Hz frequency, then averaged to produce half-hourly data (Feagin et al., 2020). Half-hourly data was used in this study due to less noise, then was linearly interpolated to exactly match P_{CO2} timestamps. The tower is accessed from UGAMI by car, boat, and then walk through the marsh.

3.3.4 Smart Rock

The Smart Rock is a low-cost submersible sensor developed by the OPEnS Lab (Openly Published Environmental Sensing Lab) and provided by the Consortium of Universities for the Advancement of Hydrologic Sciences, Inc. (~$200). It measures turbidity and salinity but can also measure water level and temperature when in calibration mode (Veach, 2019). Salinity was measured using the Gravity: Analog Total Dissolved Solids Sensor/Meter for Arduino manufactured by DF Robot, with a measurement range 0-1,000 ppm (~0-2,000 uS/cm) and accuracy within 10%. Turbidity was measured using the Gravity: Analog Turbidity Sensor for Arduino, also manufactured by DF Robot, with a measurement range of 0-4.5 V and accuracy within 0.3 V. Turbidity and salinity were recorded by the Smart Rock once every 20 minutes. Turbidity and salinity from both the Smart Rock and NOAA tide gage are presented in the results. However, only measurements from NOAA tide gages were used for analysis.

3.3.5 CO2-LAMP

The CO2-LAMP was deployed at the base of US-GCE. The CO2-LAMP measured P_{CO2} in both water and air in the tidal marsh. A waterproofed NDIR CO_2 gas analyzer was used to measure P_{CO2}. Data were logged using a low-cost Arduino monitoring platform (CO2-LAMP) recently developed by Blackstock et al. (2019). In this platform, passive equilibration of dissolved CO_2 in the water exchanges with a "headspace" volume containing the CO_2 gas analyzer enclosed by an expanded PTFE semi-permeable membrane. As previously reported by Johnson et al. (2010), diffusion of CO_2 in water primarily limits time needed for equilibration, but where runoff rapidly introduces water of dissimilar P_{CO2} values, passive equilibrators may not fully capture peak P_{CO2} values in some cases (Yoon et al., 2016).

The NDIR gas analyzer used was a K30 10% manufactured by Senseair AB (Delbo, Sweden). The K30 10 % manufacturer reported accuracy is ±300 ppm with a resolution of 10 ppm CO_2 and capability of measuring up to 100,000 ppm. Prior to deployment, reference measurements were made using 0 ppm CO_2 (99% N_2, O_2-balance) and 2000 ±40 ppm CO_2 (N_2 balance) reference gases. After deployment, reference measurements were remade using a 0 ppm CO_2 (N_2) and 550 ±2 ppm CO_2. During reference measurements, the reference gas exchanges across the semi-permeable ePTFE surface and is measured by the K30 until equilibration is reached. Pre-deployment 0 ppm CO_2 reference gas measurements were measured as 0 ppm CO_2 by the K30, and the 2000 ppm CO_2 reference measurements were measured as 1980 ppm CO_2, which were within K30 analytical and reference gas concentration uncertainty. Post-deployment 0 ppm CO_2 reference gas measurements were measured as 0 ppm CO_2 by the K30, and the 550 ppm CO_2 reference measurements were measured as 530 ppm CO_2, indicating a consistent, slight underestimation (20 ppm) of gas concentrations and negligible drift relative to the range of the gas analyzer and previous ranges observed in surface waters at Sapelo Island (Wang and Cai, 2004).

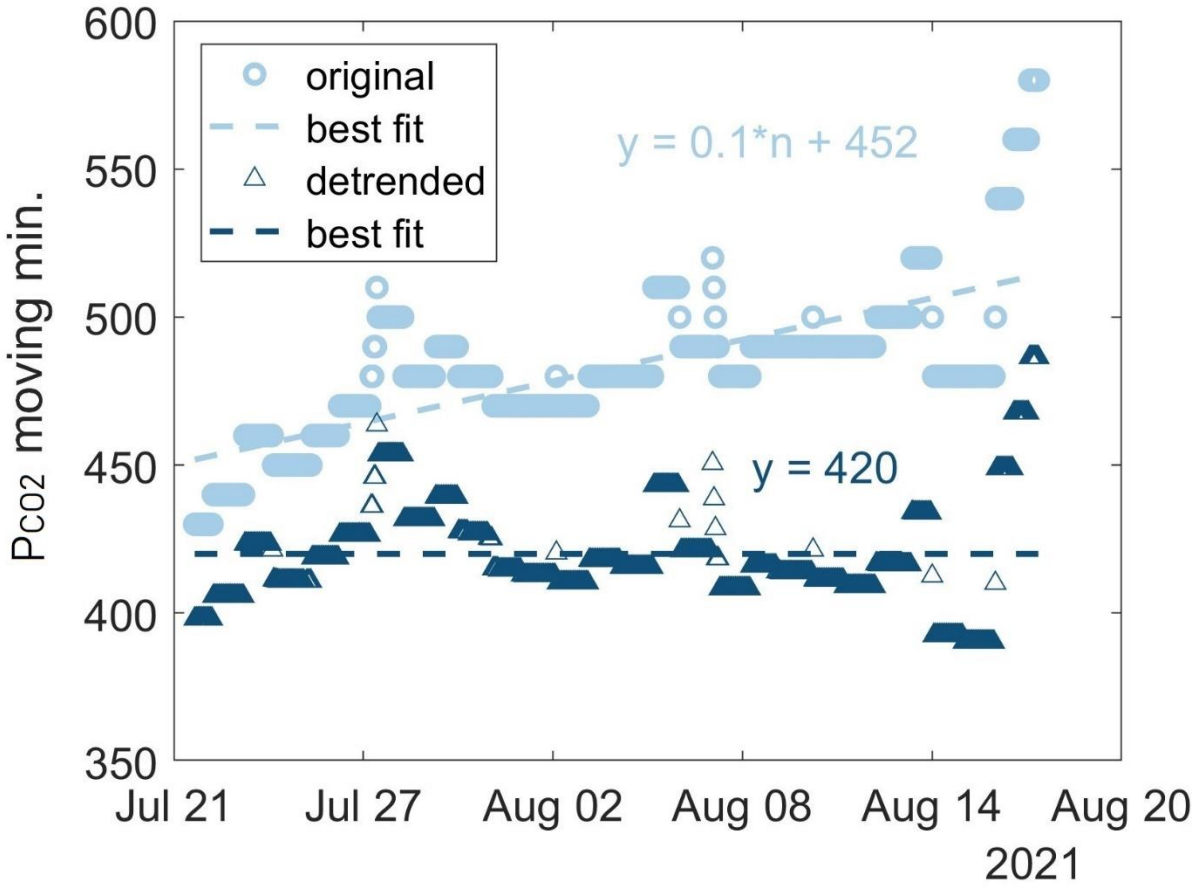

Figure 3.2. Original and detrended daily moving minimum P_{CO2} with respective linear best fit lines and their equations. The number of the observation is represented by n.

CO2-LAMP data were recorded every 10 seconds for 20 minutes, followed by 45 minutes of sleep. All measurements except the last measurement from each measurement cycle were removed during post-processing, resulting in approximately 22 datapoints per day with a resolution of 1.09 hrs each and 589 datapoints overall. Due to the unique CO2-LAMP measurement frequency, 15-minute tide data, 30-minute flux data, and hourly moon phase included in our analysis were interpolated to match the temporal resolution of P_{CO2}. Values of P_{CO2} less than or equal to 0 ppm occurred infrequently during measurement cycles but were marked as non-physical values and replaced with the value of the previous measurement.

Multiple sensors are preferred to compare P_{CO2} data, check for drift, and determine the degree of spatial variability. However, power limitations restricted simultaneous deployment of multiple CO2-LAMPs.

Another issue which impacted data collection was biological fouling, which is common when monitoring in coastal or other aquatic ecosystems. Minimum daily P_{CO2} measurements determined by the 22-point moving minimum linearly increased throughout the study, likely due to accumulation of biofilms and algae over the CO2-LAMP semi-permeable membrane (Fig 3.2). Original data were detrended by fitting the daily moving minimum P_{CO2} to a simple linear regression. Fitted data was then subtracted from the original data, and atmospheric background CO_2 of 420 ppm was added back in.

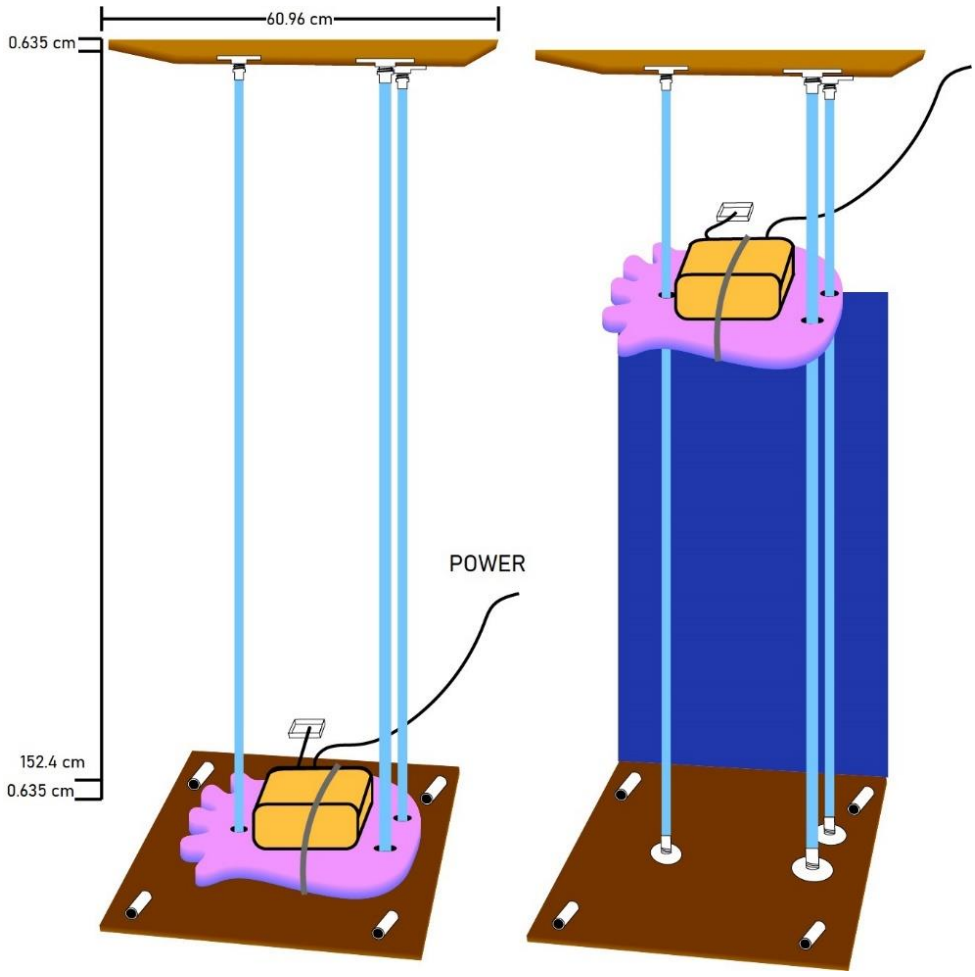

Figure 3.3. Schematic of CO2-LAMP tide-varying station, with height, width, and thickness dimensions. Blue lines represent hollow copper pipes held in place by metal flanges and adapters on the wooden top and baseboards. The black power line connects to a solar power array. The yellow waterproof sensor housing case is zip-tied onto the pink flotation device. (A) The sensor platform sits near the marsh surface at low tide, while the K30 sensor (white square) measures P_{CO2} in air. (B) The sensor platform floats upwards with the change in water level at high tide, measuring P_{CO2} just below the water surface. The dark blue square represents marsh surface water.

The CO2-LAMP was attached to a foam board capable of varying with tide height. This deployment was based on a similar, unpublished design by Thomas L. O'Halloran at Clemson University (personal communication). The CO2-LAMP protective housing was attached to a foam swimming board'' using marine epoxy and an extra-large zip tie to keep it elevated at the water surface with the waterproofed gas analyzer submerged below the water surface (Fig 3.3). Because P_{CO2} concentrations at the air-water interface are most important to wind-driven gas exchange (Wanninkhof, 2014), and P_{CO2} can vary within the water column (Beaubien et al., 2014), consistent depth of measurement near the water surface is important. The bottom baseboard was held down with four t-shaped PVC pipes with holes drilled into the piping for drainage, which prevented the pipes from moving upwards over time. The top baseboard, sized 60.96 x 60.96 x 0.635 cm, was secured to the flux tower with zip ties threaded through holes in the wood and decking. Metal flanges with male adapter fittings were screwed into the top and bottom boards with wood screws. Three hollow five-foot copper pipes were then easily placed inside the adapter fittings on both ends and pressed or hammered down, with no further seal necessary. Only metal flanges and adapters can be used because the allowances fit with copper piping. Plastic pipe fittings did not fit with the metal pipes or flanges, though transition adapters could work in the future.

Lateral C export is referred to as a "potential" throughout this study because it is solely based on contributions from P_{CO2} and does not account for the import or export of other forms of C. Tide velocity was calculated as change in tide height divided by change in time between P_{CO2} measurements. Atmospheric CO_2 (ppm) measured at the flux tower was subtracted from P_{CO2} prior to the potential tidal C export estimation (Table 3.1) and linear regression (Fig 3.5) to

eliminate any measurements potentially taken in air. Any measurements below 0 after this correction were set to zero. Lateral import was assumed to occur when tide was increasing, and export when tide was decreasing. Cumulative imported and exported C were calculated for each tide cycle. Cumulative tidal imports were subtracted from cumulative tidal exports to achieve net export (gC $m^{-2}s^{-1}$). Net export was then multiplied by the length of each tidal cycle in seconds and averaged to find the potential average C export per tidal cycle. Net export in seconds was also summed across the duration of the study to find potential total C export for the entire study. The equation used for calculations is below.

Equation 3.1: $$C\ import\ or\ export\ \left(\frac{gC}{m^2 s}\right) = \frac{PCO_2(ppm) \cdot tide\ velocity\left(\frac{m}{s}\right) \cdot \rho_{air}\left(\frac{g}{m^3}\right) \cdot 12\frac{g}{mol\ C}}{28.97\frac{g}{mol\ air} \cdot 10^6}$$

ρ_{air} was assumed to be 1225 g m^{-3}. 10^6 is the conversion factor for P_{CO2} (ppm).

3.3.6 Hypothesis testing

Vector autoregression and Granger causality were the selected methods for hypothesis testing. These methods work together and are ideal for complex datasets with multiple predictors. Vector autoregressive models are stationary, multivariate time series models which can be used to describe random stochastic processes with limited prior knowledge of the forces influencing each variable. One equation is created for each dependent variable using a linear function of the lagged dependent variable and other information. Akaike Information Criterion (AIC) of each model is calculated from the number of predictor variables and model performance. The best-fit model according to the AIC is then used in the Granger causality test.

The Granger causality test works well to examine underlying relationships in a dataset which the vector autoregression cannot. Granger causality originated in econometrics, but has

since been adopted by many other fields, including the geosciences (Granger, 1969; Detto et al., 2012; Desai, 2014). Granger causality should only be computed on stationary, modeled data rather than original or nonstationary data, and cannot be computed for singular matrices made of multiple, strongly interdependent variables. This model-test combination is a computationally simple way of assessing temporal relationships between variables. Some disadvantages of Granger causality testing are that results may be skewed by infrequent sampling, too-frequent sampling, nonlinear causal relationships, and more. Interpretations of Granger causality testing should align with the physical dynamics of a system, and not be used as stand-alone statistical results due to these limitations.

Hourly moon phase and 15-minute tide height, salinity, turbidity, and water temperature were linearly interpolated to match P_{CO2} measurement times, which had a resolution of 1.09 hours, for statistical testing. Moon phase was eliminated from statistical testing because it created a singular matrix due to its close relationship with tide height. The vector autoregression model was fitted to the dataset including tide height, salinity, turbidity, and P_{CO2} with lags ranging from 1 to 5. Model estimation was initialized using the first 6 observations as presample data. The model with the best fit, according to the lowest AIC, was then used in the Granger causality test. To evaluate the accuracy of the vector autoregression model fit, half of the data (even-numbered observations) were withheld from the fitting procedure and P_{CO2} was estimated from the fitted model. The ability of the fitted model to predict the withheld values was then assessed using correlation and significance between P_{CO2} predictions and observations. Adjusted R^2 of modeled tide height, salinity, turbidity, and P_{CO2} was also calculated. Lastly, model consistency and autopower spectral densities of the vector

autoregression were reported. Model consistency measures the proportion of the correlation structure in both the observed and modeled data. Autopower spectra can be used to determine overlapping peak frequencies between observed and modeled data.

The leave-one-out Granger causality test was performed using the Multivariate Granger Causality (MVGC) toolbox in MATLAB, which assesses whether each variable in a best-fit vector autoregression model forecasts another variable (Barnett & Seth, 2014). Results of the Granger causality test are described using p-values of each Granger causality and causal density, which is the average of Granger causalities between each pair of variables in a dataset with respect to the variables not included in each pairwise causality test. Datasets composed of variables that behave relatively independently will have higher causal densities because their predictors produce unique and useful information. Datasets with completely unrelated variables will have scores closer to zero, as the dynamics guiding each variable are different (Seth et al., 2011).

3.3.7 Uncertainty analysis

To estimate the uncertainty of our approach, we constructed one hundred P_{CO2} alternative timeseries datasets using a Monte Carlo style approach. The 100 datasets were created by randomly selecting numbers in the range of the original measurement ±300 ppm, to account for sensor accuracy. The potential tidal export was then recalculated using the simulated datasets to produce estimated upper and lower limits of tidal exports from the marsh.

3.4 Results

3.4.1 Tidal influence

The twice daily, or semidiurnal, tide at Sapelo Island had a clear influence on P_{CO2} (Fig 3.4A). Tide also influenced changes in salinity and turbidity (Fig 3.4B &C). Tide height at Hunt Dock reached a maximum of 4.5 meters during the study (Fig 3.4D). Water temperature was not strongly correlated with P_{CO2} ($R = -0.09$, $p = 0.02$). Surface water salinity as electrical conductivity surpassed the maximum limit of the Smart Rock sensor. Salinity peaks lined up well with peaks in tide height. Low tide was reflected in P_{CO2} measurements and tide height, but not by the salinity sensor. Salinity and P_{CO2} were also poorly aligned from July 31st- August 3rd when both dropped to low levels. Relative turbidity indicated murky water was consistently brought in by the tide, and was especially murky on July 25th-27th, and August 21st. Relative turbidity continued to decrease throughout the study, which means that surface water got darker with time.

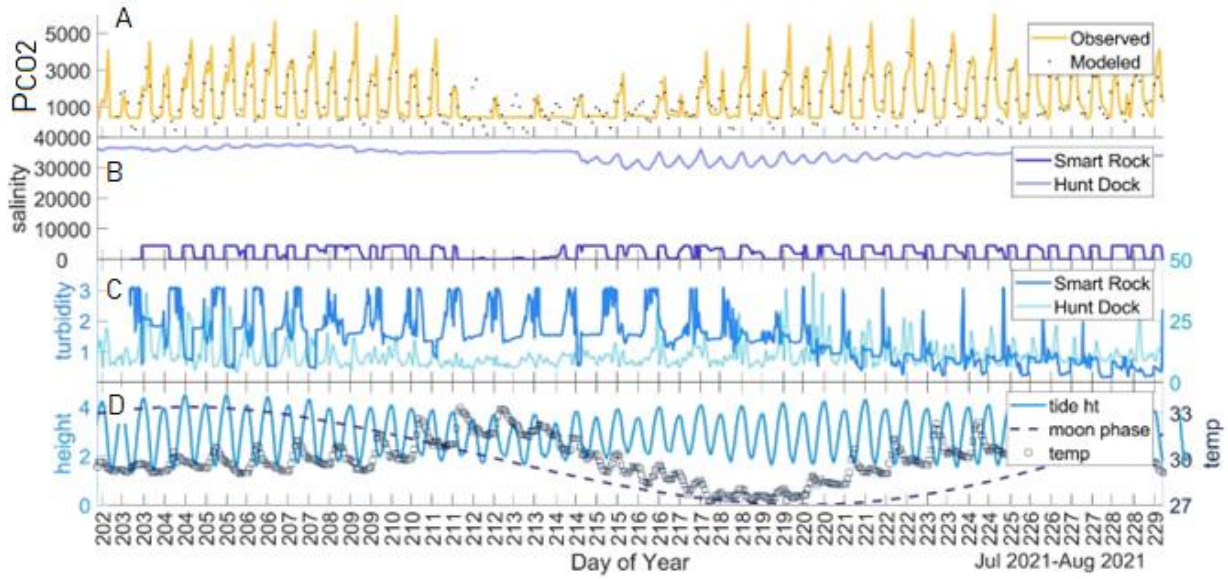

Figure 3.4. Time series at Sapelo Island Marsh. (A) Observed P_{CO2} concentrations in ppm (yellow line) and modeled by vector autoregression (black dots). (B) Salinity measured by the Smart Rock and at Hunt Dock (uS/cm). (C) Relative turbidity measured by the Smart Rock (Volts) on

the left axis and turbidity (NTU) at Hunt Dock on the right axis. Only turbidity less than 50 NTU is shown. Higher NTU indicates murkier water, while higher voltage implies clearer water. (D) Tide height at Hunt Dock (meters) and moon phase divided by 25 on the left axis and water temperature (°C) on the right axis.

Values of P_{CO2} ranged from 390-6,106 ppm ± 54 (standard error), with a mean of 1,421 ppm. This equated to a range of 0-5,596 ppm throughout the study period after accounting for atmospheric CO_2, with a mean of 1,081 ppm (0 standard error). There was a positive linear relationship (R^2 = 0.35) between mean tide height and median binned P_{CO2} (Fig 3.5). Most outliers, having P_{CO2} values greater than 1.5 times the interquartile range, occurred at tide heights below 3 m.

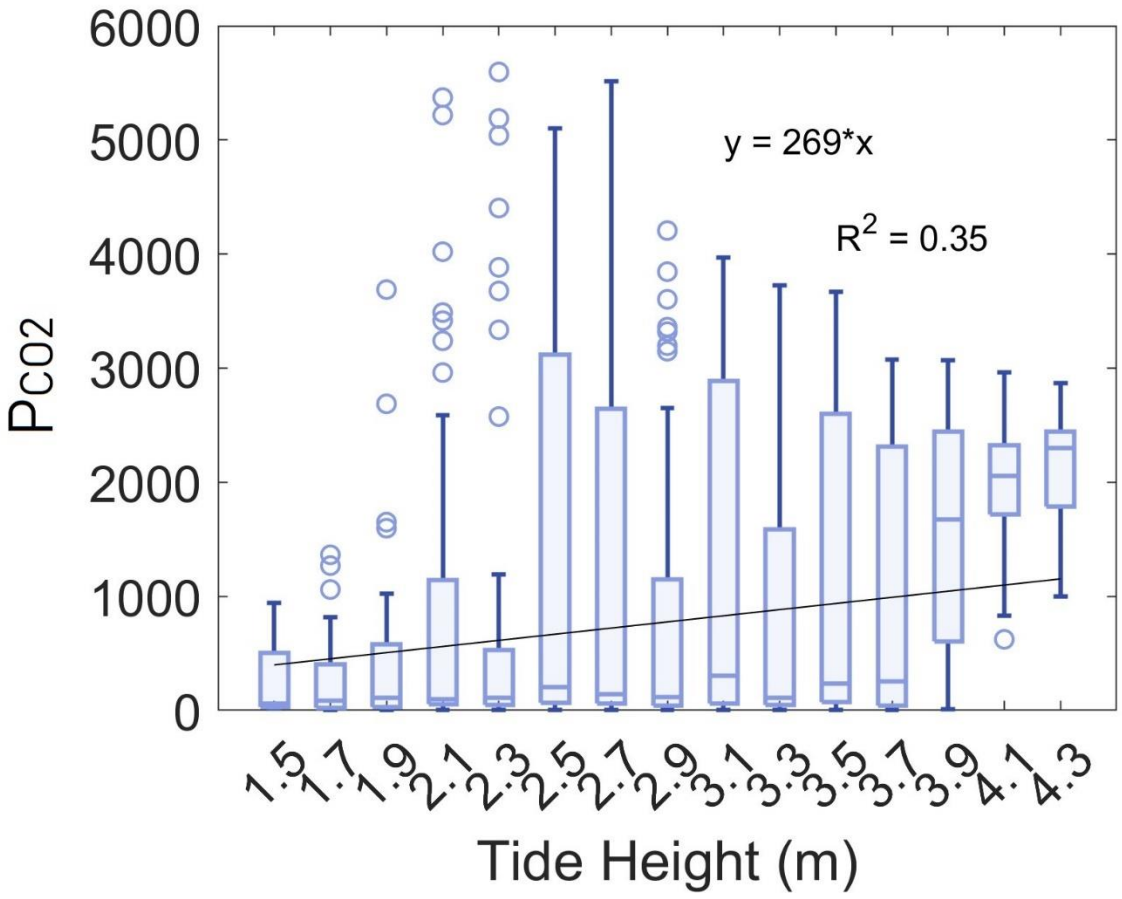

Figure 3.5. Box chart of P_{CO2} (ppm) according to tide height at Hunt Dock (blue boxes) with linear equation fitted to median P_{CO2} of each bin (black line). P_{CO2} was binned every 0.2 meters of tide height. The mean tide height for each bin, rounded to the nearest tenth of a meter, is displayed on the x-axis. Horizontal bars represent median P_{CO2} for each bin. The top and bottom of each box represent the upper and lower quartile. The whisker extending from each box represents minimum and maximum values. Outliers are shown as blue circles. Only P_{CO2} concentrations above 0 ppm after subtracting atmospheric CO_2 are shown.

3.4.2 Net tidal C export and uncertainty analysis

Station	**Lat.**	**Long.**	**Dist. (km)**	**Potential tidal export (gC m^{-2} tide $cycle^{-1}$)**		**Potential total export (gC m^{-2} study $period^{-1}$)**	
				A	B	A	B
Hunt Dock	31.48	-82.17	4.15	0.07 to 0.22	0.06	3.68 to 11.67	3.02
Cabretta Creek	31.44	-81.24	4.15	0.03 to 0.16	0.04	1.62 to 8.47	2.25
Dean Creek	31.39	-81.28	6.02	0.04 to 0.11	0.03	2.04 to 5.85	1.71

Table 3.1. Tide gage locations and distances and potential tidal and total export of P_{CO2}. Letters represent (A) Monte Carlo style estimate to account for sensor inaccuracies (B) Actual observations assuming 100% sensor accuracy.

Mean P_{CO2} during incoming tide was roughly half of mean P_{CO2} during outgoing tide, with an average concentration of 492 ppm compared to 1,569 ppm after accounting for atmospheric CO_2. This resulted in a potential net lateral C export of 0.03 to 0.06 gC m^{-2} tide $cycle^{-1}$ and 1.71 to 3.02 gC m^{-2} during the entire study period as P_{CO2} at all tide gages, assuming 100% sensor accuracy (Table 3.1). Potential tidal C export was largest when using Hunt Dock tide data.

Potential lateral net C exports per tide cycle based on tide gages at Cabretta Creek and Dean Creek were similar despite different distances from the CO2-LAMP when 100% sensor accuracy was assumed.

Flow out of the marsh was highly variable dependent on sensor accuracy. Potential lateral net C export estimated using Hunt Dock tide data was 3.20 gC m^{-2} higher than estimations based on tide data at Cabretta Creek and 5.82 gC m^{-2} higher than estimations based on tide data at Dean Creek when summed across the entire study period according to the Monte Carlo style simulation. Although the range produced by the upper and lower bounds of the Monte Carlo style simulations for each tide gage were relatively small on average per tide cycle (range of 0.12 gC m^{-2} tide $cycle^{-1}$), these led to large uncertainties in total C export for the study period overall (average range of 6.22 gC m^{-2} study $period^{-1}$). Lower bounds of the Monte Carlo style estimates were similar to observations, but upper bounds were at least two times greater than observations across all tide gages.

3.4.3 Vector autoregression and Granger causality testing

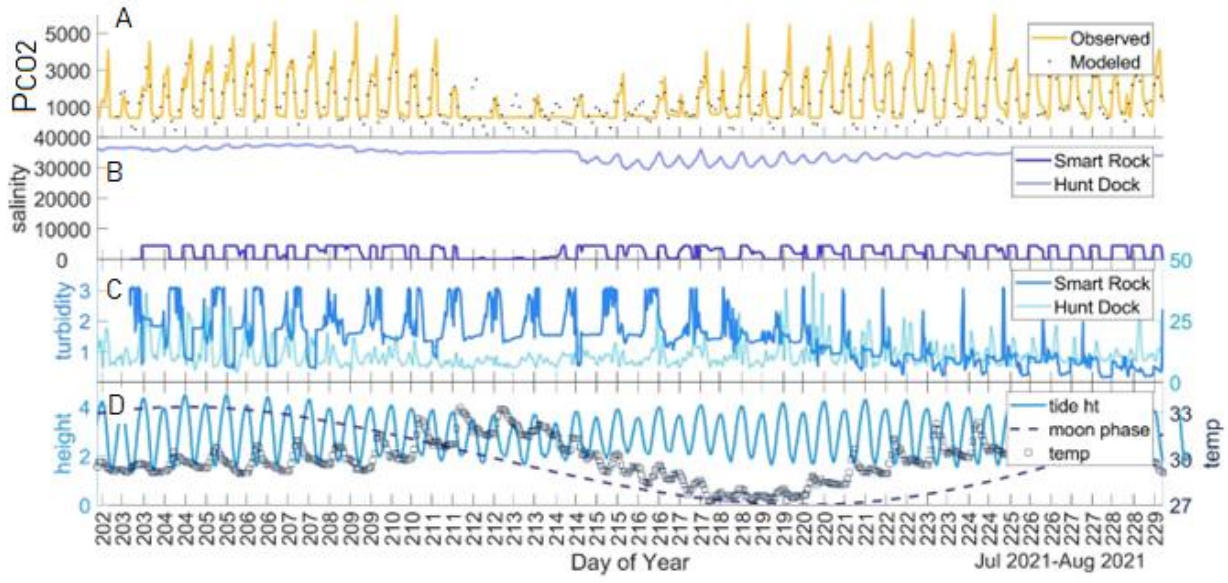

Figure 3.6. Autopower spectral densities from the vector autoregression model and time series data of (A) tide height, (B) salinity, (C) turbidity, (D) water temperature (°C), and (E) P_{CO2}. Autopower is displayed on the y-axis and has units of the representative variable squared over Hz (e.g., m^2Hz^{-1} for tide height).

The vector autoregression model explained 98% of the variation in tide height, 96% of the variation in salinity, 97% of the variation in water temperature, and 58% of the variation in P_{CO2} when considering the number of independent variables. The model results did not fit well with observations of turbidity, with an adjusted R^2 value of -0.28. Model consistency was low at only 5%. Strong peaks in the autopower spectra for tide height and P_{CO2} corresponded with the frequency of the semidiurnal tide at roughly 2.3e-5 Hz (Fig 6A &D). A similar but weaker maximum frequency was observed in the autopower spectra for salinity (Fig 3.6B). Turbidity reflected maximum autopower at the semidiurnal frequency for modeled data but not for observed data (Fig 3.6C). Vector autoregression predictions of P_{CO2} aligned well with

observations when withholding half of the data (R = 0.84) and when using the full dataset to fit the model (R = 0.83).

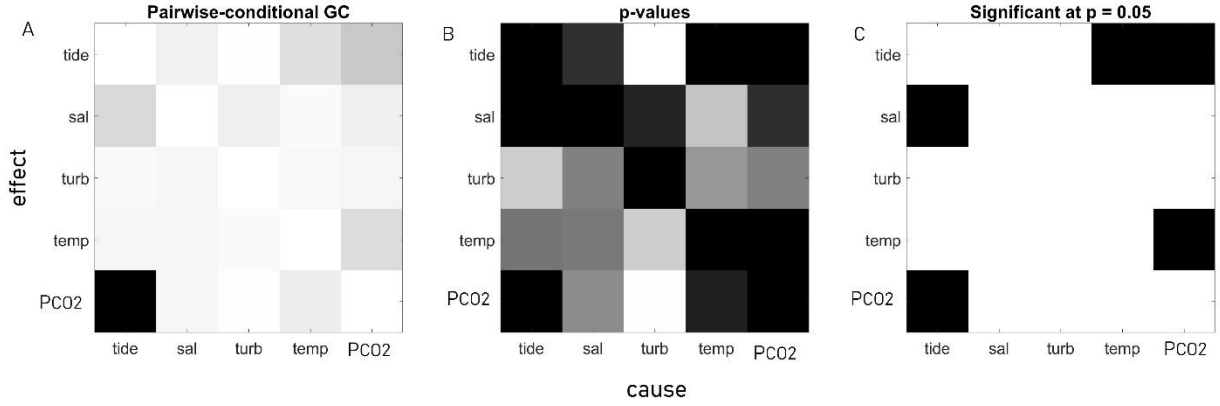

Figure 3.7. Granger causality test results. (A) Pairwise-conditional Granger causalities, with darker squares representing higher values. Granger causality units are arbitrary. (B) Corresponding p-values for each pairwise Granger causality test, with darker squares representing lower, more significant p-values. (C) Significant Granger causalities only, with dark squares representing causal relationships. In all subplots, columns represent causes; rows represent effects.

Granger causality testing of the vector autoregression model using Hunt Dock tide data revealed causal relationships between tide height and water temperature, water temperature and P_{CO2}, tide height and P_{CO2}, and tide height and salinity (Fig 3.7). Causal relationship direction (e.g., P_{CO2} -> tide ht.) was the opposite of reality in some cases. Mean causal density was 0.03.

3.5 Discussion

3.5.1 Reliability of the CO2-LAMP

We demonstrated that the CO2-LAMP could measure the influence of tides on dissolved CO_2 in a tidal marsh using a low-cost platform ($346-497 in 2022). Uncertainty in P_{CO2}

measurements due to sensor accuracy using the manufacturer-provided ranges had a large influence over potential net export, in addition to atmospheric CO_2 concentration and tide gage location. Nevertheless, it is important to note that the manufacturer-provided analytical error represents a maximum. Reference measurements inform that actual field measurements are likely much more accurate than the manufacturer-stated accuracy. A more thorough set of reference measurements would provide better statistics regarding individual sensor accuracy, which could then be used for refining the parameterization of the Monte Carlo style analysis. We assume the estimated uncertainty would be much lower in this case.

3.5.2 Cost and improvements of P_{CO2} and Smart Rock sensors

Large ranges in lateral flow estimates demonstrated difficulty with comprehensive measurement of water flow and the importance of co-located tide gages when measuring P_{CO2}. When using water flow outside of the marsh to understand lateral C imports or exports from the marsh, overland and groundwater flow corrections should be made (Wang et al., 2016), though such information was not available in this study. Overland flow is when water follows a path through the marsh not captured by a tide gage. More spatiotemporally frequent measurements of water flow are essential. One way to do this could be to use a fixed acoustic doppler current profiler or measure particle tracking velocity using video, though video may be difficult in the marsh as wind effects on apparent surface water flow can lead to erroneous flow estimations.

Despite challenges faced with maintenance and operation, the CO2-LAMP performed well in detecting tidal export of C as P_{CO2}. The sensor platform is simple to operate, lightweight, low-cost, and captures moderately frequent measurements necessary to understand influence

of a full tidal cycle on marsh biogeochemistry. Mismatched peaks in salinity and P_{CO2} indicated there was likely residual moisture with relatively high salinity still on the sensor between some tidal cycles. Decreasing turbidity and P_{CO2} drift could have been caused by fouling on sensor surfaces or increased inputs of DIC from terrestrial freshwaters. Data from nearby streams from smaller catchments would be needed to validate this claim. Additionally, more frequent cleaning may resolve this issue. In future versions of the Smart Rock, the upper limit of the salinity sensor should be increased. Adding higher quality internal clocks to both the Smart Rock and CO2-LAMP will provide more reliable timestamps. Decreasing the power draw of the CO2-LAMP would also enable simultaneous data collection by multiple sensors at stations having smaller solar arrays.

The cost of the CO2-LAMP in 2022 ranges $346-497 with an added $180 minimum for the tide-varying station (i.e., wooden boards, copper pipes, etc.), plus shipping and tax. Prices can change with individual product choices (e.g., type of K30, size of waterproof case), access to construction tools or lab supplies, and the number of supplies bought in bulk or reused. An itemized list of parts and costs are included in Table S3.1. The CO2-LAMP uses the same measurement method as other low-cost P_{CO2} sensor platforms such as the SIPCO2, which had a cost of $500 USD in 2017 (Hunt et al., 2017). A smaller, lower-cost, and submersible P_{CO2} sensor platform was developed by Hill (2018) for approximately $305 USD, though battery life was shorter. At its current price, the CO2-LAMP is still less costly than some other alternatives (Li, 2022). The Smart Rock had a low cost of around $200 but was built most easily while taking an online course workshop, which adds to the overall cost. However, the internal battery and long-lasting low-power mode make the Smart Rock simple to use and implement.

3.5.3 Vector autoregression and Granger causality testing

The autoregression model demonstrated that variations in observations of turbidity are difficult to explain with this suite of variables, and the tidal influence on modeled salinity and turbidity are present, but weak. Neither modeled nor observed water temperature demonstrated a tidal signal. Granger causality testing revealed that although P_{CO2}, turbidity, salinity, and water temperature fluctuated with tide height, any correlation between P_{CO2} and salinity is likely due to the influence of tide height on salinity. Causal density and vector autoregression model consistency were low. Low model consistency in this case could be the result of a missing key variable, such as tide direction. Nonzero causal density indicates that there was some dynamical complexity, but higher causal density might be achieved with more variables or a higher frequency and duration dataset, which would enable a greater lag capability and higher confidence in results. Alternative statistical techniques such as multiple linear regression may be better suited to describing tidal data in cases where the dataset is highly interdependent, or singular. Granger causality testing did not accurately predict the direction of some relationships potentially due to edge effects from overlapping signals, or distance between the tide gage and P_{CO2} sensor. More specifically, a sine wave of P_{CO2} may be viewed as 90° ahead of a sine wave of water temperature *or* 270° behind.

Our modeling approach could be used to increase spatial estimations of C imports and exports in salt marshes given certain assumptions. With an adequate training set and validation data collected through time, C imports and exports could be estimated. Investigators could expand C exchange monitoring using instrumentation like the CO2-LAMP to develop regression-based models where tide height and other water quality parameters are monitored.

Intermittent CO2-LAMP (or similar system) deployments at potential sites would allow validation of the regression-based model and re-evaluation of model coefficients over time should cyclical or long-term changes be present in response to C exchange dynamics.

3.5.4 Tidal effects in coastal marshes

Fluctuation of P_{CO2} with the tide supported other studies which show tidal amplitude is a key variable in porewater discharge (Seyfferth et al., 2020; Bouillon et al., 2007; Call et al., 2015; Linto et al., 2014; Maher et al., 2013) and groundwater discharge (Tamborski et al., 2021; Wang & Cai, 2004). Porewater and groundwater also contribute to lateral export of dissolved inorganic C, which includes CO_2, bicarbonate (HCO_3^-), carbonate (CO_3^{2-}), and carbonic acid (H_2CO_3). As a result, low tides may result in higher concentrations of CO_2 partial pressure (P_{CO2}) in surface water than high tides at some sites as high P_{CO2} porewater and groundwater become more dominant (Taillardat et al., 2018; Zablocki, Andersson, and Bates, 2011; Burgos et al., 2018; Mayen, 2020), especially during periods of low flow (Marescaux et al., 2018). There was no strong evidence for that relationship in bin-averaged P_{CO2} and tide height in the marsh, though most P_{CO2} outliers existed at low tide heights. The marsh surface was also exposed during low tide, leading to a lack of underwater P_{CO2} measurements during low tide to compare with high tide. Tidal oscillation of P_{CO2} at Sapelo contrasted with coastal ecosystems of the English Channel, which have a much stronger diurnal variability despite a semidiurnal tide (Yang et al., 2019). Measurements of groundwater and surface water flow from within the marsh were a limitation of this study but are crucial for understanding coastal C dynamics.

Potential net tidal export based on tide velocity at all stations was expected, as tidal marshes typically export more C than they import through lateral flow. A salt marsh in North

Carolina demonstrated summertime lateral dissolved inorganic C export of approximately 0.5 gC m^{-2} tidal $cycle^{-1}$, which was larger but similar in magnitude to the upper limits of C export based on tide velocity at Hunt Dock and Dean Creek using the Monte Carlo style simulation (Czapla et al., 2020). Potential net C export for the entire month of study was lower than dissolved inorganic C export of more than 30 gC m^{-2} for the month of July in a Massachusetts salt marsh in all cases (Wang et al., 2016). The cumulative annual C sink for the marsh in Sapelo ranges from approximately 130-300 gC m^{-2} yr^{-1} (Nahrawi, 2019) and can range from 380-890 gC m^{-2} yr^{-1} in other subtropical marshes (Liu et al, 2020; Gomez-Casanovas et al., 2020). Total lateral C export during the month of study alone would account for approximately 0.5-9% of the cumulative annual C sink of the marsh. The estimates presented here were based on measurements taken during the peak of the growing season when photosynthetic productivity and respiration rates are high, and they should not be extrapolated throughout the rest of the year. Granger causality of tide height means that small changes in tide height across the marsh surface could have a large impact on seasonal and long-term fluctuations in C export due to P_{CO2}.

Additionally, subtropical salt marshes can display “hot” moments of high C export or import, such as the coastal marsh in Codden et al. (2022) where as much as 12% of annual organic C sequestration was exported as DOC in one summer month across a 16-month study. Longer term monitoring would be necessary to determine whether our measurements reflect a “hot” moment. Our lateral C export estimate likely underestimates actual lateral C export from the marsh because it does not consider the import or export of other forms of C, such as particulate organic C, dissolved organic C, or C in CH_4. Subtropical coastal salt marshes such as

Sapelo Island are among the most productive ecosystems on Earth and given high spatiotemporal variability of these types of measurements, continual monitoring is important.

A weak, positive linear relationship between marsh surface water P_{CO2} and tide height was in line with results from previous studies at this site. Specifically, aquatic P_{CO2} concentrations aligned well with previous measurements of ~3,250 and ~2,500 ppm during low tide and high tide, respectively in June 2001 at Barn Creek (Wang & Cai, 2004). Maximum P_{CO2} concentrations were still lower than those of a tidal creek in Delaware, USA of around 8,400 ppm (Trifunovic et al., 2020). Surface water P_{CO2} aligned with the observations of ~1,086 ppm and ~493 ppm during low tide and high tide respectively at the mouth of Doboy Sound in June 2003, when accounting for atmospheric CO_2 (Jiang, Cai, and Wang, 2008).

3.6 Conclusion

Here, we evaluated a low-cost P_{CO2} sensor platform at Sapelo Island, Georgia, USA as an approach to address the desire for more frequent and more extensive sampling of P_{CO2} in coastal marshes. We hypothesized that (1) CO2-LAMP measurements of P_{CO2} would support previous research findings that Sapelo Island marshes are a lateral C source, and (2) comparison of P_{CO2} measurements with tidal data would demonstrate known biogeochemical mechanisms, including positive correlations with turbidity and salinity, a weak inverse correlation with water temperature, and higher concentrations during ebb tide than flood tide.

In accordance with our first hypothesis, we found that the CO2-LAMP is an effective tool for studying aquatic biogeochemistry and capturing tidal signals using semi-frequent measurements. Results of P_{CO2} tidal variability demonstrated net lateral C export as P_{CO2} and

higher P_{CO2} concentrations during outgoing tide (ebb) than incoming tide (flood), but some difficulties remain when teasing apart signal from complex tidal data.

Our second hypothesis was partially supported by Granger causality results showing that tide height was a significant driver of P_{CO2}, salinity, and water temperature, although the direction of causality was incorrect. P_{CO2} had a weak inverse relationship with water temperature, a positive linear relationship with tide height, and was higher during outgoing tide (ebb) than incoming tide (flood).

As coastal wetlands begin to migrate landwards or disappear because of urbanization, topography, and rising seas, the pressure to understand and conserve them increases (Borchert et al., 2018; Thorne et al., 2018). Scientific collaboration and a clearer understanding of biogeochemistry in tidal ecosystems could contribute to better modeling of coastal environments influenced by hurricanes, sea-level rise, groundwater abstraction, and more (White & Kaplan, 2017). In combination with other measurements, P_{CO2} can provide a window into the biogeochemistry of coastal ecosystems.

3.7 Acknowledgements

We would like to thank the dedicated team of researchers and field technicians at UGA and UGAMI, including Jacob Shalack, Peter Hawman, and Dr. Deepak Mishra, and our reviewers for their valuable feedback. This work also benefitted from insights on Granger causality testing from Dr. Paul Stoy and Dr. Matteo Detto, and post-deployment lab testing by Jonathan Thom of the Space Science and Engineering Center at UW-Madison. This material is based upon work supported by the -. Any opinions, findings, and conclusions or recommendations expressed in this material are those of the authors and do not necessarily reflect the views of the National

Science Foundation or the USDA. Any mention of commercial names or products does not imply USDA endorsement.

3.8 Data availability

The data that support the findings of this study are openly available at various locations. MATLAB scripts and datasets created for this research are available on GitHub (turner-j, 2022) and through the Environmental Data Initiative (EDI) Data Portal (Turner, 2022). Others can be found using the in-text citations (NOAA NERRS, 2022; NOAA Tides & Currents, 2021). Flux data from US-GCE are available from the site Prinicipal Investigators upon reasonable request using contact information on AmeriFlux.

3.9 References

Ardón, M., Helton, A.M. & Bernhardt, E.S. Salinity effects on greenhouse gas emissions from wetland soils are contingent upon hydrologic setting: a microcosm experiment. Biogeochemistry 140, 217–232 (2018). https://doi.org/10.1007/s10533-018-0486-2

Barnett, L., & Seth, A. K. (2014). The MVGC multivariate Granger causality toolbox: a new approach to Granger-causal inference. *Journal of neuroscience methods*, *223*, 50-68.

Beaubien, S. E., Graziani, S., Annunziatellis, A., Bigi, S., Ruggiero, L., Tartarello, M. C., & Lombardi, S. (2014). Spatial-temporal water column monitoring using multiple, low-cost GasPro-pCO2 sensors: implications for monitoring, modelling, and potential impact. Energy Procedia, 63, 3840-3847.

Blackstock, J. M., Covington, M. D., Perne, M., & Myre, J. M. (2019). Monitoring atmospheric, soil, and dissolved CO2 using a low-cost, Arduino monitoring platform (CO2-LAMP): theory, fabrication, and operation. *Frontiers in Earth Science*, *7*, 313.

Borchert, S. M., Osland, M. J., Enwright, N. M., & Griffith, K. T. (2018). Coastal wetland adaptation to sea level rise: Quantifying potential for landward migration and coastal squeeze. *Journal of Applied Ecology*, *55*(6), 2876-2887.

Burgos, M., Ortega, T. & Forja, J. Carbon Dioxide and Methane Dynamics in Three Coastal Systems of Cadiz Bay (SW Spain). Estuaries and Coasts 41, 1069–1088 (2018). https://doi.org/10.1007/s12237-017-0330-2

Call, M., Maher, D. T., Santos, I. R., Ruiz-Halpern, S., Mangion, P., Sanders, C. J., ... & Eyre, B. D. (2015). Spatial and temporal variability of carbon dioxide and methane fluxes over semi-diurnal and spring–neap–spring timescales in a mangrove creek. *Geochimica et Cosmochimica Acta*, *150*, 211-225.

Call, M., Santos, I. R., Dittmar, T., de Rezende, C. E., Asp, N. E., & Maher, D. T. (2019). High pore-water derived CO2 and CH4 emissions from a macro-tidal mangrove creek in the Amazon region. *Geochimica et Cosmochimica Acta*, *247*, 106-120.

Chambers, L. G., Reddy, K. R., & Osborne, T. Z. (2011). Short-term response of carbon cycling to salinity pulses in a freshwater wetland. *Soil Science Society of America Journal*, *75*(5), 2000-2007.

Chamberlain, S. D., Hemes, K. S., Eichelmann, E., Szutu, D. J., Verfaillie, J. G., & Baldocchi, D. D. (2020). Effect of drought-induced salinization on wetland methane emissions, gross ecosystem productivity, and their interactions. *Ecosystems*, *23*(3), 675-688.

Cheng, J., Karambelkar, B., and Xie, Y. (2022). leaflet: Create Interactive Web Maps with the JavaScript 'Leaflet' Library. R package version 2.1.1. https://CRAN.R-project.org/package=leaflet

Chanda, A., Das, S., Bhattacharyya, S., Akhand, A., Das, I., Samanta, S., ... & Hazra, S. (2020). CO2 effluxes from an urban tidal river flowing through two of the most populated and polluted cities of India. *Environmental Science and Pollution Research*, *27*(24), 30093-30107.

Jones, C. R. (1980). Productivity of algal epiphytes in a Georgia salt marsh: effect of inundation frequency and implications for total marsh productivity. *Estuaries*, *3*(4), 315-317.

Codden, C. J., Edwards, C. R., & Stubbins, A. (2022). Non-conservative behavior of dissolved organic carbon in a Georgia salt marsh creek indicates summer outwelling. *Estuarine, Coastal and Shelf Science*, *265*, 107709.

Czapla, Kenneth M., Iris C. Anderson, and Carolyn A. Currin. (2020). Net ecosystem carbon balance in a North Carolina, USA, salt marsh. *Journal of Geophysical Research: Biogeosciences* 125.10: e2019JG005509.

Dai, Minhan, Lu, Zhongming, Zhai, Weidong, Chen, Baoshan, Cao, Zhimian, Zhou, Kuanbo, Cai, Wei-Jun, Chenc, Chen-Tung Arthur. (2009). Diurnal variations of surface seawater pCO2 in contrasting coastal environments, *Limnology and Oceanography*, 54, doi: 10.4319/lo.2009.54.3.0735.

Desai, A. R. (2014). Influence and predictive capacity of climate anomalies on daily to decadal extremes in canopy photosynthesis. *Photosynthesis Research*, *119*(1), 31-47.

Detto, M., Molini, A., Katul, G., Stoy, P., Palmroth, S., & Baldocchi, D. (2012). Causality and persistence in ecological systems: a nonparametric spectral Granger causality approach. *The American Naturalist*, *179*(4), 524-535.

Fagherazzi, S., Wiberg, P.L., Temmerman, S. et al. Fluxes of water, sediments, and biogeochemical compounds in salt marshes. Ecol Process 2, 3 (2013). https://doi.org/10.1186/2192-1709-2-3

Feagin, R. A., Forbrich, I., Huff, T. P., Barr, J. G., Ruiz-Plancarte, J., Fuentes, J. D., et al (2020). Tidal wetland gross primary production across the continental United States, 2000–2019. Global Biogeochemical Cycles, 34, e2019GB006349. https://doi.org/10.1029/2019GB006349

Friedlingstein, P., O'sullivan, M., Jones, M. W., Andrew, R. M., Hauck, J., Olsen, A., ... & Zaehle, S. (2020). Global carbon budget 2020. *Earth System Science Data*, *12*(4), 3269-3340.

Golub, M., Desai, A. R., McKinley, G. A., Remucal, C. K., & Stanley, E. H. (2017). Large uncertainty in estimating pCO2 from carbonate equilibria in lakes. *Journal of Geophysical Research: Biogeosciences*, *122*(11), 2909-2924.

Gomez-Casanovas, N., DeLucia, N. J., DeLucia, E. H., Blanc-Betes, E., Boughton, E. H., Sparks, J., & Bernacchi, C. J. (2020). Seasonal controls of CO2 and CH4 dynamics in a temporarily flooded subtropical wetland. *Journal of Geophysical Research: Biogeosciences*, *125*(3), e2019JG005257.

Granger, C. W. (1969). Investigating causal relations by econometric models and cross-spectral methods. *Econometrica: journal of the Econometric Society*, 424-438.Han, G., Luo, Y., Li, D., Xia, J., Xing, Q., & Yu, J. (2014). Ecosystem photosynthesis regulates soil respiration on a diurnal scale with a short-term time lag in a coastal wetland. *Soil Biology and Biochemistry*, *68*, 85-94.

Hill, K. S. (2018). *Development of a low-cost marine pCO2 sensor to characterise the natural variability of coastal carbonate chemistry in the context of global change* (Doctoral dissertation, University of Glasgow).

Hunt, C. W., Snyder, L., Salisbury, J. E., Vandemark, D., & McDowell, W. H. (2017). SIPCO2: a simple, inexpensive surface water pCO2 sensor. Limnology and Oceanography: Methods, 15(3), 291-301.

Jiang, L. Q., Cai, W. J., & Wang, Y. (2008). A comparative study of carbon dioxide degassing in river-and marine-dominated estuaries. *Limnology and Oceanography*, *53*(6), 2603-2615.

Kara, E., & Shade, A. (2009). Temporal dynamics of South End tidal creek (Sapelo Island, Georgia) bacterial communities. *Applied and Environmental Microbiology*, *75*(4), 1058-1064.

Kirwan, M., Megonigal, J. Tidal wetland stability in the face of human impacts and sea-level rise. Nature 504, 53–60 (2013). https://doi.org/10.1038/nature12856

Kuwae, T., Kanda, J., Kubo, A., Nakajima, F., Ogawa, H., Sohma, A., & Suzumura, M. (2019). CO 2 uptake in the shallow coastal ecosystems affected by anthropogenic impacts. In *Blue Carbon in Shallow Coastal Ecosystems* (pp. 295-319). Springer, Singapore.

Li, M., Du, B., Guo, J. *et al.* A low-cost in-situ CO2 sensor based on a membrane and NDIR for long-term measurement in seawater. *J. Ocean. Limnol.* (2022). https://doi-org.ezproxy.library.wisc.edu/10.1007/s00343-021-1133-7

Liu, J., & Lai, D. Y. (2019). Subtropical mangrove wetland is a stronger carbon dioxide sink in the dry than wet seasons. *Agricultural and Forest Meteorology*, *278*, 107644.

Liu, J., Zhou, Y., Valach, A., Shortt, R., Kasak, K., Rey-Sanchez, C., ... & Lai, D. Y. (2020). Methane emissions reduce the radiative cooling effect of a subtropical estuarine mangrove wetland by half. *Global Change Biology*, *26*(9), 4998-5016.

Lovelock, C. E., & Reef, R. (2020). Variable impacts of climate change on blue carbon. *One Earth*, 3(2), 195-211.

Macreadie, P.I., Anton, A., Raven, J.A. et al. The future of Blue Carbon science. Nat Commun 10, 3998 (2019). https://doi.org/10.1038/s41467-019-11693-w

Mayen, J. (2020). Spatial and temporal variations in pCO2 and atmospheric CO2 exchanges in a temperate salt marsh system.

Mendelssohn, I. A., & Morris, J. T. (2000). Eco-physiological controls on the productivity of Spartina alterniflora Loisel. In: M. Weinstein & D. A. Kreeger (Eds.), *Concepts and controversies in tidal marsh ecology* (pp. 59–80). Dordrecht, Netherlands: Kluwer Academic Publishing.

Mudd, S. M., D'Alpaos, A., and Morris, J. T. (2010), How does vegetation affect sedimentation on tidal marshes? Investigating particle capture and hydrodynamic controls on biologically mediated sedimentation, J. Geophys. Res., 115, F03029, doi:10.1029/2009JF001566.

Nahrawi, H. (2019). Exchange of Carbon Dioxide between a Southeastern Salt Marsh and the Atmosphere (Doctoral dissertation, University of Georgia).

NOAA National Estuarine Research Reserve System (NERRS). System-wide Monitoring Program. Data accessed from the NOAA NERRS Centralized Data Management Office website: http://cdmo.baruch.sc.edu/; accessed 3 March 2022.

NOAA Tides & Currents. (2021). 8675622 OLD TOWER, SAPELO ISLAND, DOBOY SOUND, GA. Retrieved December 1, 2021, from https://tidesandcurrents.noaa.gov/noaatidepredictions.html?id=8675622

Pinton, D., Canestrelli, A., & Fantuzzi, L. (2020). A UAV-based dye-tracking technique to measure surface velocities over tidal channels and salt marshes. *Journal of Marine Science and Engineering*, *8*(5), 364.

Ragotzkie, R. A., & Bryson, R. A. (1955). Hydrography of the Duplin River, Sapelo Island, Georgia. *Bulletin of Marine Science*, *5*(4), 297-314.

Raymond, P. A., Bauer, J. E., & Cole, J. J. (2000). Atmospheric CO2 evasion, dissolved inorganic carbon production, and net heterotrophy in the York River estuary. *Limnology and Oceanography*, *45*(8), 1707-1717.

Sanders, S. C. (2021). *Groundwater Flow and Transport at the Forest-Marsh Boundary: A Modeling Study* (Doctoral dissertation, University of South Carolina).

Seth, A. K., Barrett, A. B., & Barnett, L. (2011). Causal density and integrated information as measures of conscious level. *Philosophical Transactions of the Royal Society A: Mathematical, Physical and Engineering Sciences, 369*(1952), 3748-3767.

Seyfferth, A. L., Bothfeld, F., Vargas, R., Stuckey, J. W., Wang, J., Kearns, K., ... & Sparks, D. L. (2020). Spatial and temporal heterogeneity of geochemical controls on carbon cycling in a tidal salt marsh. *Geochimica et cosmochimica acta*, *282*, 1-18.

Song, C., Wang, G., Hu, Z., Zhang, T., Huang, K., Chen, X., & Li, Y. (2020). Net ecosystem carbon budget of a grassland ecosystem in central Qinghai-Tibet Plateau: Integrating terrestrial and aquatic carbon fluxes at catchment scale. *Agricultural and Forest Meteorology*, *290*, 108021.

Sutter, L. A., Perry, J. E., & Chambers, R. M. (2014). Tidal freshwater marsh plant responses to low level salinity increases. Wetlands, 34(1), 167–175. https://doi.org/10.1007/s13157-013-0494-x

Taillardat, P., Willemsen, P., Marchand, C., Friess, D. A., Widory, D., Baudron, P., ... & Ziegler, A. D. (2018). Assessing the contribution of porewater discharge in carbon export and CO2 evasion in a mangrove tidal creek (Can Gio, Vietnam). *Journal of hydrology*, *563*, 303-318.

Thorne, K., MacDonald, G., Guntenspergen, G., Ambrose, R., Buffington, K., Dugger, B., ... & Takekawa, J. (2018). US Pacific coastal wetland resilience and vulnerability to sea-level rise. *Science Advances*, *4*(2), eaao3270.

Tobias, C., & Neubauer, S. C. (2019). Salt marsh biogeochemistry—an overview. *Coastal wetlands*, 539-596.

Trifunovic, B., Vázquez-Lule, A., Capooci, M., Seyfferth, A. L., Moffat, C., & Vargas, R. (2020). Carbon dioxide and methane emissions from a temperate salt marsh tidal creek. *Journal of Geophysical Research: Biogeosciences*, *125*(8), e2019JG005558.

Turner, J.L. 2022. Sapelo Island Marsh pCO2, turbidity, and salinity, Summer 2021 ver 1. Environmental Data Initiative. https://doi.org/10.6073/pasta/972e85c197c3e30e27312ec6515ea2e9 (Accessed 2022-10-07).

turner-j. (2022). turner-j/pCO2sapelo: Sapelo Marsh pCO2 Plots and Analysis (v1.0.0). Zenodo. https://doi.org/10.5281/zenodo.6403170

Veach, A. (2019, December). An Open-Sourced Sensor Package for Low-Cost Remote Stream Monitoring. In *AGU Fall Meeting Abstracts* (Vol. 2019, pp. H53S-2078).

Wang, Z. A., Kroeger, K. D., Ganju, N. K., Gonneea, M. E., & Chu, S. N. (2016). Intertidal salt marshes as an important source of inorganic carbon to the coastal ocean. *Limnology and Oceanography*, *61*(5), 1916-1931.

Wang, F., Sanders, C.J., Santos, I.R., Tang, J., Schuerch, M., Kirwan, M.L., et al… (2021). Global blue carbon accumulation in tidal wetlands increases with climate change. *National Science Review* https://doi.org/10.1093/nsr/nwaa296

Wanninkhof, R. (2014). Relationship between wind speed and gas exchange over the ocean revisited. *Limnology and Oceanography: Methods*, *12*(6), 351-362.

Ward, N. D., Bianchi, T. S., Medeiros, P. M., Seidel, M., Richey, J. E., Keil, R. G., & Sawakuchi, H. O. (2017). Where carbon goes when water flows: carbon cycling across the aquatic continuum. *Frontiers in Marine Science*, *4*, 7.

Weiss, R. F., Jahnke, R. A., & Keeling, C. D. (1982). Seasonal effects of temperature and salinity on the partial pressure of CO2 in seawater. *Nature*, *300*(5892), 511-513.

White, E., and Kaplan, D.. 2017. Restore or retreat? Saltwater intrusion and water management in coastal wetlands. Ecosystem Health and Sustainability 3(1):e01258. doi: 10.1002/ehs2.1258

Wright, E., Ladd, D., Petro, N., & Keller, J. (n.d.). *SVS: Moon Phase and libration, 2021*. NASA's Scientific Visualization Studio. Retrieved March 8, 2022, from https://svs.gsfc.nasa.gov/4874

Yang, M., Bell, T. G., Brown, I. J., Fishwick, J. R., Kitidis, V., Nightingale, P. D., ... & Smyth, T. J. (2019). Insights from year-long measurements of air–water CH 4 and CO 2 exchange in a coastal environment. *Biogeosciences*, *16*(5), 961-978.

Yoon, T. K., Jin, H., Oh, N. H., & Park, J. H. (2016). Assessing gas equilibration systems for continuous pCO 2 measurements in inland waters. *Biogeosciences*, *13*(13), 3915-3930.

Zablocki, J. A., Andersson, A. J., & Bates, N. R. (2011). Diel aquatic CO 2 system dynamics of a Bermudian mangrove environment. *Aquatic geochemistry*, *17*(6), 841-859.

Zhang, W., Cao, Y., Zhu, Y., Zheng, J., Ji, X., Xu, Y., ... & Hoitink, A. J. F. (2018). Unravelling the causes of tidal asymmetry in deltas. *Journal of Hydrology*, *564*, 588-604.

3.10 Supplemental Information

Table S3.1. CO2-LAMP and floating platform parts list.

Item **(shaded blue if a bulk or reusable item)	**Link**	**Cost**
Grove 2-coil Latching Relay	https://www.seeedstudio.com/Grove-2-Coil-Latching-Relay.html	6.90
K30 10% CO2 Sensor	https://gaslab.com/products/k-30-3-co2-sensor	129.00 (99 for 1%)
Pololu 6V Step-Up/Step-Down Voltage Regulator	https://www.pololu.com/product/2575	24.95
Adafruit Assembled Data Logging Shield for Arduino	https://www.amazon.com/gp/product/B00OKCRZ7A/ref=ppx_od_dt_b_asin_title_s00?ie=UTF8&psc=1	14.99
SanDisk 128GB Extreme PRO SDXC UHS-I Card - C10, U3, V30, 4K UHD, SD Card - SDSDXXY-128G-GN4IN	https://www.amazon.com/gp/product/B07H9DVLBB/ref=ppx_od_dt_b_asin_title_s00?ie=UTF8&psc=1	33.25
Houseables 22 Gauge Solid Core Wire, Hookup Wires, 6 Spools (25 Feet Each), Red, Black, Green, Yellow, White & Blue Electrical AWG Assortment, Electric, Electronic Wiring, Thin Coated		16.83
Gasket Material Disc Compressible PTFE, 4" Diameter, 1/16" Thick 1084N86	https://www.mcmaster.com/ptfe-gaskets/	8.02

14/2 or 14/3 outdoor extension cord, 25 ft.	https://www.homedepot.com/p/Husky-25-ft-14-3-Indoor-Outdoor-Extension-Cord-Red-and-Black-HD-277-533/100650642	26.67
ARDUINO UNO R3 [A000066]	https://www.amazon.com/gp/product/B008GRTSV6/ref=ppx_od_dt_b_asin_title_s01?ie=UTF8&psc=1	22.86
5-Year Warranty CELEWELL CR1220 3V Lithium Battery 40mAh for Fairy Pearls/LED Light/Bracelet/Flashlight/Clock (5-Pack)	https://www.amazon.com/gp/product/B06XQ1C5TN/ref=ppx_od_dt_b_asin_title_s01?ie=UTF8&psc=1	4.97
eTECH Collection 20 Pack of Clear Plastic SD/SDHC/SDXC/MicroSD/MicroSDHC/MicroSDXC Memory Card Case Holder for SanDisk/Kingston/Transcend/Samsung Memory Card (Case Only, Memory Card Not Included)	https://www.amazon.com/gp/product/B00M6YEZQ8/ref=ppx_od_dt_b_asin_title_s01?ie=UTF8&psc=1	5.99
10 Male 12v DC Power Jack Adapter Connector for Led Strip CCTV Camera	https://www.amazon.com/gp/product/B015OCV5XY/ref=ppx_od_dt_b_asin_title_s01?ie=UTF8&psc=1	4.20
USB A to B cable	https://www.dell.com/en-us/work/shop/c2g-5m-usb-cable-usb-a-to-usb-b-cable-m-m-usb-cable-usb-m-to-usb-type-b-m-usb-20-164-ft-black/apd/a6992990/printers-ink-toner?gacd=9646510-1025-5761040-266794296-0&dgc=st&ds_rl=1282786&gcli	10.99

	d=Cj0KCQjwspKUBhCvARIsAB2IYuuZJDQjPkM-Y4KwjDUUK_JMaM0G5KVM3ivt8ysxAopGYdzJoMdej7IaAiYqEALw_wcB&gclsrc=aw.ds&ncid=eZ8DdBnfAmcsjAzxeiOhTC09C6HrKPQCyB8dXQu7lDKGRbZb0vgatSEEGevGmZsl	
Paint Brushes for Acrylic Painting, Nylon Hair Artist Detail Paintbrushes Set for Oil Watercolor Painting Face Nail Body Art Craft Model, Blue	https://www.amazon.com/gp/product/B089ZYM416/ref=ppx_od_dt_b_asin_title_s01?ie=UTF8&psc=1	2.99
Medical Nitrile Examination Gloves Blue Disposable Medium 100 Count Care Plus	https://www.discountsafetygear.com/pulin-nitrile-gloves.html?utm_source=googlepepla&utm_medium=adwords&id=&gclid=Cj0KCQjwspKUBhCvARIsAB2IYuvba1UOGjhYXZyKsoL-goVh9S37CRYSDMlD7Ko_7sa5FXBXyJqSJkwaAn6qEALw_wcB	4.40
TICONN 200PCS Heat Shrink Butt Connectors Kit, Insulated Waterproof Electrical Marine Automotive Wire Crimp Terminals, Butt Splice (3 Colors / 3 Sizes)	https://www.amazon.com/gp/product/B07HCPFPD2/ref=ppx_od_dt_b_asin_title_s01?ie=UTF8&psc=1	19.95
WYCTIN Lead Free Solder Wire Sn99.3-Cu0.7 0.6mm with Rosin Core for Electrical Soldering and DIYs	https://www.amazon.com/gp/product/B075GKDLXT/ref=ppx_od_dt_b_asin_title_s02?ie=UTF8&psc=1	8.39

SEEKONE Heat Gun 1800W Heavy Duty Hot Air Gun Kit Variable Temperature Control with 2-Temp Settings 4 Nozzles 122℉~1202℉（50℃- 650℃）with Overload Protection for Crafts, Shrinking PVC, Stripping Paint	https://www.amazon.com/gp/product/B078S5QMFG/ref=ppx_od_dt_b_asin_title_s02?ie=UTF8&psc=1	29.99
Gorilla Glue Beige 2 oz Mounting Putty Pre-Cut Squares, 84 Count	https://www.walmart.com/ip/Gorilla-Glue-Beige-2-oz-Mounting-Putty-Pre-Cut-Sqaures-84-Count/489565353?wmlspartner=wlpa&selectedSellerId=0&wl13=3201&adid=22222222277489565353_117755028669_12420145346&wmlspartner=wmtlabs&wl0=&wl1=g&wl2=c&wl3=501107745824&wl4=pla-293946777986&wl5=9010812&wl6=&wl7=&wl8=&wl9=pla&wl10=8175035&wl11=local&wl12=489565353&wl13=3201&veh=sem_LIA&gclid=Cj0KCQjwspKUBhCvARIsAB2IYuttRzGklDkwVdAAQ8TQ4eXw6zJDLqcQYE5qjtTJ5k2sgHzCTFlF2w0aAhwaEALw_wcB&gclsrc=aw.ds	3.18
650pcs Heat Shrink Tubing Black innhom Heat Shrink Tube Wire Shrink Wrap UL Approved Ratio 2:1 Electrical Cable Wire Kit Set Long Lasting Insulation Protection, Safe and Easy, Eco-Friendly Material	https://www.amazon.com/gp/product/B07WWWPR2X/ref=ppx_od_dt_b_asin_title_s02?ie=UTF8&psc=1	9.79
Grove - 2-Coil Latching Relay	https://www.seeedstudio.com/Grove-2-Coil-Latching-Relay.html	6.90

Seahorse SE-520 Waterproof Protective Hardcase without Foam (Black), Small	https://www.amazon.com/gp/product/B001A1PTAE/ref=ppx_yo_dt_b_asin_title_o01_s00?ie=UTF8&psc=1	65.57
½" cable glands (2)	https://cableglandsdirect.com/product/npt-12-10-14mm-cable-range/	1.34
Antrader 40 Pin 2.54mm Right Angle Male Pin Header Connector Strip Pack of 30	https://www.amazon.com/gp/product/B07M88GRHG/ref=ppx_yo_dt_b_asin_title_o02_s00?ie=UTF8&psc=1	7.37
Plasti Dip Performix 11603-06 Blk	https://www.amazon.com/gp/product/B00QU553YC/ref=ppx_yo_dt_b_asin_title_o03_s00?ie=UTF8&psc=1	18.33
Cat8 Ethernet Cable, Outdoor&Indoor, 6FT Heavy Duty High Speed 26AWG Cat8 LAN Network Cable 40Gbps, 2000Mhz with Gold Plated RJ45 Connector, Weatherproof S/FTP UV Resistant for Router/Gaming/Modem *MUST BE ROUND*	https://www.amazon.com/Ethernet-Outdoor-Connector-Weatherproof-Resistant/dp/B07QLXC6QR/ref=sr_1_4?crid=NV2PIFE5OHDG&keywords=round%2Bcat%2B7%2F8%2Bstandard%2Bethernet%2Bcable&qid=1652983753&s=electronics&sprefix=round%2Bcat%2B7%2F8%2Bstandard%2Bethernet%2Bcable%2B%2Celectronics%2C70&sr=1-4&th=1	8.99
Marine epoxy		
Total for Reusable or Bulk Parts Total for Non-reusable Parts Total for all parts Estimated tax (10%) and shipping		120.65 376 (346 for 1% K30) 497 (468 for 1% K30) 100

SENSOR PLATFORM TOTAL		597
Boogie board	https://www.amazon.com/Sunlite-Sports-Blue-Kickboard-Lightweight/dp/B07VVSTC14/ref=sr_1_1_sspa?crid=7V6UK1UIG89G&keywords=kickboard&qid=1652890270&sprefix=kick%2Caps%2C80&sr=8-1-spons&spLa=ZW5jcnlwdGVkUXVhbGlmaWVyPUEzMDFDVTBYSkswM1NDJmVuY3J5cHRlZElkPUEwNzExNDgzMzJXREhTSFNYMDMyRiZlbmNyeXB0ZWRBZElkPUEwNTIxMzYyMlgzTVo3QTA0QVFGRiZ3aWRnZXROYW1lPXNwX2F0ZiZhY3Rpb249Y2xpY2tSZWRpcmVjdCZkb05vdExvZ0NsaWNrPXRydWU&th=1	14.49
4’ x 2’ x 0.25” wooden board	https://www.homedepot.com/p/1-4-in-x-2-ft-x-4-ft-Sanded-Plywood-1502100/203116838	18.76
.25” hollow copper pipes (3)	https://www.homedepot.com/p/Mueller-Streamline-1-2-in-x-5-ft-Copper-Type-M-Pipe-MH04005/100558487	42.48
Extra-large zip ties *will likely need all of these*	https://www.homedepot.com/p/HDX-14-in-UV-Resist-Zip-Ties-Black-20-Pack-FT-370STUV-20/307799374	4.21
small zip ties	https://www.homedepot.com/p/Commercial-Electric-8-in-UV-Cable-Tie-Black-100-Pack-GT-200STCB/203531910	10.86
½” t-shaped PVC pipe (4)	https://www.homedepot.com/p/Charlotte-Pipe-1-2-in-PVC-	3.00

	Schedule-40-S-x-S-x-S-Tee-PVC024000600HD/203812195	
½" x 10 ft PVC pipe (cut into 4)	https://www.homedepot.com/p/JM-EAGLE-1-2-in-x-10-ft-600-PSI-Schedule-40-PVC-Plain-End-Pipe-530048/100113200	5.82
reciprocating saw	https://www.homedepot.com/p/Makita-18-Volt-LXT-Lithium-Ion-Cordless-Reciprocating-Saw-Tool-Only-XRJ04Z/300065680	129.00
drill with bits	https://www.amazon.com/BLACK-DECKER-BDCD8HDPK-Home-Project/dp/B079WGV6FB/ref=asc_df_B079WGV6FB/?tag=hyprod-20&linkCode=df0&hvadid=309812340191&hvpos=&hvnetw=g&hvrand=14388982965856360 8&hvpone=&hvptwo=&hvqmt=&hvdev=c&hvdvcmdl=&hvlocint=&hvlocphy=9010761&hvtargid=pla-644193401979&th=1	34.60
¾" iron flanges (6)	https://www.acehardware.com/departments/plumbing/parts-and-repair/flanges/4010751?store=17735&gclid=Cj0KCQjwspKUBhCvARIsAB2IYusog6BXePtnL-VJpHauzExfl9yeMKbNqv-V07PYddXERQt7eWbbBLsaAntOEALw_wcB&gclsrc=aw.ds	60
½" metal male adapter fittings (6)	https://www.homedepot.com/p/Everbilt-1-2-in-Copper-Pressure-Cup-x-MIP-Male-	12.78

	Adapter-Fitting-C604HD12/204620255	
.25” wood screws (24)	https://www.amazon.com/JQK-Electroplating-Stainless-100-Piece-SB3514-P100/dp/B089KGSZTD/ref=sr_1_11?keywords=small+wood+screws&qid=1652890126&sr=8-11	6.60
Total for reusable parts Total for non-reusable parts Total for all parts Estimated tax (10%) and shipping BOOGIE BOARD TOTAL		163.60 179.00 342.60 60 404.60

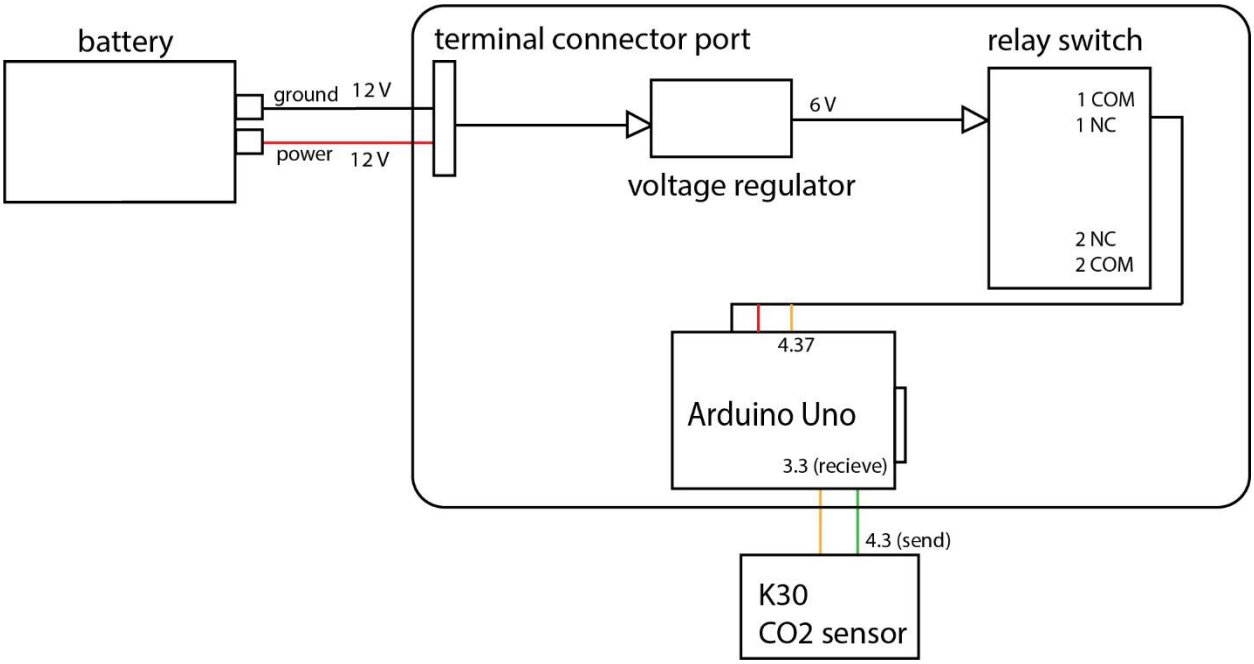

Figure S3.1. Schematic of CO2-LAMP connections with selected voltages when K30 is on. All connections are not shown.

3.10.1 CO2-LAMP Troubleshooting Guide

When the CO2-LAMP is working properly, you will have these signs:

- Clicking noise from the latching relay after the warm-up period and between measurement cycles
- Constant green light on top and bottom of Adafruit data logger shield
- A flash of red light next to label “SD” on the Adafruit data logger shield at the start of each measurement cycle
- Voltage running throughout the CO2-LAMP during measurement, limited voltage during sleep
- Blinking yellow/white light on the K30 (only visible before waterproofing) during measurement

1. If the date and time stamps are correctly formatted (e.g., YYYY/MM/DD HH:mm:SS) but are incorrectly assigned (e.g., 2018 instead of 2020), follow the protocol for sketch not properly uploaded.

2. If the sketch is not properly uploaded, follow this protocol:

A. Insert SD card into the Adafruit data logger shield.

B. Attach the CO2-LAMP to a 12V power source.

C. Attach the Arduino to a laptop or computer using USB A to B cable.

G. Download the CO2-LAMP sketch that you wish to use from github.

D. Open the sketch on the Arduino IDE App (downloadable from Arduino website)

E. Go to “tools” on the taskbar and make sure it reads “Board: Arduino Uno” on the dropdown list. Then, select “port” on the dropdown list and make sure “COM4: Arduino” is selected.

F. Go to “tools” then “Manage Libraries…” in the dropdown on the taskbar. Once the dialog box is open, enter “RTClib” where it says “Filter your search” and wait for the results to update. Once it appears, hit the button that says “install” with the option for the latest version.

G. Hit the arrow button just below the task bar. This will upload the sketch to the Arduino. There is no need to hit the “reset” button on the Arduino board, or to verify the sketch. There will be three warnings that appear which you can ignore. If there is a missing library, repeat step F with the library name.

3. If the SD card is producing a 0 KB size file, follow this protocol:

A. Check voltage at each solder point or connection point along the wire paths from power source to the K30. Below is a diagram of what the voltages should be at each solder point. If all of these voltages are correct, then move on to the next step. If they are not, stop and resolder the joint. Be especially careful to check ring terminals that were crimped on to end wires as they can become loose over time despite looking solidly connected. Lightly tug on wire connections to check for weak spots. Ensure connections are metal to metal. Melted wire insulation or other substances mixed in to solder connections will weaken connections that appear solid.

B. If all voltage readings match the diagram above, then solder joints can be ruled out as the problem. However, the other potential problems are: sketch not properly uploaded, faulty data logger, faulty step-down voltage regulator, faulty latching relay switch, or faulty K30. Try going through the protocols for each of these to determine the source of the problem.

4. If the hardware (i.e., data logger, voltage regulator, or relay switch) itself is faulty, replace it and follow protocol for SD card producing a 0 KB file size.

5. If you suspect a faulty K30, follow this protocol:

A. Insert SD card into the Adafruit data logger shield.

B. Attach the CO2-LAMP to a 12V power source.

C. Attach the Arduino to a laptop or computer using USB A to B cable.

D. Under “tools” on the taskbar select “Serial monitor”. Once the dialog box opens, wait for information about new measurements from the K30 to appear. If there are no CO2 measurements, there is either no power going to the K30 and the soldering connections need to be strengthened, or the K30 is faulty and must be replaced. If there are CO2 measurements, move on to the next step.

E. If there are accurate CO2 measurements, there is either a faulty SD card reader or faulty connections through the yellow, green, or black wires coming from the sensor. Give them a light tug to see if any connections are loose. If so, resolder the joints. Check the voltage readings to see if a connection that appears to be strong is still loose, and recut and resolder the wires if they are.

4 Coupling between lateral and vertical CO_2 exchange in some of the world's key wetland types

4.1 Abstract

To understand patterns in CO_2 partial pressure (P_{CO2}) over time in wetlands, we examined the relationship between P_{CO2} and land-atmosphere flux of CO_2 at the ecosystem scale at 22 Northern Hemisphere wetland sites synthesized through an open call. Wetlands spanned 6 major wetland types (tidal, alpine, fen, bog, marsh, and prairie pothole/karst), 7 Köppen climates, and 16 different years. Ecosystem respiration (Reco) and gross primary production (GPP), components of vertical CO_2 flux, were compared to P_{CO2}, a component of lateral CO_2 flux, to determine if photosynthetic rates and root respiration consistently influence wetland surface and porewater CO_2 concentrations across wetlands. Like drivers of primary productivity at the ecosystem scale, P_{CO2} was strongly positively correlated with air temperature (T_{air}) at most sites. Monthly average P_{CO2} tended to peak towards the middle of the year and was more strongly related to Reco than GPP. Our results suggest root respiration (R_{root}) may have a causal influence on temperature-normalized or biologically driven P_{CO2} in wetlands, but the relationship is site-specific and could be an artifact of differently timed seasonal cycles or other factors. Higher levels of discharge do not alter the relationship between Reco and P_{CO2}. This work offers a brief overview of the interplay between vertical and lateral C processes across wetland types and provides a basis for conceptualizing the role of lateral C export within the wetland C sink.

4.2 Introduction

4.2.1 Refining our understanding of the wetland C cycle

Global wetlands may contain as much as 71% of the biological C stored on land, despite making up less than 9% of global land area (Mitra et al., 2005; Zedler & Kercher, 2005). Evaluating lateral C export from wetlands is a crucial part of understanding global wetland C storage. Comparing wetland dissolved CO_2 concentrations to net ecosystem exchange (NEE, the net CO_2 flux from ecosystem to atmosphere [negative for CO_2 uptake]) rates could improve our understanding of the relationship between vertical C fluxes (NEE, GPP, and Reco) and lateral loss or movement of C (dissolved organic carbon (DOC), dissolved inorganic carbon (DIC)) (Bogard et al., 2020). NEE, unlike net ecosystem production (NEP), excludes gains and losses of DIC from biotic sources but includes abiotic CO_2 fluxes (e.g., from fire) (Chapin et al., 2006).

While vertical fluxes explain the exchange of C between ecosystems and the atmosphere, lateral fluxes are indicative of the exchange of C within and between ecosystems. Lateral fluxes depend on landscape connectedness, the concentration of C in surface water, and water flow (whether from groundwater, surface water, or precipitation). CO_2 partial pressure (P_{CO2}) is a component of DIC related to the concentration of dissolved CO_2 in water, mediated air-water gas exchange and Henry's law. It is thus an important aspect of measuring lateral gas exchange. We ask three main questions about lateral and vertical CO_2 flux through this work:

1. What are the average wetland soil porewater and surface water P_{CO2} concentrations?
2. Why might a relationship exist between lateral and vertical wetland CO_2 flux?
3. How does discharge mediate that relationship, if at all?

We hypothesize that GPP and Reco contribute to the biologically derived component of P_{CO2} in wetlands when there is low lateral import and therefore negligible external influence on P_{CO2}. Environmental factors such as air and water temperature (T_{air} and T_{water}), groundwater, and surface water are some examples of external influences which could obstruct a biological signal in P_{CO2}. Root respiration (R_{root}) and leaching of other root exudates could convert a fraction of CO_2 uptake by plants (GPP) into dissolved C in soil and water, which can then become part of lateral C flux. This is not unlike the plant-mediated relationship between GPP and subsequent FCH_4 in wetlands (Gomez-Casanovas et al., 2020; Turner et al., 2021). Relating lateral and vertical fluxes could become a challenge due to the compounding effects of T_{air} and water level. T_{air} will generally enhance wetland GPP but reduce P_{CO2}, while rising water level will typically increase GPP and P_{CO2} (Pugh et al., 2018).

4.2.2 Estimating wetland lateral carbon flows

Some evidence already exists for the complicated relationship between lateral and vertical CO_2 flux in wetlands (Santos et al., 2019; Schneider et al., 2020) and forests (Öquist et al., 2014). This relationship needs to be explored across different timescales, as environmental controls that affect lateral and vertical fluxes could change from the daily to annual scale. Measuring the strength of correlation between lateral and vertical wetland CO_2 exchanges using NEE, GPP, Reco, and dissolved CO_2 in wetland surface and porewater could improve estimations of wetland C sequestration rate and storage.

Table 4.1. Mean area-weighted average hydraulic residence times (HRTs) according to ecosystem type. Details about references used to make this table can be found in the Supplementary Information.

Ecosystem	**Marsh**	**Tidal**	**Fen**	**Bog**	**Alpine**	**Porewater**
Hydraulic residence time	0.4 hrs	5.6 hrs	1.6 days	2.9 days	17.5 days	23.7 days

In theory, wetland type as defined by hydrology (e.g., groundwater-fed fens, precipitation-fed bogs, tidal marshes, etc.) should impact the relationship between GPP and dissolved CO_2 due, in part, to differing hydraulic residence times, or HRTs (Table 1). Research shows tidal wetland HRT is typically shorter than other wetland types, followed by tidal creeks. Fen wetland HRTs are even greater and are inversely related to stage and discharge. Unsurprisingly, HRTs in bogs are much longer than other wetland types due to their unique precipitation-dependent hydrology. Coupling between vertical and lateral CO_2 exchanges in wetland surface and porewater could disaggregate similarly to wetland types and HRTs, with stronger coupling in alpine wetlands and porewater due to longer HRTs, lower flow rate, and therefore less external influence on P_{CO2}. Comparing lateral and vertical fluxes across wetland types can help categorize P_{CO2} concentrations and expand our understanding of how GPP or Reco relate to P_{CO2} and whether this conceptual framework is supported by observations.

4.2.3 How P_{CO2} relates to ecosystem fluxes

The primary objective of this study is to determine how GPP and Reco, components of vertical flux, relate to P_{CO2}, a component of lateral flux, in wetlands. We will do this by comparing GPP and Reco to P_{CO2} concentrations at different timescales, measuring the strength of coupling, and determining whether it is a direct or indirect link. We hypothesize that GPP and Reco are coupled to P_{CO2} in wetlands because of the physical connection between photosynthesizing plants, CO_2-respiring roots, and surface and porewater. Furthermore, there should be a stronger link between lateral and vertical flux during times with low lateral flow due to less signal noise from other inputs like groundwater, which can contribute incoming water of different chemistry and age characteristics (Pint et al., 2006).

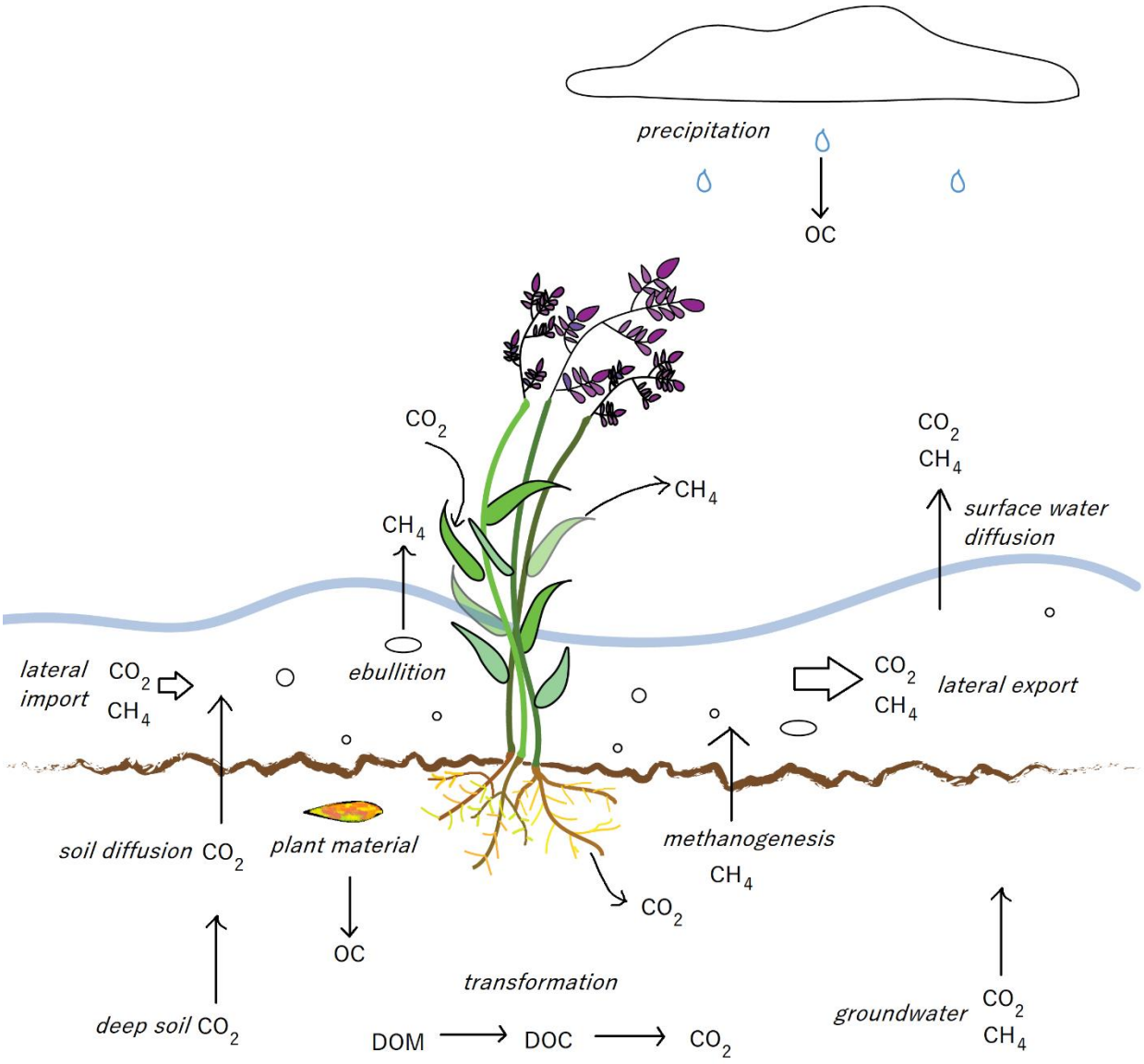

Figure 4.1. Examples of various contributions to lateral and vertical CO_2 and CH_4 wetland flux.

Numerous processes factor into lateral and vertical exchange of wetland CO_2 and CH_4 (Fig 4.1). Precipitation mixes with plant volatile organic compound emissions, pollution, and dust to provide organic matter to soils below (Ward et al., 2017). Photosynthetic uptake of atmospheric CO_2 prompts the release of CO_2 (though not necessarily the same molecule that was absorbed) through roots. Precipitation, root respiration of CO_2 and other exudates, and

decaying plant material provide organic carbon (OC) for soil organisms to consume. Methane produced by methanogenic soil microbes is then absorbed by plants. As xylem sap ascends from plant roots to leaves, dissolved CO_2 and CH_4 can diffuse through the stem or be released through leaves during transpiration, ultimately being emitted into the atmosphere (Vroom et al., 2022). Alternatively, methane and CO_2 produced in soils may be transported from soils to surface waters, then from surface waters into the air through diffusion or ebullition.

Groundwater is rich in CO_2 and CH_4 and its upwelling represents another important but highly variable gas source to soil porewater, surface water, and eventually the atmosphere. Groundwater to surface water turnover time is estimated to be 6-14 years, which necessitates long term monitoring studies to accurately estimate landscape-level carbon budgets and their decadal variability (Downing & Striegl). Similarly, deep soil may release CO_2 to surface soils during the transition from warmer to colder months, which can then diffuse into surface and porewater (Campeau et al., 2021). Lateral import of CO_2 and CH_4 tends to be lower than export in wetlands but is still a fundamental and understudied aspect of wetland C cycling.

C is continuously transformed as these dynamic wetland processes take place. Labile DOC is oxidized to DIC (of which CO_2 is one form), which is then exported laterally or diffused from surface water to the atmosphere. Organic substrates and DOC are biologically transformed (e.g., decomposition or degradation) into inorganic C. Additional processes contributing to the transformation and cycling of wetland C include weathering, snowfall, coastal outwelling, anthropogenic disturbances, and more. Transformation of wetland DOC into

DIC is more thoroughly discussed from the coastal ecosystem perspective in Santos et al., (2021).

4.3 Methods

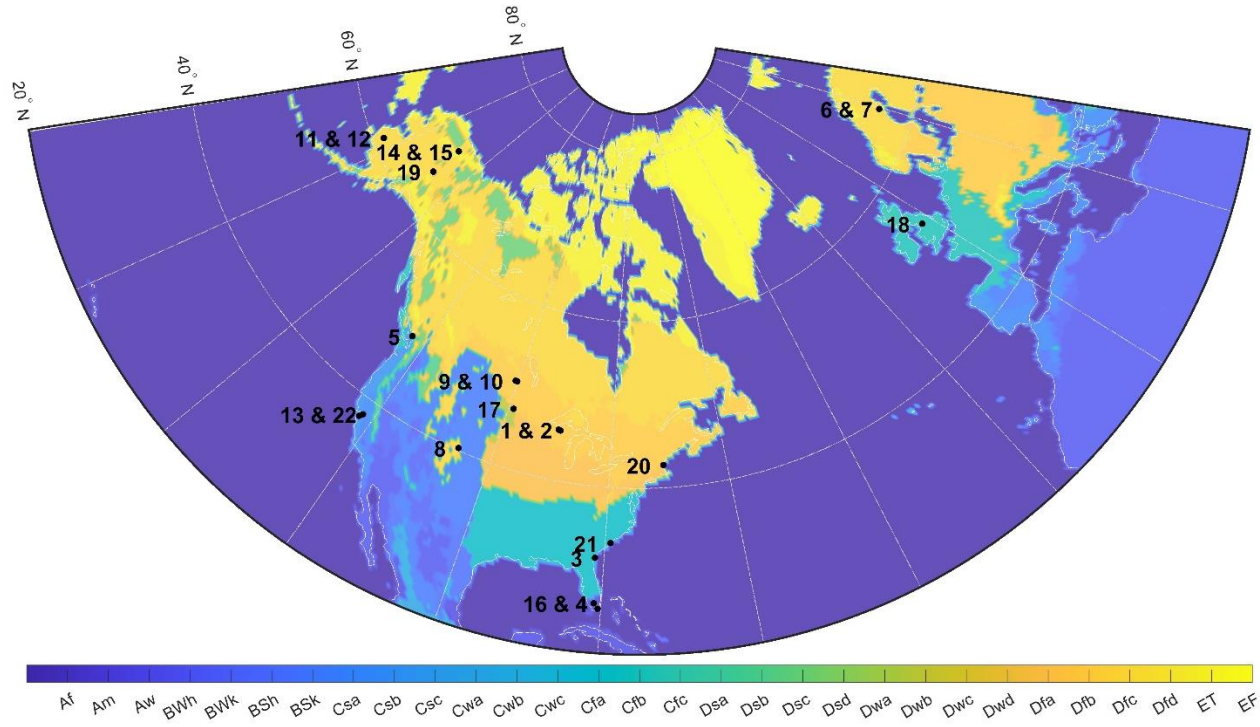

Figure 4.2. Köppen climate map of study sites. Numbers represent each site listed in Table 4.2. Köppen classifications in the legend are listed according to the codes in Table S3 (Supplementary Information). Meridians are shown every 20° from -180 to 30°.

4.3.1 Experimental Design

Through an open call, we synthesized measurements of lateral and vertical CO_2 flux across 22 Northern Hemisphere wetland sites (Fig 4.2). Our goal was to collect data on GPP, Reco, $P_{CO2,}$ and related variables (i.e., T_{air}, T_{water}, WTD, discharge) across sub-diel, diel, and monthly scales to test the relationship between lateral and vertical wetland flux. To determine typical wetland soil porewater and surface water P_{CO2} concentrations (Question 1), we

compared high-frequency P_{CO2} time series measurements from multiple wetland types and locations and identified significant differences using ANOVA testing.

To establish whether a relationship exists between lateral and vertical wetland CO_2 flux (Question 2), we needed data on daily and seasonal cycling of vertical fluxes at sites with lateral flux. We tested our hypothesis that lateral and vertical wetland CO_2 fluxes are related by comparing diel and seasonal cycles and performing nonparametric regressions of lateral and vertical flux at sites with at least three months of concurrent half-hourly or hourly data.

The question of how discharge mediates the relationship between lateral and vertical flux (Question 3) required concurrent sub-daily scale data on wetland Reco or GPP, P_{CO2}, and discharge from multiple sites. To test our hypotheses, we identified a subset of three wetlands (Eden Landing Ecological Reserve (US-EDN), Allequash Creek Wetland Site (US-ALQ), and Degerö Stormyr (SE-Deg)) with sufficient data for further analysis. Lateral and vertical fluxes from the subset were compared across times with no, low, medium, and high discharge rates at each site. These flow regimes were defined as 0-25th percentile, 25th-50th percentile, 50th-75th, and 75th-100th percentile discharge rates at each site.

4.3.2 Site Descriptions

Sites were found through web search (Google Scholar), solicited online (FLUXNET listserv, Twitter, email) and by word-of-mouth (Table 4.2). Sites included in the synthesis needed to have *in-situ* P_{CO2} data from within the wetland or in a nearby (<1 km) wetland stream outlet, as well as light chamber flux measurements only for sites with dominant low-lying vegetation or eddy covariance flux measurements for sites with scrubs, shrubs, tall grasses, or tree cover.

Observations of water table depth (WTD) and air or water temperature (T_{air} or T_{water}) were helpful but not necessary for sites to be included in analysis.

Although high frequency measurement was not a criterion for site selection, only sites with at least 5 months of data coverage were included in seasonal cycle plots, and those with at least 5 measurements for each hour, for at least 10 hours per day, were included in diel cycle plots. Sites with a WTD range of 0.4 m or more were included in comparisons of WTD and P_{CO2}. Sites with a T_{air} range of at least 10°C were included in the comparison of T_{air} and P_{CO2}. Sites with at least three continuous months of daily-scale resolution or finer P_{CO2}, GPP, Reco, and T_{air} or T_{water} were used in signal analysis, which included evaluations of magnitude-squared coherence between temperature-normalized P_{CO2} and GPP and linear correlation of biologically derived P_{CO2} ($P_{CO2\ BIO}$), GPP, and Reco.

Table 4.2. Study sites used in analysis. Years do not necessarily represent continuous periods of measurement.

Years	2020	2021 (NEE & porewater P_{CO2})	2021	2022	2016-2017	2015-2018 (surface water	2018-2022 (P_{CO2}), 2021-	1996 (NEE), 2013-2019
Latitude, Longitude	46.0827, -89.9792	46.0308, -89.6067	31.4441, -81.2835	25.3539, -80.3810	49.1293, -122.9849	64.1833, 19.5500		40.2900, -105.6670
Köppen Climate	Humid continental	Humid continental	Humid subtropical	Savanna	Mediterranean	Subarctic	Subarctic	Subarctic
Location	Rhinelander, Wisconsin, USA	Rhinelander, Wisconsin, USA	Sapelo Island, Georgia, USA	Greater Everglades Ecosyste	Delta, British Columbia, Canada	Vindeln, Sweden	Gävleborg County, Sweden	Rocky Mountain National Park,
Site Abbreviation	Lost Creek Wetland (US-Los)	Allequash Creek Site (US-ALQ)	Georgia Coastal Ecosystems LTER	Everglades Saltwater Intrusion	Delta Burns Bog (CA-DBB)	Degerö Stormyr (SE-Deg)	Trollberget rewetted peatland	Loch Vale (LV)
Reference	Desai, 2022	Crawford et al., 2017; Olson,	Hawman et al., 2021; Turner et		D' Acunha et al., 2019; Christen	Nilsson & Peichl, 2020; Campeau		Mast et al., 1998; Wickland et al.,
Site #	1	2	3	4	5	6	7	8

2021	2021	2022	2022	2017-2021	2007-2017	2016
50.3705, -100.5339	50.3623, -100.2024	61.2723, -163.2228	61.2548, -163.2590	38.0499, -121.7650	68.6058, -149.3110	41.3795, -82.5125
Humid continental	Humid continental	Subarctic	Subarctic	Mediterranean	Tundra	Humid continental
Manitoba, Canada	Manitoba, Canada	Yukon Delta National Wildlife	Yukon Delta National Wildlife Refuge, Bethel, Alaska and St. Mary's Village, Alaska, USA	Sherman Island, Sacramento County, California, USA	Imnavait Creek, Alaska, USA	Huron, Ohio, USA
Manitoba Prairie Pothole Wetland,	Manitoba Prairie Pothole Wetland,	Yukon-Kuskokwim Delta, Izaviknek-	Yukon-Kuskokwim Delta, Izaviknek-Kingaglia uplands, Unburned (YKD2)	Mayberry wetland (US-Myb)	Imnavait Creek Watershed Wet Sedge Tundra (US-ICs)	Old Woman Creek (US-OWC)
		Zolkos et al., 2022	Zolkos et al., 2022	Hatala Matthes et al., 2021	Kling, 2019	Bohrer et al., 2019; Bohrer & Kerns, 2022
9	10	11	12	13	14	15

2015-2016 (P_{CO2} only)	2010–2016 (P_{CO2} only)	2022	2016	2018-2019	2020
25.9896, -80.9279	47.0992, -99.0992	53.5158, -1.9837	64.701, -148.313	42.7345, -70.8382	33.3455, -79.1957
Savanna	Humid continental	Temperate oceanic	Subarctic	Humid continental	Humid subtropical
Greater Everglades Ecosystem, Florida, USA	Jamestown, North Dakota, USA	South Pennines, UK	Fairbanks, Alaska, USA	Plum Island Sound, Massachusetts, USA	Georgetown, South Carolina, USA
Big Cypress National Preserve (Big Cypress)	Cottonwood Lake Study Area	Restored peatlands of south Pennines (SP)	Alaska Peatland Experiment (APEX)	Plum Island Ecosystem (PIE)	North Inlet Crab Haul Creek (US-HB1)
	Gleason et al., 2009; Tangen &		Euskirchen, 2022; Euskirchen et al., 2019; Rupp 2019		Forsythe, 2020a
16	17	18	19	20	21

2021
37.6156, -122.1140
Mediterranean
San Francisco Bay, California, USA
Eden Landing Ecological Reserve (US-EDN)
Shahan, 2022
22

4.3.2.1 Tidal

Tidal wetlands featured in the study occupied both the east and west coasts of the United States (Fig 4.2, Table 4.2). Different fluctuations in tide height were observed during each tidal cycle across sites, with water level at some wetlands fully receding below the marsh surface every day and staying above the surface for the entire study duration at others. More information on all wetlands included in the study can be found in the Supplementary Information.

4.3.2.2 Alpine

One alpine wetland located within the Loch Vale watershed of Rocky Mountain National Park was included in the study. The wetland is vegetated, but the surrounding watershed is dominated by bare rock. Snow cover can last up to 8 months of the year, making snowmelt and buildup of gases under snow and ice important means of gas production and transport.

4.3.2.3 Prairie Potholes and Karsts

Prairie potholes featured in the study included ecosystems of both Canadian and US Prairie Pothole Regions (PPR), which have been the subject of many studies on soil organic C stocks under different land management practices (Loder & Finkelstein, 2020; Tangen & Bansal, 2020; Bansal et al., 2021). These wetlands are shallow freshwater marshes formed by glaciers retreating from the landscape during the Pleistocene. Surface water is sourced mainly by precipitation, leading to bog-like hydrology.

Seasonally flooded karst wetlands of the Big Cypress National Preserve in Florida have similar shallow depths, with bedrock interface occurring around 2 meters or less (Ward et al.,

2020). However, these depressional wetlands formed under much different conditions (e.g., bedrock dissolution by acid-rich rainwater) slightly more recently, during the transition from Pleistocene to Holocene. Groundwater lies on a shallow aquifer directly below the soil surface.

4.3.2.4 Bogs, Fens, and Marshes

Bogs featured in the study were previously disturbed for different reasons but have since been restored through active or passive rewetting techniques. Wetlands of South Pennines, United Kingdom were dominated by sedge (*Eriophorum vaginatum* and *E. angustifolium*) whereas the Canadian peat bog was dominated by both sedge and moss (*Sphagnum spp.*).

Fens incorporated in the study had a range of freshwater sources, from upland forest runoff to river flow to mountain snowmelt. Fen wetlands had a range of disturbance levels, including preservation, natural burning, and draining followed by rewetting. Site locations included Alaska, the midwestern USA, and Sweden.

Surface water from only one freshwater marsh was included in the study. The wetland was impounded for restoration purposes, leading to low surface water flows between inlets and outlets controlled by wind and environmental management. Droughts in the region can lead to salinization due to saltwater intrusion and reduction of typically constant water table levels.

4.3.2.5 Porewater

Sites with porewater data included two riverine fens, a boreal rich fen peatland, a range of wetland types (peatland plateaus, peatland ponds, and fen channels) in Alaska, and a

frequently flooded natural freshwater estuary with marsh hydrology. Dominant vegetation types varied across wetlands with porewater data. More details can be found in the Supplementary Information.

4.3.3 Data Processing

P_{CO2} was measured directly through automatic or manual sampling at each site. P_{CO2} concentrations of manual samples were determined using gas chromatography with flame ionization detection (GC-FID) or isotope ratio mass spectrometry (IRMS). Automated sampling of P_{CO2} was performed with different infrared gas analyzers (IRGAs) across sites (Table S4.2). Eddy covariance CO_2 flux data (NEE) were gap-filled and partitioned into GPP and ecosystem respiration (Reco) using marginal distribution sampling (MDS) and the daytime-based algorithm available through the online tool, REddyProc (Lasslop, 2010; Wutzler et al., 2018). Raw flux data were made available upon request following site data sharing policies or collected through those available under the CC-BY4 license on FLUXNET or AmeriFlux archives. More details on sampling techniques, methods, and references can be found in Supplementary Information.

4.3.4 Statistical testing

Significant differences in daily and annual average P_{CO2} concentrations according to wetland type were determined with ANOVA testing. Sites with at least 5 representative months from a single year were included in the seasonal analysis, and monthly data was averaged together across years. Sites with at least 5 measurements per hour for at least 10 hours per day were used in diel cycle analysis. The influence of T_{water} was removed using Equation 1 (Takahashi et al., 2002). T_{mean} is the average T_{water} in °C during the study period and T_{obs} is the

observed T_{water}. T_{air} is used if there is no T_{water} data for the site. P_{CO2} at T_{mean} is the temperature normalized P_{CO2} (ppmv). Biologically derived P_{CO2} ($P_{CO2\ BIO}$) was estimated from P_{CO2} according to Equation 2 (Takahashi et al., 2002). Max and min are the maximum and minimum daily average concentrations for each month.

Equation 4.1:

$$P_{CO2\ at\ Tmean} = P_{CO2} e^{[0.0423(T_{mean} - T_{obs})]}$$

Equation 4.2:

$$P_{CO2\ BIO} = (P_{CO2\ at\ Tmean})_{max} - (P_{CO2\ at\ Tmean})_{min}$$

4.4 Results

4.4.1 P_{CO2} varies according to wetland type

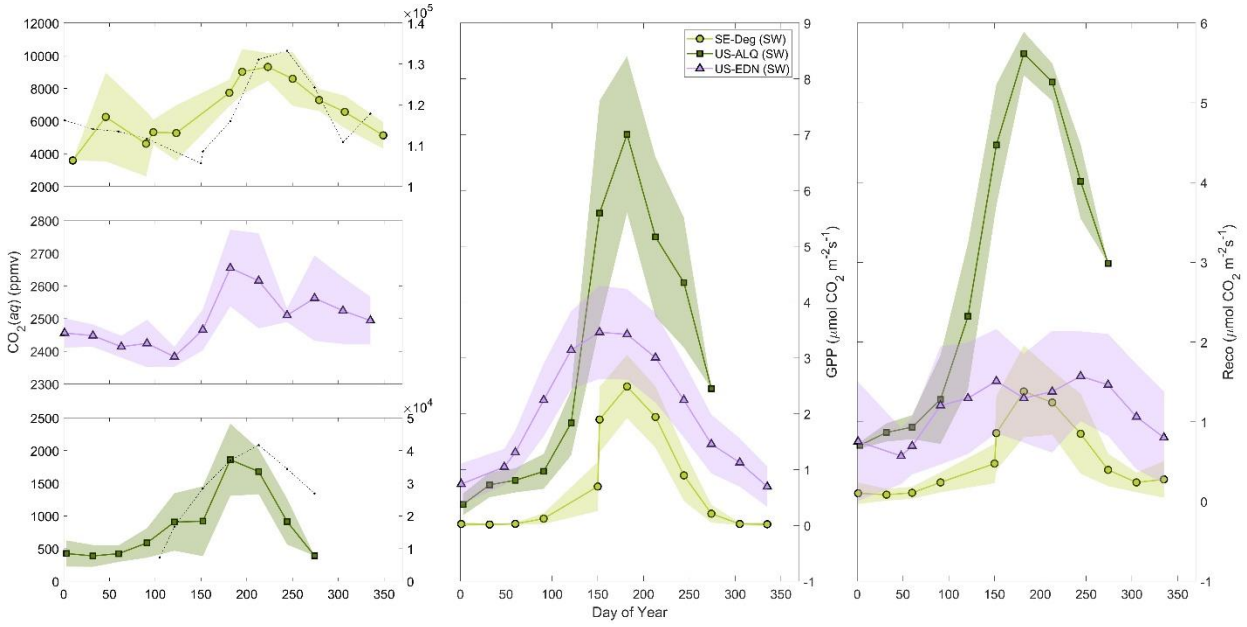

Figure 4.3. Monthly averages of P_{CO2} in (A) surface water (left axis) and soil porewater (right axis) at SE-Deg (B) surface water at US-EDN (C) surface water (left axis) and soil porewater (right axis) at US-ALQ (D) GPP and (E) Reco.

Overall, there were more than 120,000 P_{CO2} datapoints. The greatest amount of datapoints were recorded between noon and 1 pm (4.2%), and the lowest amount of datapoints were recorded at 5 am (4.1%). All wetlands included in the study demonstrated seasonal and diel cycles of P_{CO2}, GPP, and Reco (Fig 4.3; Figs S4.1-4.6). Monthly average photosynthetic CO_2 uptake reached a maximum in June for all wetland types. Fens and bogs demonstrated the lowest monthly average GPP compared to other wetland types. Annual mean GPP at the alpine wetland Loch Vale was on the higher end of published ranges for alpine tundra wetlands (118-631 gC m^{-2} yr^{-1}; Lu et al., 2017; Table S4.4). Cumulative annual GPP for the impounded marsh US-Myb was on the higher end of published ranges for intertidal marshes (1,023-1513 gC m^{-2} yr^{-1}). Annual mean GPP for fens, bogs, and prairie potholes/karsts in this study aligned with published ranges for other peatlands (201-869 gC m^{-2} yr^{-1}) and freshwater shrub swamps (248-856 gC m^{-2} yr^{-1}).

Daily and monthly average P_{CO2} was more strongly correlated with Reco than GPP, in both surface and soil porewater. The strongest relationships between daily average Reco and P_{CO2} occurred at US-ALQ in porewater ($R = 0.84$, $p<<0.01$) and surface water ($R = 0.77$, $p<<0.01$). The weakest correlations between P_{CO2} and GPP or Reco were in US-EDN surface water ($R = 0.05$ and 0.07, respectively, $p<<0.01$). Surface water P_{CO2} was more closely related to daily average GPP and Reco at SE-Deg ($R = 0.61$ and 0.68, respectively, $p<<0.01$) than porewater P_{CO2} ($R = 0.12$ and 0.22, respectively, $p<<0.01$).

Wetland type did not influence annual average P_{CO2} concentrations (ANOVA $p=0.24$). However, shifts in P_{CO2} concentrations throughout the year did appear to be related to wetland

type (Fig S4). Monthly average P_{CO2} typically reached the highest concentrations of the year sometime in August for most fens, bogs, marshes, prairie potholes and karsts, and porewater. The highest monthly average P_{CO2} at these wetlands were observed at least one month after peak CO_2 uptake. The exception was the alpine wetland, where P_{CO2} peaked in April, prior to the month with the highest photosynthetic CO_2 uptake. Monthly average P_{CO2} at the alpine wetland appeared to be linked to snow depth (Fig S4.7). More concurrent alpine wetland data would be necessary to confirm this.

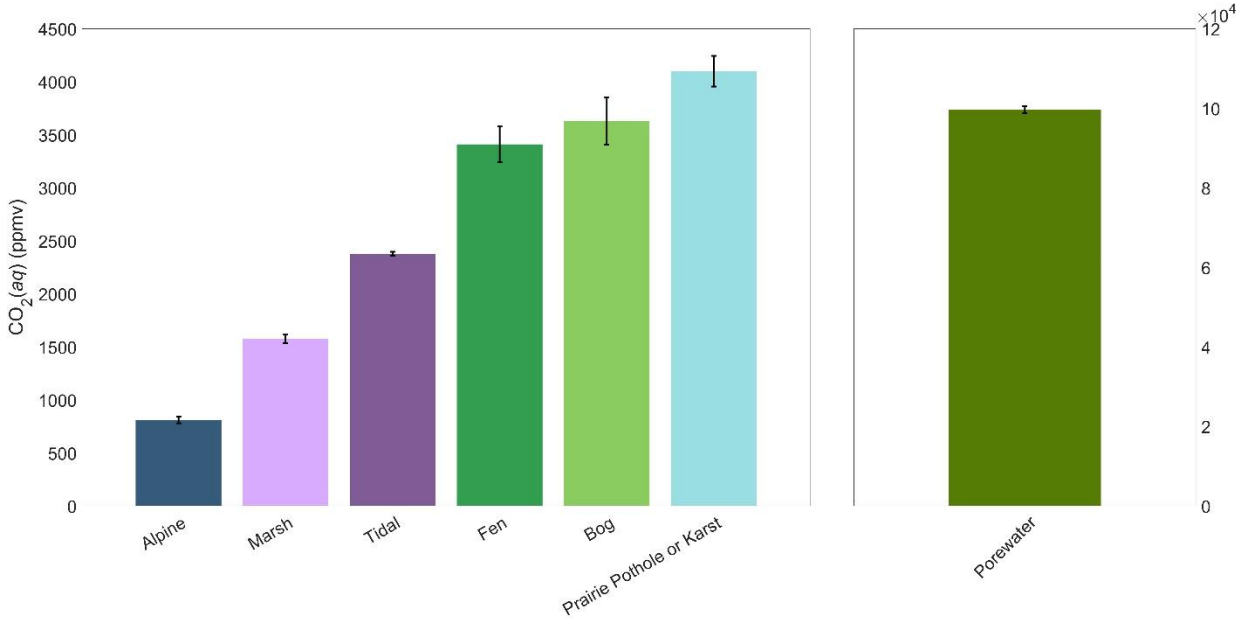

Figure 4.4. Bar graph of daily average P_{CO2} across (A) wetland types and (B) porewater. Error bars represent standard error of the mean.

Diel P_{CO2} cycles varied across and within wetland types (Figs S4.1 & 4.2). For example, P_{CO2} followed a semidiurnal pattern (i.e., completing a full cycle twice a day) at only three of 4 tidal wetlands (Fig S4.6). P_{CO2} also appeared to fluctuate with T_{water} in some tidal wetlands (Fig S4.8) but was driven by changes in tide height in others (Fig S4.9). Daily average P_{CO2} was also dependent on wetland type (ANOVA p<1e-10). Daily average P_{CO2} was lowest at the alpine

wetland at 811 ppm on average and was statistically significantly different from the next highest categories of marshes and tidal wetlands, which exhibited very similar daily average P_{CO2} concentrations of 1,574 and 1,755 ppm, respectively (Fig 4.3). Fens had neither the highest nor the lowest daily average P_{CO2} concentrations and were distinct from other wetland categories, averaging 3,040 ppm. Bogs and prairie potholes or karsts showed the highest daily average P_{CO2} concentrations of 3,629 and 4,099 ppm, respectively and had no statistically significant differences between wetland types. Daily average porewater P_{CO2} was an order of magnitude higher than the highest daily average surface water concentrations at 18,014 ppm.

All wetland types demonstrated similar diel CO_2 cycling, emitting less than 5 $\mu molm^{-2}s^{-1}$ CO_2 at night, and absorbing up to 14 $\mu molm^{-2}s^{-1}$ CO_2 during the day through photosynthesis from approximately 5 am until 8 pm. The highest photosynthetic CO_2 uptake occurred towards the middle of the day for all sites, despite differences in diel cycles of P_{CO2}. Within wetland categories, some wetlands were weaker C sinks than others.

4.4.2 Relationship of P_{CO2} to drivers

Wetland type influenced the relationship between P_{CO2} and T_{air}, as was evidenced by the strong correlation between P_{CO2} and T_{air} at the alpine wetland ($R^2 = 0.93$), which was higher than any other wetland site (Fig S4.11). T_{air} only had a negative impact on P_{CO2} at the alpine wetland and one tidal wetland. Fens, bogs, and marshes presented the highest positive correlations between daily average P_{CO2} and T_{air} (R^2 = 0.38 to 0.89), followed by porewater (R_2 = 0.48 to 0.75), with an average R^2 of approximately 0.6 for wetlands from both categories. The

correlation between P_{CO2} and T_{air} was weakest at prairie potholes/karsts (R^2 = 0.15) and tidal wetlands (R^2 = 0.22 to 0.41).

The relationship between P_{CO2} and WTD was not as distinct. Higher WTD corresponded to higher P_{CO2} in some wetlands but corresponded with lower P_{CO2} at others (Fig S4.12). WTD and P_{CO2} were strongly linked in some wetlands, but there was a wide range of R^2 within and across categories, ranging from R^2 = 0.03 at the lowest (a prairie pothole) to R = 0.94 at the highest (a bog). Wetland type did not appear to have an impact on the strength of correlation or whether the relationship was positive or negative.

4.4.3 Direct and indirect links of vertical to lateral wetland CO_2 flux

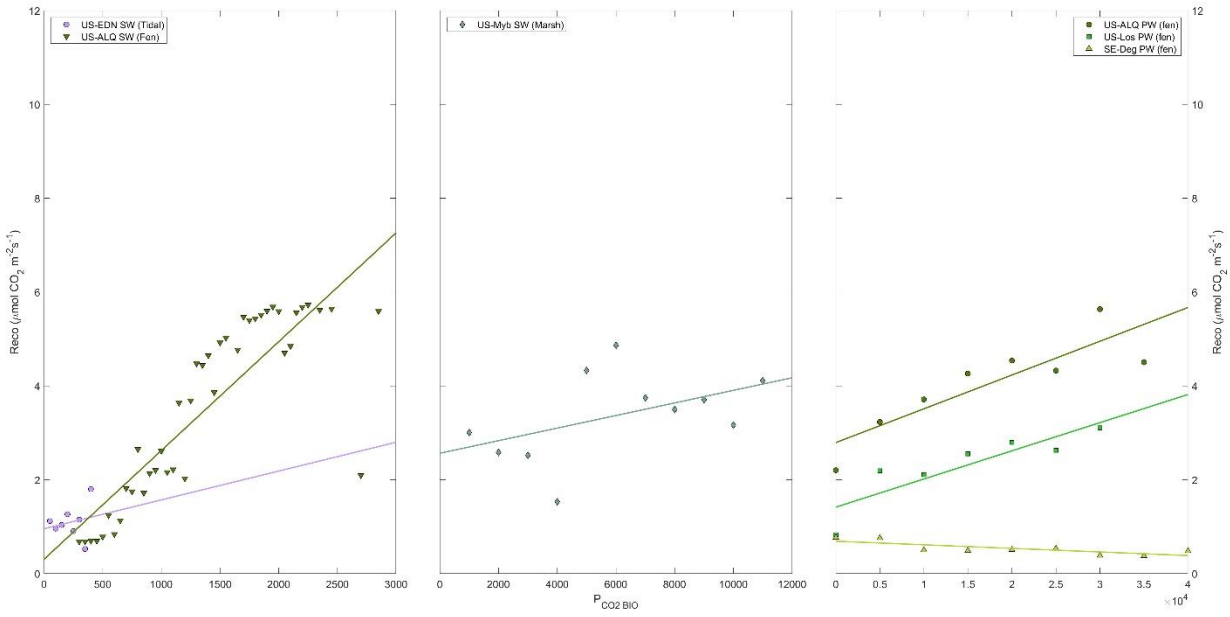

Figure 4.5. Biologically derived daily resolution $P_{CO2\ BIO}$ versus Reco in (A) surface water in a tidal wetland and fen bin-averaged every 50 ppmv, (B) nontidal marsh bin-averaged every 1,000 ppmv, and (C) porewater bin-averaged every 5,000 ppmv. Solid lines represent the linear fit.

T_{water} influence was removed prior to analysis for fen SE-Deg, which reduced the correlation coefficient of daily average T_{water} and P_{CO2} from R = 0.54 to -0.47. T_{water} did not have a positive influence on daily average surface water P_{CO2} at marsh US-Myb, tidal wetland US-EDN, or fen US-ALQ, and therefore was not removed. T_{air} had a positive influence on daily average porewater P_{CO2} at fens US-Los and US-ALQ (R = 0.68 and 0.71, respectively), which was reduced after removal (R = -0.38 and 0.25, respectively). There was a consistent relationship between daily resolution Reco and $P_{CO2\ BIO}$ in porewater and surface water at four out of 5 sites, although the strength of correlation was site-specific (Fig 4.5).

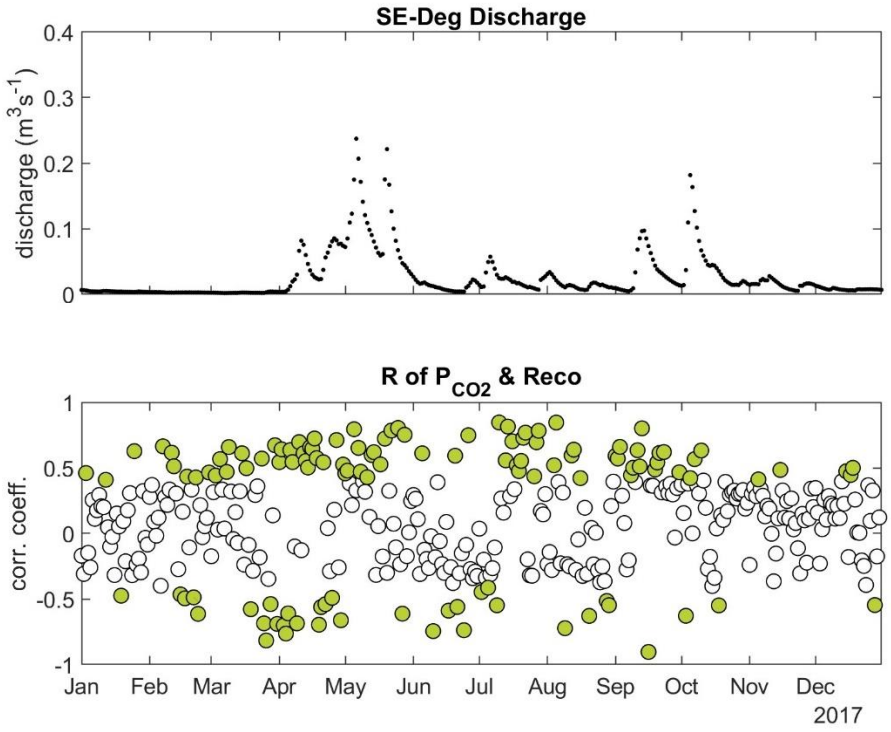

Figure 4.6. (A) Daily average discharge and (B) correlation coefficient between hourly porewater P_{CO2} and Reco for each day at SE-Deg in 2017. Filled circles represent significant correlations.

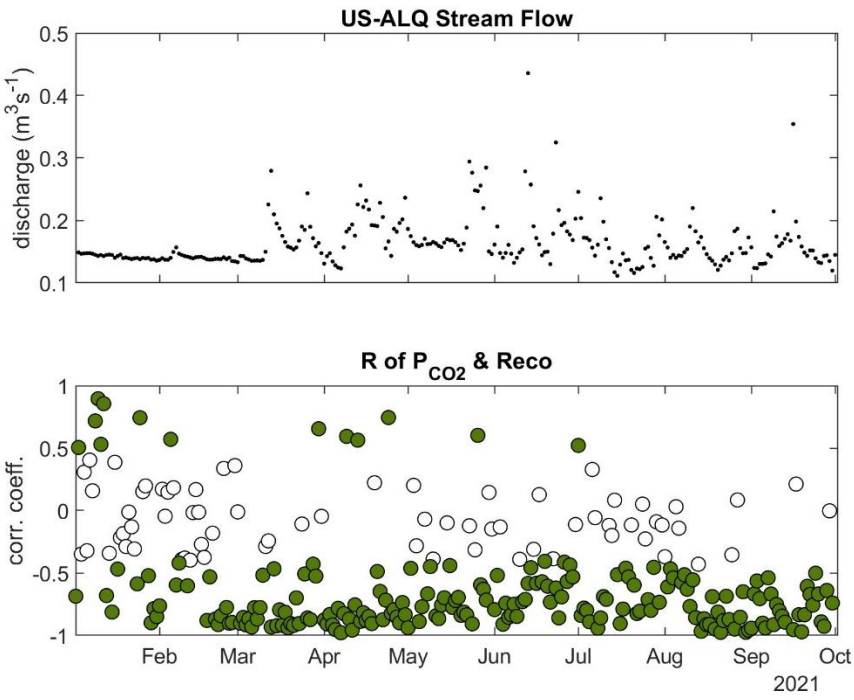

Figure 4.7. (A) Daily average discharge and (B) correlation coefficient between half-hourly surface water P_{CO2} and Reco for each day at US-ALQ. Filled circles represent significant correlations.

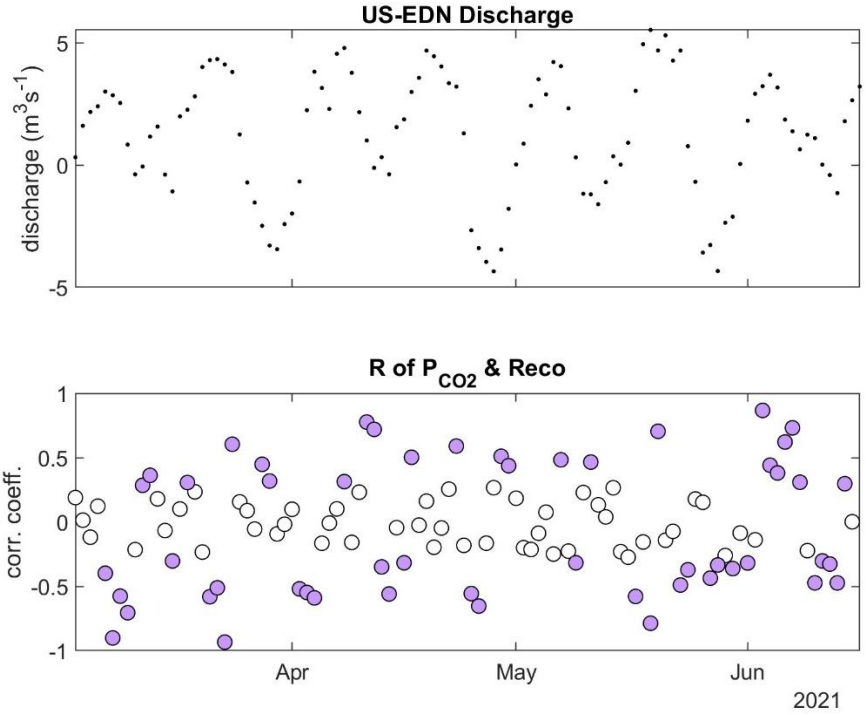

Figure 4.8. (A) Daily average discharge and (B) correlation coefficient between half-hourly surface water P_{CO2} and Reco for each day at US-EDN. Filled circles represent significant correlations.

Flow did not appear to mediate the relationship between P_{CO2} and Reco (Figs 4.6-4.8), or GPP (data not shown). Days with significant correlations between P_{CO2} and Reco or GPP were randomly distributed amongst flow regimes. For example, at US-EDN there were 24 low or no flow days with significant correlations between P_{CO2} and GPP (R = 0.16, on average) and 27 low or no flow days with significant correlations between P_{CO2} and Reco (R = -0.06, on average). There were 21 medium or high flow days with significantly correlated P_{CO2} and GPP at US-EDN (R = -0.12, on average) and 25 medium or high flow days with significantly correlated P_{CO2} and Reco (R = -0.06, on average).

Results at US-ALQ and SE-Deg were similar, with significant correlations in sub-daily scale measurements being randomly distributed amongst flow regimes. There were 119 no-flow days with significant but weak correlation between P_{CO2} and GPP at SE-Deg (R = 0.20, on average) and 145 high-flow days with significant correlation between P_{CO2} and GPP (R = 0.33, on average). Twenty-six high flow days showed significant correlation between P_{CO2} and GPP at US-ALQ (R = -0.61). Similar correlations between P_{CO2} and GPP at US-ALQ also existed on low (R = -0.40) and no flow days (R = -0.60).

4.5 Discussion

4.5.1 Diel and seasonal cycles of lateral and vertical wetland fluxes

We hypothesized that R_{root} and root exudates would cause physical coupling between GPP or Reco and P_{CO2}, with the strongest links occurring during times of low flow or in wetlands with longer HRTs and therefore lower flow rates. Results showed that GPP, Reco, and P_{CO2} have similar seasonal cycles across all wetland types except alpine wetlands and are related on the daily scale but not at other frequencies. Daily average P_{CO2} was more variable within and across wetland types than monthly averages. Hydraulic residence times did appear to have a general impact on P_{CO2}, with daily average concentrations increasing from marshes to tidal wetlands, fens, bogs, and then porewater (Fig 4.4), except for alpine wetlands. This could be due to HRT being lowest immediately following snowmelt in alpine ecosystems, then returning to a longer residence time for the rest of the year. However, information on residence times at each site throughout the study period would be necessary to confirm this.

The diel signal of wetland P_{CO2} observed at all sites in this study was unique compared to other systems such as headwater streams, where some sites lack any diel signal (Crawford et al., 2017). Diel P_{CO2} reached a maximum at nighttime in some wetlands, suggesting that root respiration increases P_{CO2} in surface water at night and strengthening our hypothesis that lateral and vertical CO_2 exchange are potentially related. This finding aligns well with results from another study on stream P_{CO2} (Attermeyer et al., 2021). However, this could also be due to higher midday water temperatures decreasing CO_2 solubility and releasing surface water CO_2 into the atmosphere. Other wetlands achieved maximum concentrations at midday, which was

opposite to expectations if the two variables are linked. This relationship has previously been observed in an ultra-oligotrophic lake, where photosynthetic uptake was not clearly related to dissolved CO_2 (Eugster et al., 2022). Our analyses supported the idea that lateral and vertical CO_2 exchange in wetlands are linked on a daily scale but not at lower frequencies, such as the seasonal scale.

4.5.2 Optimal measurement frequencies

The location of single P_{CO2} sensor may not necessarily be representative of wetland P_{CO2} within the entire eddy covariance tower footprint or whole wetland. Additionally, light soil respiration chambers placed over vegetated zones will likely capture higher CO_2 fluxes as result of their influence on microbial respiration and other factors (Wang et al., 2016). Annual average fluxes can also range between sinks and sources at different locations within the same forested site, as in Sakabe et al (2015). As a result, we focused on seasonal and diel cycles of P_{CO2} and GPP, averages across entire study periods, and direct links rather than P_{CO2} concentrations at individual sites or at specific times.

Optimal measurement frequency was determined to be the point at which the linear relationship between a subset of the original data and the original dataset had a correlation coefficient of R decreased below 0.8. There was a steep decline in representativeness of daily average P_{CO2} if measurements were made less than 40 times per day, highlighting the importance of continuous half-hourly measurement of P_{CO2} (Figure S4.10). Sub-daily scale measurements are also important for capturing the coherence between daily cycles of GPP and temperature normalized P_{CO2} in some wetlands. Measurements should be made at least 50

times per year to accurately estimate annual average concentrations (R = 0.8 with annual means), and 3 or more times per month for accurate monthly average estimations (R = 0.8 with monthly means).

4.5.3 Study limitations

Complexities in wetland C cycling make it difficult to compare GPP, Reco, and dissolved CO_2 in surface and soil porewater. A multitude of biological processes, such as groundwater upwelling, create statistical noise that could interfere with the signal of plant productivity or R_{root} in dissolved CO_2 concentrations. The main limitation of this study was the lack of data on the multiple external influences on wetland surface and soil porewater CO_2, followed by a lack of wetland sites with concurrent high-frequency lateral and vertical flux measurements. High-frequency, concurrent measurements of discharge rate and lateral import of P_{CO2} are also essential to calculate net lateral export as P_{CO2}. Groundwater, surface water, and precipitation all play varying roles in P_{CO2} concentrations and fluctuations across wetland types and are often site-specific.

Despite the difficulty in parsing out biological signal from P_{CO2}, its measurement is valuable because it exchanges more readily with the atmosphere than other forms of DIC. Inorganic C is also the least measured NECB term and makes up the majority of hydrologic C export and the majority of soil C (Bogard et al., 2020; Zhao et al., 2018). Although wetland DOC export at some sites is estimated to be an order of magnitude lower than DIC export, its measurement is equally as important because it is often a limiting factor on biota and plays a

role in microbial metabolism, nutrient cycling, and UV light in the water column (Megonigal & Neubauer, 2009; Korbel & Hose, 2011).

New research is attempting to refine these less understood aspects of the wetland C cycle by quantifying the coastal wetland contribution of DIC to the ocean or developing new frameworks for analyzing landscape-level fluxes. In fact, viewing wetland C within the context of watersheds as part of a net watershed exchange (NWE) could be the solution to improving estimations of lateral export (Casas-Ruiz et al., 2023). Our work suggests that as the planet warms and the contributions of different sources to runoff increase (e.g., rainfall) or decrease (e.g., snow and glacier melt), the influence on lateral export as P_{CO2} may be unpredictable (Cui et al., 2023). Long-term monitoring of discharge, GPP, Reco, WTD, T_{air}, P_{CO2}, and HRTs could help improve our understanding of drivers of lateral CO_2 export from global wetlands.

Scientific understanding of wetland lateral CO_2 flux will also benefit from better spatial data resolution. There were no wetlands in our study from South America, which contains the largest wetland surface area out of any continent (Junk, 2013). Concentrations of surface water P_{CO2} in floodplain wetlands of the northwestern Brazilian Amazon ranged 896-13,530 ppmv, the upper end of which is higher than the monthly average of most sites presented in this study (Belger et al., 2011). Forested wetlands near Lake Janauacá in the central Amazon basin of Brazil also had high P_{CO2}, ranging from 664-11,006 ppmv (Amaral et al., 2020). P_{CO2} in a sewage-fed aquaculture pond in the East Kolkata wetlands of India were even higher, reaching as high as 21,140 ppmv (Bhattacharyya et al., 2020). A study on wetland plant physiological performance under flooding stress in the Pantanal determined that the wetland plant communities are well adapted to changing soil conditions caused by intense flooding followed

by an intense dry season (Dalmagro et al., 2016). Comparing seasonal and diel cycles of surface water and porewater P_{CO2} and GPP in tropical wetlands such as these will likely reveal unique and surprising relationships among environmental variables.

4.6 Summary

This study explored possible linkages between lateral and vertical CO_2 exchange according to wetland type by comparing seasonal and diel cycles, measuring the strength of coupling, and determining whether there was a direct or indirect link by removing the influence of T_{water} or T_{air} and estimating $P_{CO2\ BIO}$. Initially, it was believed that a possible relationship might exist between GPP, Reco, and P_{CO2} due to the physical connection of photosynthesizing plants to surface and porewater through roots. We hypothesized that a signal from root respiration of CO_2 and other exudates would appear in dissolved CO_2 in wetlands with longer HRTs and during periods of low flow.

Results showed that there were no statistically significant differences in yearly average P_{CO2} according to wetland type. However, daily average P_{CO2} was affected by wetland type, with alpine wetlands producing the lowest amounts of surface water dissolved CO_2, and the highest concentrations existing in bogs and prairie potholes/karsts. Porewater P_{CO2} was an order of magnitude greater than the highest daily average surface water concentrations, likely due to the dampened influence of T_{air} below the soil surface. Air temperature was negatively correlated with bin averaged P_{CO2} at an alpine wetland and one tidal wetland but had a positive correlation with P_{CO2} in all other wetland sites, with the strongest relationship occurring in fens, bogs, and marshes. The connection between WTD and P_{CO2} was not consistent across or within

wetland categories. Periods of low discharge did not lead to higher correlations between GPP or Reco and P_{CO2}.

Finally, $P_{CO2\ BIO}$ was not consistently related to Reco or GPP, although it was positively correlated with Reco at four out of 5 sites in both soil porewater and surface water. Further study of wetland porewater and surface water P_{CO2} is essential to understand its complex relationships with other environmental variables and improve wetland C budgeting and ecosystem modeling. Our findings suggest that simple or direct universal relationships with eddy covariance flux tower estimates of GPP or Reco and *in-situ* measurements of P_{CO2} to estimate or link lateral and vertical exchanges of carbon dioxide at wetlands are not likely to be easily found. Further research on wetland lateral CO_2 exchange should seek out drivers of site-specific differences in P_{CO2} concentrations such as site-specific hydrology, spatial variability, and lag effects, and incorporate those relationships into ecosystem models. There remains a need for concurrent high resolution, long-term measurements of lateral and vertical greenhouse gas flux along with relevant ancillary data such as tide height or water table height and air or water temperature. Higher quality data will help to remove the influence of external effects (e.g., weathering or tides) and better identify environmental drivers of wetland gas emissions.

4.7 Acknowledgements

We would like to thank the scientists who helped us in the beginning stages of formulating our methods, especially Kenta Suzuki and Shin-ichiro S. Matsuzaki at the National Institute for Environmental Studies, and Nick Marzolf at Duke University. Jess Turner acknowledges support from the UW-Madison Student Research Grant Competition, PeatNeeds Microgrant from PeatECR Action Team, NSF, and the Eco-meteorology lab at UW-Madison.

Funding for the AmeriFlux data portal is provided by the U.S. Department of Energy Office of Science. US-EvM is supported in part by funds from the Department of Energy's National Institute for Climate Change Research grant (07-SC-NICCR-1059) and the National Science Foundation Division of Atmospheric & Geospace Sciences Atmospheric Chemistry Program awards (1561139, 1233006, and 1807533). The Koppen climate basemap was from Beck et al, (2018).

4.8 Data Availability

Previously published data can be accessed through the following citations (Clow et al., 2021a; Mast et al., 1998; Wickland et al., 2001; Turner et al., 2022; Hawman et al., 2021; Campeau et al., 2021b; Leach et al., 2016; Nilsson & Peichl, 2020; Rupp, 2019; Euskirchen et al., 2019; Euskirchen , 2022; D'Acunha et al., 2019; Christen & Knox, 2021; Kling, 2019; Zolkos et al., 2022; Gleason et al., 2009; Hatala Matthes et al., 2021; Crawford et al., 2017; Olson, 2022; Desai, 2022; Forsythe, 2020a; Bohrer et al., 2019; Bohrer & Kerns, 2022; Tangen & Bansal, 2017) and are listed in Table S2. Data from the following sites is available in this study: US-EvM, Big Cypress, YKD 1&2, US-Myb, US-ALQ.

4.9 References

Anderson, M.P. and Lowry, C.S. (2007). Transient Functioning of a Groundwater Wetland Complex, Allequash Basin, Wisconsin [PDF].

Arega, F., Armstrong, S., & Badr, A. W. (2008). Modeling of residence time in the East Scott Creek Estuary, South Carolina, USA. *Journal of Hydro-environment Research*, *2*(2), 99-108.

Amaral, J. H. F., Melack, J. M., Barbosa, P. M., MacIntyre, S., Kasper, D., Cortés, A., ... & Forsberg, B. R. (2020). Carbon dioxide fluxes to the atmosphere from waters within flooded forests in the Amazon basin. Journal of Geophysical Research: Biogeosciences, 125(3), e2019JG005293.

Attermeyer, K., Casas-Ruiz, J. P., Fuss, T., Pastor, A., Cauvy-Fraunié, S., Sheath, D., ... & Bodmer, P. (2021). Carbon dioxide fluxes increase from day to night across European streams. *Communications earth & environment*, *2*(1), 1-8.

Bansal, S., Tangen, B. A., Gleason, R. A., Badiou, P., & Creed, I. F. (2021). Land Management Strategies Influence Soil Organic Carbon Stocks of Prairie Potholes of North America. *Wetland Carbon and Environmental Management*, 273-285.

Bhattacharyya, S., Hazra, S., Das, S., Samanta, S., Mukhopadhyay, A., Dutta, D., ... & Chanda, A. (2020). Characterizing nutrient dynamics with relation to changes in partial pressure of CO2 in a tropical sewage-fed aquaculture pond situated in a Ramsar wetland. Water and environment journal, 34(2), 259-273.

Beck, P. (2018). future Köppen-Geiger climate classification maps at 1-km resolution, Sci. *Data https://doi. org/10.1038/sdata*.

Belger, L., Forsberg, B. R., & Melack, J. M. (2011). Carbon dioxide and methane emissions from interfluvial wetlands in the upper Negro River basin, Brazil. Biogeochemistry, 105(1), 171-183.

Bogard, M. J., Bergamaschi, B. A., Butman, D. E., Anderson, F., Knox, S. H., & Windham-Myers, L. (2020). Hydrologic export is a major component of coastal wetland carbon budgets. Global Biogeochemical Cycles, 34(8), e2019GB006430. https://doi.org/10.1029/2019GB006430

Bohrer, G., Ju, Y., Arend, K., Morin, T., Rey-Sanchez, C., Wrighton, K., & Villa, J. (2019). *Methane and CO2 chamber fluxes and porewater concentrations US-OWC Ameriflux wetland site, 2015-2018*. Environmental System Science Data Infrastructure for a Virtual Ecosystem (ESS-DIVE) (United States); AmeriFlux Management Project.

Bohrer, G., Kerns, J. (2022), AmeriFlux BASE US-OWC Old Woman Creek, Ver. 3-5, AmeriFlux AMP, (Dataset). https://doi.org/10.17190/AMF/1418679

Brugger, A., Wett, B., Kolar, I., Reitner, B., & Herndl, G. J. (2001). Immobilization and bacterial utilization of dissolved organic carbon entering the riparian zone of the alpine Enns River, Austria. *Aquatic Microbial Ecology*, *24*(2), 129-142.

Buytaert, W., & Beven, K. (2011). Models as multiple working hypotheses: hydrological simulation of tropical alpine wetlands. *Hydrological Processes*, *25*(11), 1784-1799.

Campeau, A., Vachon, D., Bishop, K. et al. Autumn destabilization of deep porewater CO2 store in a northern peatland driven by turbulent diffusion. Nat Commun 12, 6857 (2021a). https://doi.org/10.1038/s41467-021-27059-0

Campeau, A. Swedish University of Agriculture (2021b). Dataset for research article: Autumn destabilization of deep porewater CO2 store in a northern peatland driven by turbulent diffusion. . Swedish national data service. Version 1. https://doi.org/10.5878/ggdt-ew12

Chang, C. W., Miki, T., Ushio, M., Ke, P. J., Lu, H. P., Shiah, F. K., & Hsieh, C. H. (2021). Reconstructing large interaction networks from empirical time series data. *Ecology Letters*, *24*(12), 2763-2774.

Chapin, F. S., Woodwell, G. M., Randerson, J. T., Rastetter, E. B., Lovett, G. M., Baldocchi, D. D., ... & Schulze, E. D. (2006). Reconciling carbon-cycle concepts, terminology, and methods. *Ecosystems*, *9*, 1041-1050.

Clow, D.W., Qi, S.L., and Akie, G.A., 2021a, Continuous water-quality data for selected streams in Rocky Mountain National Park, Colorado, water years 2011-19: U.S. Geological Survey data release, https://doi.org/10.5066/P9RNS5FP.

Clow, D. W., Striegl, R. G., & Dornblaser, M. M. (2021b). Spatiotemporal dynamics of CO2 gas exchange from headwater mountain streams. *Journal of Geophysical Research: Biogeosciences*, *126*(9), e2021JG006509.

Crawford, J. T., Stanley, E. H., Dornblaser, M. M., & Striegl, R. G. (2017). CO2 time series patterns in contrasting headwater streams of North America. *Aquatic Sciences*, *79*(3), 473-486.

Cui, T., Li, Y., Yang, L., Nan, Y., Li, K., Tudaji, M., ... & Tian, F. (2023). Non-monotonic changes in Asian Water Towers' streamflow at increasing warming levels. *Nature Communications*, *14*(1), 1176.

D'Acunha, B., Morillas, L., Black, T. A., Christen, A., & Johnson, M. S. (2019). Net ecosystem carbon balance of a peat bog undergoing restoration: integrating CO2 and CH4 fluxes from eddy covariance and aquatic evasion with DOC drainage fluxes. Journal of Geophysical Research: Biogeosciences, 124(4), 884-901.

Dalmagro, H. J., Lathuilliere, M. J., Vourlitis, G. L., Campos, R. C., Pinto Jr, O. B., Johnson, M. S., ... & Couto, E. G. (2016). Physiological responses to extreme hydrological events in the Pantanal wetland: heterogeneity of a plant community containing super-dominant species. *Journal of Vegetation Science*, *27*(3), 568-577.

Desai, A. R., Murphy, B. A., Wiesner, S., Thom, J. E., Butterworth, B. J., Koupaei-Abyazani, N., ... & Davis, K. J. (2022). Drivers of decadal carbon fluxes across temperate ecosystems. *Journal of Geophysical Research: Biogeosciences*, e2022JG007014.

Etheridge, J. R., Burchell II, M. R., & Birgand, F. (2017). Can created tidal marshes reduce nitrate export to downstream estuaries?. *Ecological Engineering*, *105*, 314-324.

Eugster, W., DelSontro, T., Laundre, J. A., Dobkowski, J., Shaver, G. R., & Kling, G. W. (2022). Effects of long-term climate trends on the methane and CO2 exchange processes of Toolik Lake, Alaska. *Frontiers in Environmental Science*, 1457.

Euskirchen, E. S., Bret-Harte, M. S., Shaver, G. R., Edgar, C. W., & Romanovsky, V. E. (2017). Long-term release of carbon dioxide from arctic tundra ecosystems in Alaska. *Ecosystems*, *20*(5), 960-974.

Euskirchen, E. (2022), AmeriFlux BASE US-BZF Bonanza Creek Rich Fen, Ver. 4-5, AmeriFlux AMP, (Dataset). https://doi.org/10.17190/AMF/1756433

Euskirchen, E. S., Bret-Harte, M. S., Shaver, G. R., Edgar, C. W., & Romanovsky, V. E. (2019). Arctic Observatory Network: Imnavait fen eddy covariance. Arctic Observatory Network. http://aon.iab.uaf.edu/data_access

Forsythe, J. D., Kline, M. A., & O'Halloran, T. L. (2020a). *AmeriFlux AmeriFlux US-HB1 North Inlet Crab Haul Creek*. Lawrence Berkeley National Lab.(LBNL), Berkeley, CA (United States). AmeriFlux; Clemson Univ., SC (United States). https://doi.org/10.17190/AMF/1660341

Forsythe, J. D., O'Halloran, T. L., & Kline, M. A. (2020b). An eddy covariance mesonet for measuring greenhouse gas fluxes in coastal South Carolina. *Data*, *5*(4), 97.

Frost, G. V., Loehman, R. A., Saperstein, L. B., Macander, M. J., Nelson, P. R., Paradis, D. P., & Natali, S. M. (2020). Multi-decadal patterns of vegetation succession after tundra fire on the Yukon-Kuskokwim Delta, Alaska. Environmental Research Letters, 15(2), 025003. https://doi.org/10.1088/1748-9326/ab5f49

Gibson, J. J., Price, J. S., Aravena, R., Fitzgerald, D. F., & Maloney, D. (2000). Runoff generation in a hypermaritime bog–forest upland. *Hydrological Processes*, *14*(15), 2711-2730.

Gleason, R. A., Tangen, B. A., Browne, B. A., & Euliss Jr, N. H. (2009). Greenhouse gas flux from cropland and restored wetlands in the Prairie Pothole Region. *Soil Biology and Biochemistry*, *41*(12), 2501-2507.

Gomez-Casanovas, N., DeLucia, N. J., DeLucia, E. H., Blanc-Betes, E., Boughton, E. H., Sparks, J., & Bernacchi, C. J. (2020). Seasonal controls of CO2 and CH4 dynamics in a temporarily flooded subtropical wetland. *Journal of Geophysical Research: Biogeosciences*, *125*(3), e2019JG005257.

Hatala Matthes, J. A., Sturtevant, C., Oikawa, P. Y., Chamberlain, S. D., Szutu, D., Arias-Ortiz, A., ... & Baldocchi, D. (2021). AmeriFlux BASE US-Myb Mayberry Wetland, Ver. 12-5, AmeriFlux AMP,(Dataset). *AmeriFlux AMP*.

Hawman, P. A., Mishra, D. R., O'Connell, J. L., Cotten, D. L., Narron, C. R., & Mao, L. (2021). Salt Marsh Light Use Efficiency is Driven by Environmental Gradients and Species-Specific Physiology and Morphology. *Journal of Geophysical Research: Biogeosciences*, *126*(5), e2020JG006213.

Hayashi, M., van der Kamp, G., & Rosenberry, D. O. (2016). Hydrology of prairie wetlands: understanding the integrated surface-water and groundwater processes. *Wetlands*, *36*(2), 237-254.

Holloway, Randall W., "Annual Sediment Retention and Hydraulic Residence Time Variability in a Riverine Wetland Receiving Unregulated Inflow from Agricultural Runoff" (2010). SNS Master's Theses. 28. https://digitalcommons.csumb.edu/sns_theses/28

Holmes, M. E., Chanton, J. P., Tfaily, M. M., & Ogram, A. (2015). CO2 and CH4 isotope compositions and production pathways in a tropical peatland. *Global Biogeochemical Cycles*, 29(1), 1-18.

Itoh, M., Ohte, N., Koba, K., Sugimoto, A., & Tani, M. (2008). Analysis of methane production pathways in a riparian wetland of a temperate forest catchment, using δ13C of pore water CH4 and CO2. *Journal of Geophysical Research: Biogeosciences*, 113(G3).

Jankowski, K. J., Mejia, F. H., Blaszczak, J. R., & Holtgrieve, G. W. (2021). Aquatic ecosystem metabolism as a tool in environmental management. *Wiley Interdisciplinary Reviews: Water*, *8*(4), e1521.

Jordan, T. E., Whigham, D. F., Hofmockel, K. H., & Pittek, M. A. (2003). Nutrient and sediment removal by a restored wetland receiving agricultural runoff. *Journal of environmental quality*, *32*(4), 1534-1547.

Junk, W. J. (2013). Current state of knowledge regarding South America wetlands and their future under global climate change. *Aquatic Sciences*, *75*(1), 113-131.

Kaushal, S. S., Mayer, P. M., Vidon, P. G., Smith, R. M., Pennino, M. J., Newcomer, T. A., ... & Belt, K. T. (2014). Land use and climate variability amplify carbon, nutrient, and contaminant pulses: a review with management implications. *JAWRA Journal of the American Water Resources Association*, *50*(3), 585-614.

Klaus, F. (2022). Impacts of peatland drainage on soil properties.

Knox, A. K., Dahlgren, R. A., Tate, K. W., & Atwill, E. R. (2008). Efficacy of natural wetlands to retain nutrient, sediment and microbial pollutants. *Journal of environmental quality*, *37*(5), 1837-1846.

Kominoski, J. S., Pachón, J., Brock, J. T., McVoy, C., & Malone, S. L. (2021). Understanding drivers of aquatic ecosystem metabolism in freshwater subtropical ridge and slough wetlands. *Ecosphere*, *12*(12), e03849.

Kling, G. 2019. Biogeochemistry data set for Imnavait Creek Weir on the North Slope of Alaska 2002-2018. Arctic Data Center. https://pasta.lternet.edu/package/metadata/eml/knb-lter-arc/10531/8.

Leach, J. A., Larsson, A., Wallin, M. B., Nilsson, M. B., & Laudon, H. (2016). Twelve year interannual and seasonal variability of stream carbon export from a boreal peatland catchment. *Journal of Geophysical Research: Biogeosciences*, *121*(7), 1851-1866.

Lee, S. C., Christen, A., Black, A. T., Johnson, M. S., Jassal, R. S., Ketler, R., ... & Merkens, M. (2017). Annual greenhouse gas budget for a bog ecosystem undergoing restoration by rewetting. *Biogeosciences*, *14*(11), 2799-2814.

Liu, X., Wan, S., Su, B., Hui, D., & Luo, Y. (2002). Response of soil CO2 efflux to water manipulation in a tallgrass prairie ecosystem. *Plant and soil*, *240*(2), 213-223.

Lizotte Jr, R. E., Shields Jr, F. D., Murdock, J. N., Kröger, R., & Knight, S. S. (2012). Mitigating agrichemicals from an artificial runoff event using a managed riverine wetland. *Science of the Total Environment*, *427*, 373-381.

Loder, A. L., & Finkelstein, S. A. (2020). Carbon accumulation in freshwater marsh soils: A synthesis for temperate North America. *Wetlands*, *40*(5), 1173-1187.

Lu, W., Xiao, J., Liu, F., Zhang, Y., Liu, C. A., & Lin, G. (2017). Contrasting ecosystem CO 2 fluxes of inland and coastal wetlands: a meta-analysis of eddy covariance data. *Global Change Biology*, *23*(3), 1180-1198.

Malerba, M. E., Friess, D. A., Peacock, M., Grinham, A., Taillardat, P., Rosentreter, J. A., ... & Macreadie, P. I. (2022). Methane and nitrous oxide emissions complicate the climate benefits of teal and blue carbon wetlands. *One Earth*, *5*(12), 1336-1341.

Mast, M. A., Wickland, K. P., Striegl, R. T., & Clow, D. W. (1998). Winter fluxes of CO2 and CH4 from subalpine soils in Rocky Mountain National Park, Colorado. *Global Biogeochemical Cycles*, *12*(4), 607-620.

Maynard, J. J., O'Geen, A. T., & Dahlgren, R. A. (2009). Bioavailability and fate of phosphorus in constructed wetlands receiving agricultural runoff in the San Joaquin Valley, California. *Journal of environmental quality*, *38*(1), 360-372.

McJannet, D., Wallace, J., Keen, R., Hawdon, A., & Kemei, J. (2012). The filtering capacity of a tropical riverine wetland: II. Sediment and nutrient balances. *Hydrological Processes*, *26*(1), 53-72.

Mitra, S., Wassmann, R., & Vlek, P. L. (2005). An appraisal of global wetland area and its organic carbon stock. *Current science*, *88*(1), 25-35.

Mommer, L., & Visser, E. J. (2005). Underwater photosynthesis in flooded terrestrial plants: a matter of leaf plasticity. *Annals of botany*, *96*(4), 581-589.

Morris, P. J., & Waddington, J. M. (2011). Groundwater residence time distributions in peatlands: Implications for peat decomposition and accumulation. *Water Resources Research*, *47*(2). doi:10.1029/2010WR009492.

Mushet, D.M, 2019, Cottonwood Lake Study Area - Boundary Polygon: U.S. Geological Survey data release. https://doi.org/10.5066/P9B0GADT

Oikawa, P. (2020). AmeriFlux BASE US-EDN Eden Landing Ecological Reserve, Ver. 2-5, AmeriFlux AMP, (Dataset). https://doi.org/10.17190/AMF/1543381

Oquist, M. G., Bishop, K., Grelle, A., Klemedtsson, L., Kohler, S. J., Laudon, H., ... & Nilsson, M. B. (2014). The full annual carbon balance of boreal forests is highly sensitive to precipitation. *Environmental Science & Technology Letters*, *1*(7), 315-319.

Pang, R., Xu, X., Tian, Y., Cui, X., Ouyang, H., & Kuzyakov, Y. (2021). In-situ 13CO2 labeling to trace carbon fluxes in plant-soil-microorganism systems: Review and methodological guideline. *Rhizosphere*, *20*, 100441.

Pedron, S. A., Welker, J. M., Euskirchen, E. S., Klein, E. S., Walker, J. C., Xu, X., & Czimczik, C. I. (2022). Closing the Winter Gap—Year-Round Measurements of Soil CO2 Emission Sources in Arctic Tundra. Geophysical Research Letters, 49(6), e2021GL097347. https://doi.org/10.1029/2021GL097347

Pint, C. D., Hunt, R. J., & Anderson, M. P. (2003). Flowpath delineation and ground water age, Allequash Basin, Wisconsin. *Groundwater*, *41*(7), 895-902.

Podzorski, H. L. (2018). Expression of geochemical controls on water quality in Loch Vale, Rocky Mountain National Park. *2018-Mines Theses & Dissertations*.

Pugh, C. A., Reed, D. E., Desai, A. R., & Sulman, B. N. (2018). Wetland flux controls: how does interacting water table levels and temperature influence carbon dioxide and methane fluxes in northern Wisconsin? *Biogeochemistry*, *137*(1), 15-25.

Rosentreter, J. A. (2022). Water-air gas exchange of CO2 and CH4 in coastal wetlands. In *Carbon Mineralization in Coastal Wetlands* (pp. 167-196). Elsevier.

Rupp, D. L. (2019). *Biogeochemical response to vegetation and hydrologic change in an Alaskan boreal fen ecosystem* (Doctoral dissertation, Michigan Technological University).

Sagerfors, J., A. Lindroth, A. Grelle, L. Klemedtsson, P. Weslien, and M. Nilsson (2008), Annual CO2 exchange between a nutrient-poor, minerotrophic, boreal mire and the atmosphere, *J. Geophys. Res.,* 113, G01001, doi:10.1029/2006JG000306.

Sakabe, A., Kosugi, Y., Takahashi, K., Itoh, M., Kanazawa, A., Makita, N., & Ataka, M. (2015). One year of continuous measurements of soil CH4 and CO2 fluxes in a Japanese cypress forest: Temporal and spatial variations associated with Asian monsoon rainfall. *Journal of Geophysical Research: Biogeosciences*, *120*(4), 585-599.

Santos, I. R., Maher, D. T., Larkin, R., Webb, J. R., & Sanders, C. J. (2019). Carbon outwelling and outgassing vs. burial in an estuarine tidal creek surrounded by mangrove and saltmarsh wetlands. *Limnology and Oceanography*, *64*(3), 996-1013.

Santos, I. R., Burdige, D. J., Jennerjahn, T. C., Bouillon, S., Cabral, A., Serrano, O., et al. (2021). The renaissance of Odum's outwelling hypothesis in "Blue Carbon" science. Estuarine, Coastal and Shelf Science, 255, 107361. https://doi.org/10.1016/j.ecss.2021.107361

Schneider, C. L., Herrera, M., Raisle, M. L., Murray, A. R., Whitmore, K. M., Encalada, A. C., ... & Riveros-Iregui, D. A. (2020). Carbon dioxide (CO2) fluxes from terrestrial and aquatic environments in a high-altitude tropical catchment. *Journal of Geophysical Research: Biogeosciences*, *125*(8), e2020JG005844.

Shahan, J., Chu, H., Windham-Myers, L., Matsumura, M., Carlin, J., Eichelmann, E., ... & Oikawa, P. (2022). Combining eddy covariance and chamber methods to better constrain CO2 and CH4 fluxes across a heterogeneous restored tidal wetland. *Journal of Geophysical Research: Biogeosciences*, *127*(9), e2022JG007112.

Sirianuntapiboon, S., Kongchum, M., & Jitmaikasem, W. (2006). Effects of hydraulic retention time and media of constructed wetland for treatment of domestic wastewater. *African Journal of Agricultural Research*, *1*(2), 027-037.

Skogssällskapet (2020) Ny forskning ska visa hur skog på torvmark kan göra bäst klimatnytta. Retrieved April 18, 2022, from https://www.skogssallskapet.se/kunskapsbank/artiklar/2020-10-27-ny-forskningska-visa-hur-skog-pa-torvmark-kan-gora-bast-klimatnytta.html

Sponseller, R. A. (2007). Precipitation pulses and soil CO2 flux in a Sonoran Desert ecosystem. *Global Change Biology*, *13*(2), 426-436.

Steinmann, K., Siegwolf, R.T.W., Saurer, M. et al. Carbon fluxes to the soil in a mature temperate forest assessed by 13C isotope tracing. Oecologia 141, 489–501 (2004).

STOY, P.C., PALMROTH, S., OISHI, A.C., SIQUEIRA, M.B.S., JUANG, J.-Y., NOVICK, K.A., WARD, E.J., KATUL, G.G. and OREN, R. (2007), Are ecosystem carbon inputs and outputs coupled at short time scales? A case study from adjacent pine and hardwood forests using impulse–response analysis. Plant, Cell & Environment, 30: 700-710. https://doi.org/10.1111/j.1365-3040.2007.01655.x

Sullivan, J. C., Torres, R., & Garrett, A. (2019). Intertidal creeks and overmarsh circulation in a small salt marsh basin. Journal of Geophysical Research: Earth Surface, 124, 447–463. https://doi.org/ 10.1029/2018JF004861

Sun, R., Chen, A., Chen, L., & Lü, Y. (2012). Cooling effects of wetlands in an urban region: The case of Beijing. *Ecological Indicators*, *20*, 57-64.

Sun, L., Ataka, M., Kominami, Y., & Yoshimura, K. (2017). Relationship between fine-root exudation and respiration of two Quercus species in a Japanese temperate forest. *Tree physiology*, *37*(8), 1011-1020.

Suzuki, K., Matsuzaki, S. I. S., & Masuya, H. (2022). Decomposing predictability to identify dominant causal drivers in complex ecosystems. *bioRxiv*.

Takahashi, T., Sutherland, S. C., Sweeney, C., Poisson, A., Metzl, N., Tilbrook, B., ... & Nojiri, Y. (2002). Global sea–air CO2 flux based on climatological surface ocean pCO2, and seasonal biological and temperature effects. *Deep Sea Research Part II: Topical Studies in Oceanography*, *49*(9-10), 1601-1622.

Tangen, B. A., & Bansal, S. (2020). Soil organic carbon stocks and sequestration rates of inland, freshwater wetlands: Sources of variability and uncertainty. *Science of the Total Environment*, *749*, 141444.

Tangen, B.A., and Bansal, S., 2017, Soil properties and greenhouse gas fluxes of Prairie Pothole Region wetlands: a comprehensive data release. U.S. Geological Survey data release. https://doi.org/10.5066/F7KS6QG2.

Tans, P. P. (1998). *Why carbon dioxide from fossil fuel burning won't go away* (pp. 271-291). Oxford Univ. Press.

Thompson, Y., Sandefur, B. C., Karathanasis, A. D., & D'Angelo, E. (2009). Redox potential and seasonal porewater biogeochemistry of three mountain wetlands in Southeastern Kentucky, USA. *Aquatic geochemistry*, 15(3), 349-370.

Toet, S., Van Logtestijn, R. S., Kampf, R., Schreijer, M., & Verhoeven, J. T. (2005). The effect of hydraulic retention time on the removal of pollutants from sewage treatment plant effluent in a surface-flow wetland system. *Wetlands*, *25*(2), 375-391.

Troxler, T. G., Barr, J. G., Fuentes, J. D., Engel, V., Anderson, G., Sanchez, C., ... & Davis, S. E. (2015). Component-specific dynamics of riverine mangrove CO2 efflux in the Florida coastal Everglades. *Agricultural and Forest Meteorology*, *213*, 273-282.

Turner, J., Desai, A. R., Blackstock, J., & Smith, D. (2022). Tidal influence on dissolved CO2 at Sapelo Island, Georgia, USA. Environmental Research: Ecology. doi:10.1088/2752-664X/aca0f4.

Turner, J., Desai, A. R., Thom, J., & Wickland, K. P. (2021). Lagged wetland CH4 flux response in a historically wet year. *Journal of Geophysical Research: Biogeosciences*, *126*(11), e2021JG006458.

Turner, J., Desai, A. R., Thom, J., Wickland, K. P., & Olson, B. (2019). Wind sheltering impacts on land-atmosphere fluxes over fens. *Frontiers in Environmental Science*, 179.

Ushio, M., Hsieh, C. H., Masuda, R., Deyle, E. R., Ye, H., Chang, C. W., ... & Kondoh, M. (2018). Fluctuating interaction network and time-varying stability of a natural fish community. *Nature*, *554*(7692), 360-363.

Valach, A. C., Kasak, K., Hemes, K. S., Anthony, T. L., Dronova, I., Taddeo, S., ... & Baldocchi, D. D. (2021). Productive wetlands restored for carbon sequestration quickly become net CO2 sinks with site-level factors driving uptake variability. *PloS one*, *16*(3), e0248398.

Van Dam, B. R., Lopes, C., Osburn, C. L., & Fourqurean, J. W. (2019). Net heterotrophy and carbonate dissolution in two subtropical seagrass meadows. *Biogeosciences*, *16*(22), 4411-4428.

Van Dam, B. R., Lopes, C. C., Polsenaere, P., Price, R. M., Rutgersson, A., & Fourqurean, J. W. (2021). Water temperature control on CO2 flux and evaporation over a subtropical seagrass meadow revealed by atmospheric eddy covariance. *Limnology and Oceanography*, *66*(2), 510-527.

Vroom, R. J. E., van den Berg, M., Pangala, S. R., van der Scheer, O. E., & Sorrell, B. K. (2022). Physiological processes affecting methane transport by wetland vegetation-a review. *Aquatic Botany*, 103547.

Wang, H., Liao, G., D'Souza, M., Yu, X., Yang, J., Yang, X., & Zheng, T. (2016). Temporal and spatial variations of greenhouse gas fluxes from a tidal mangrove wetland in Southeast China. *Environmental Science and Pollution Research*, *23*(2), 1873-1885.

Wang, Z. P., Li, L. H., Han, X. G., Li, Z. Q., & Chen, Q. S. (2007). Dynamics and allocation of recently photo-assimilated carbon in an Inner Mongolia temperate steppe. *Environmental and experimental botany*, *59*(1), 1-10.

Ward, N. D., Bianchi, T. S., Martin, J. B., Quintero, C. J., Sawakuchi, H. O., & Cohen, M. J. (2020). Pathways for Methane Emissions and Oxidation that Influence the Net Carbon Balance of a Subtropical Cypress Swamp. *Frontiers in Earth Science*, 8, 573357.

Webb, J. R., Santos, I. R., Maher, D. T., & Finlay, K. (2019). The importance of aquatic carbon fluxes in net ecosystem carbon budgets: a catchment-scale review. *Ecosystems*, *22*(3), 508-527.

Wickland, K. P., Striegl, R. G., Mast, M. A., & Clow, D. W. (2001). Carbon gas exchange at a southern Rocky Mountain wetland, 1996–1998. *Global Biogeochemical Cycles*, *15*(2), 321-335.

Winkler, G., Wagner, T., Pauritsch, M., Birk, S., Kellerer-Pirklbauer, A., Benischke, R., ... & Hergarten, S. (2016). Identification and assessment of groundwater flow and storage components of the relict Schöneben Rock Glacier, Niedere Tauern Range, Eastern Alps (Austria). *Hydrogeology Journal*, *24*(4), 937.

Yao Li, Xuan Yang, Xuejuan Bai et al. Contribution of Stipa bungeana root exudates to soil organic carbon fractions in the Loess Plateau, 05 May 2022, PREPRINT (Version 1) available at Research Square [https://doi.org/10.21203/rs.3.rs-1579134/v1]

Zedler, J. B., & Kercher, S. (2005). Wetland resources: status, trends, ecosystem services, and restorability. *Annu. Rev. Environ. Resour.*, *30*, 39-74.

Zolkos, S., MacDonald, E., Hung, J. K., Schade, J. D., Ludwig, S., Mann, P. J., ... & Natali, S. (2022). Physiographic Controls and Wildfire Effects on Aquatic Biogeochemistry in Tundra of the Yukon-Kuskokwim Delta, Alaska. Journal of Geophysical Research: Biogeosciences, 127(8), e2022JG006891.

4.10 Supplemental Information

Table S4.1. References used in calculating area-weighted HRTs in Table 4.1.

Location	Ecosystem	Area	Hydraulic residence time	Reference
East Scott Creek Estuary, South Carolina, USA	Tidal	1 km^2 (inundated during high tide)	22 – 86 hrs	Arega et al., 2008
Carteret County, North Carolina, USA	Tidal	0.056 km^2	3 – 4.1 hrs	Etheridge et al., 2017
Groves Creek, Georgia, USA	Tidal	1.4 km^2	1.86 d	Sullivan et al., 2015
Enns River, Central Alps, Austria	Alpine	6,080 km^2 (area catchment)	0.56 – 6.75 d	Brugger et al., 2001
Schöneben Rock Glacier, Eastern Alps, Austria	Alpine	0.17 km^2 (Glacier)	7 months	Winkler et al., 2016
Huagrahuma catchment, the Andes, Ecuador	Alpine	2.58 km^2	80 days (optimized model average res. time)	Buytaert & Beven, 2010
Kyambul Lagoon, Queensland, Australia	Fen	0.25 km^2	<6 hrs (90% of flow)	McJannet et al., 2012
Allequash Creek wetland, Wisconsin, USA	Fen groundwater	0.32 km^2	3 – 791 days (135 days on average)	Anderson & Lowry, 2007
	Groundwater (entire basin)	22 km^2 (entire watershed)	25 – 150 yrs	Pint et al., 2003
San Joaquin River, California, USA	Fen	0.023 km^2	11 hrs	Maynard et al., 2009
	Marsh	0.073 km^2	31 hrs	
Sierra Nevada foothills, Yuba County, California, USA	Fen (channelized wetland)	0.002 km^2	18 – 47 mins	Knox et al., 2008
	Marsh (“reference” wetland)	0.002 km^2	38 mins – 2 hrs	

"Triple M Wetlands" of Carneros Creek, California, USA	Marsh	0.22 km^2	3 – 28 hrs	Holloway, 2010
Kent Island, Maryland, USA	Marsh	0.013 km^2	12 – 19 days	Jordan et al., 2003
North Coast Forest District, British Columbia, Canada	Bog and forest	0.33 km^2	2 months	Gibson et al., 2000
Theoretical model results	Bog porewater	0.1 – 0.5 km^2	0.8 – 1 year	Morris & Waddington, 2011

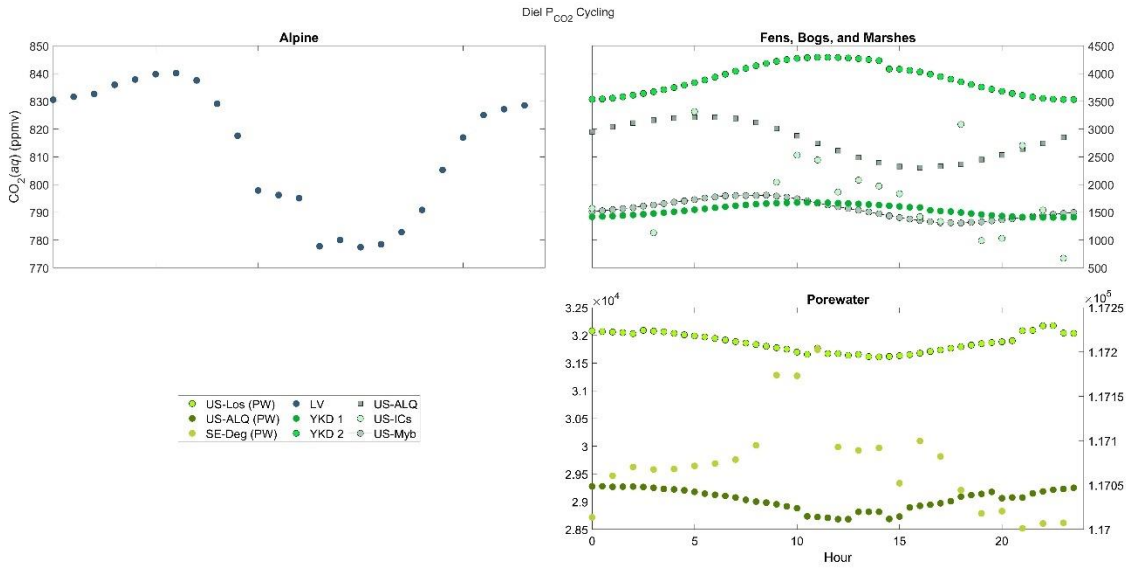

Figure S4.1. Diel cycles of P_{CO2} in (A) an alpine wetland (B) fens, bogs, and marshes (C) porewater. Data was averaged across each half-hour for the entire study duration at each site.

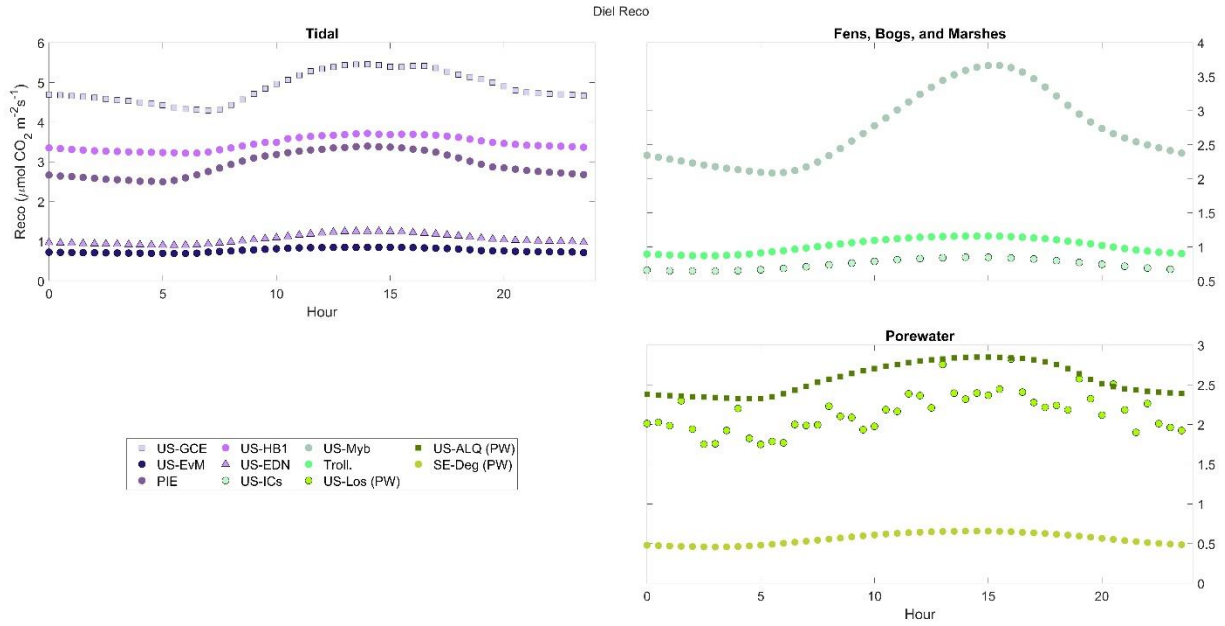

Figure S4.2. Diel cycles of Reco in (A) tidal wetlands (B) fens, bogs, and marshes and (C) porewater. Data was averaged across each half-hour for the entire study duration at each site.

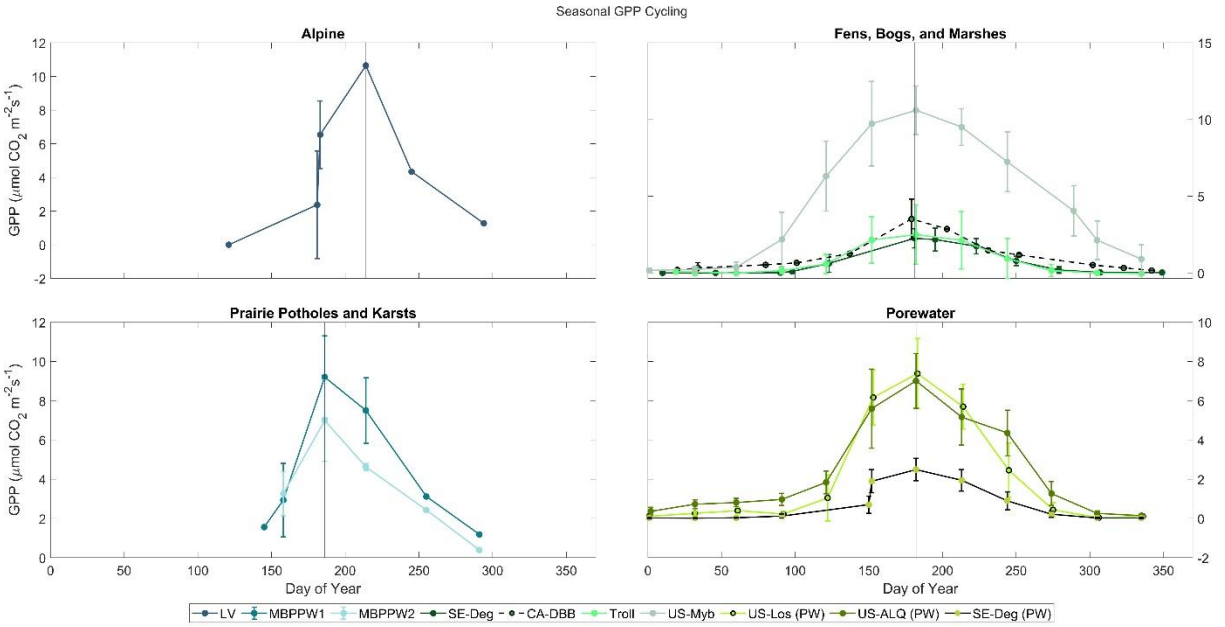

Figure S4.3. Seasonal cycles of GPP in (A) an alpine wetland (B) fens, bogs, and marshes (C) prairie potholes and karsts and (D) porewater. The vertical line represents when peak monthly averages occurred across the sites within each category.

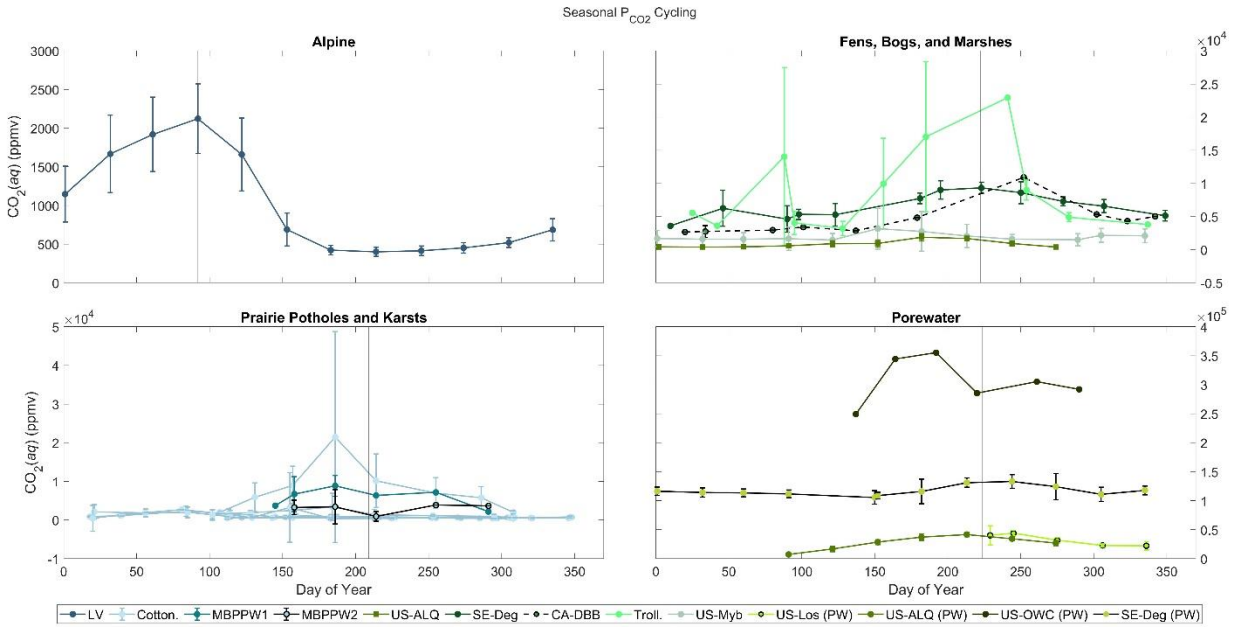

Figure S4.4. Seasonal cycles of P_{CO2} in (A) an alpine wetland (B) fens, bogs, and marshes (C) prairie potholes and karsts and (D) porewater. The vertical line represents when peak monthly averages occurred across the sites within each category.

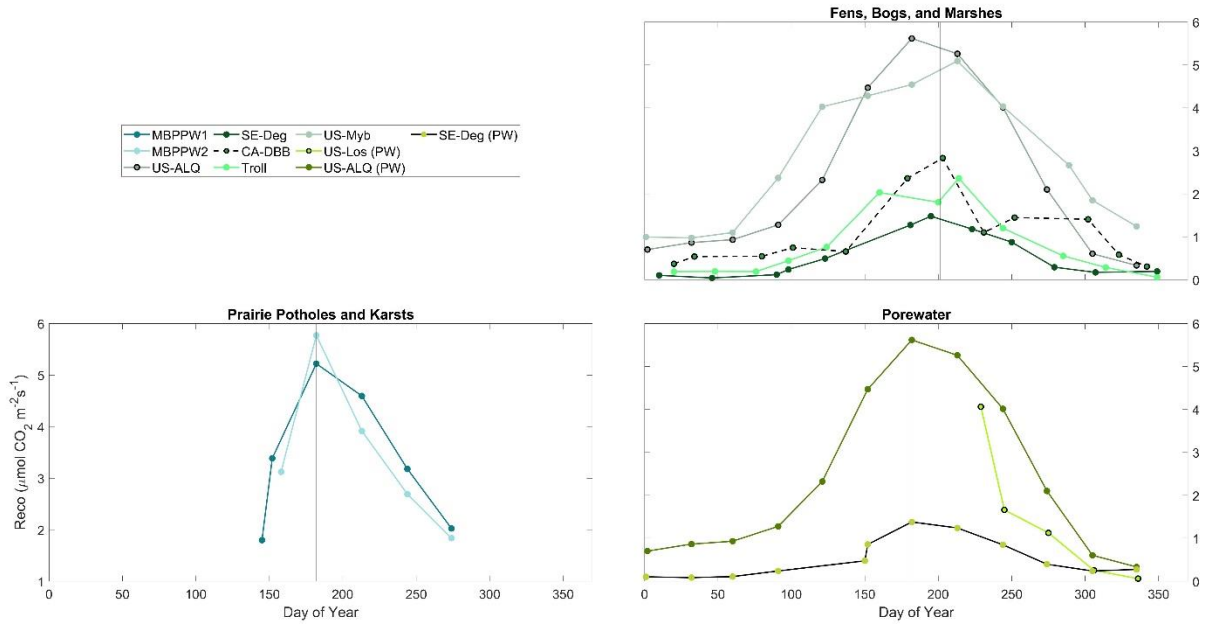

Figure S4.5. Seasonal cycles of Reco in (A) an alpine wetland (B) fens, bogs, and marshes (C) prairie potholes and karsts and (D) porewater. The vertical line represents when peak monthly averages occurred across the sites within each category.

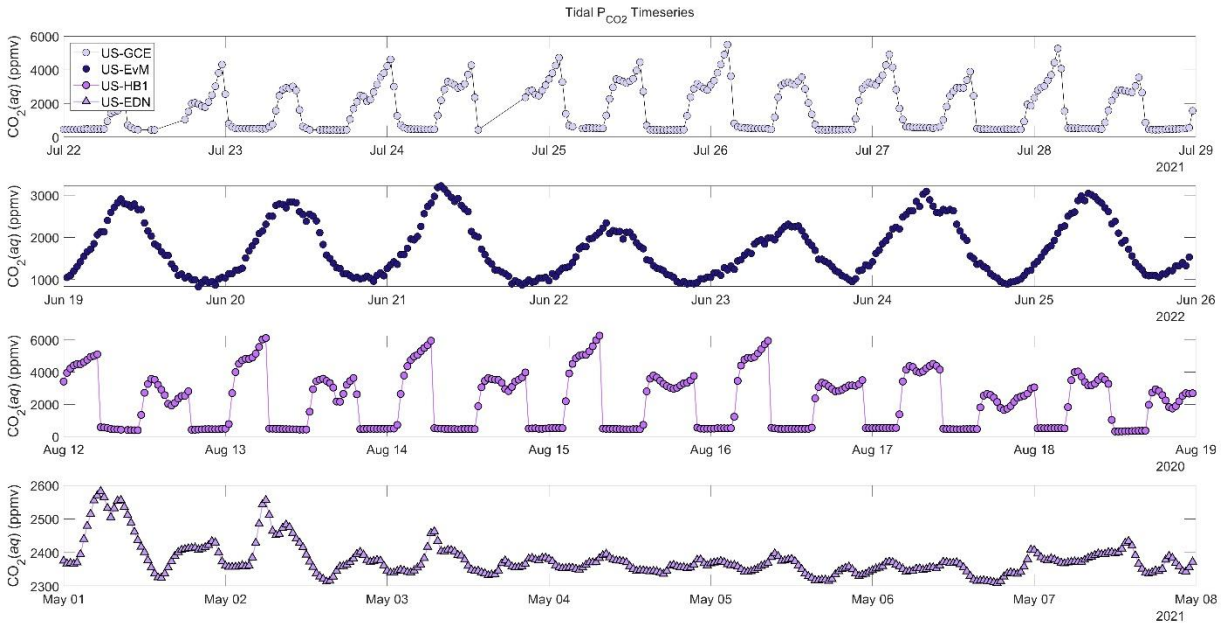

Figure S4.6. Tidal wetland surface water P_{CO2} timeseries in continuous 10-day increments.

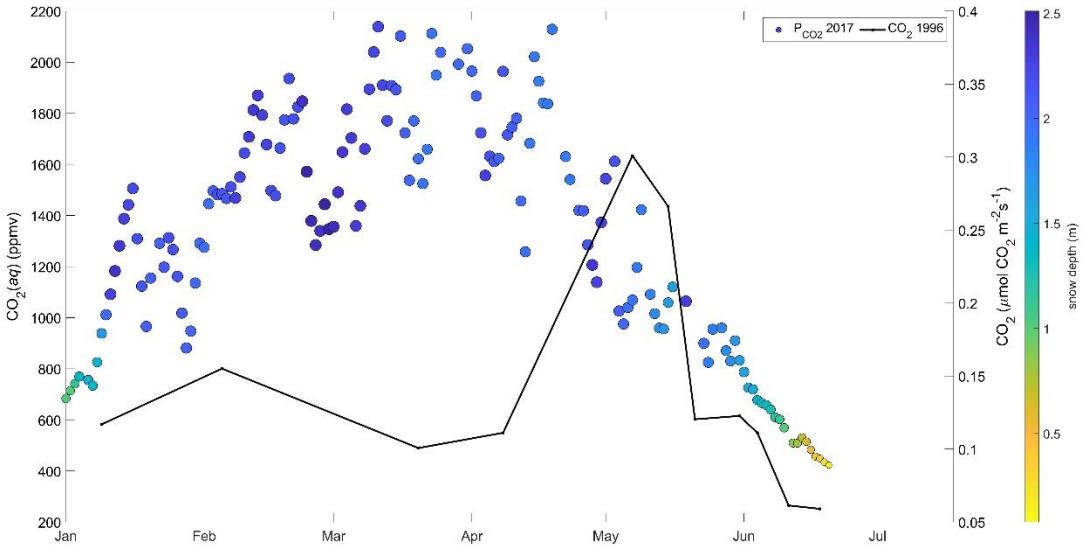

Figure S4.7. Loch Vale daily average P_{CO2} in 2017 (circles) compared to chamber-based CO_2 flux measured in 1996 (black line). Color bar represents daily average snow depth at Loch Vale in 2017. Higher snow depths have larger, darker circles.

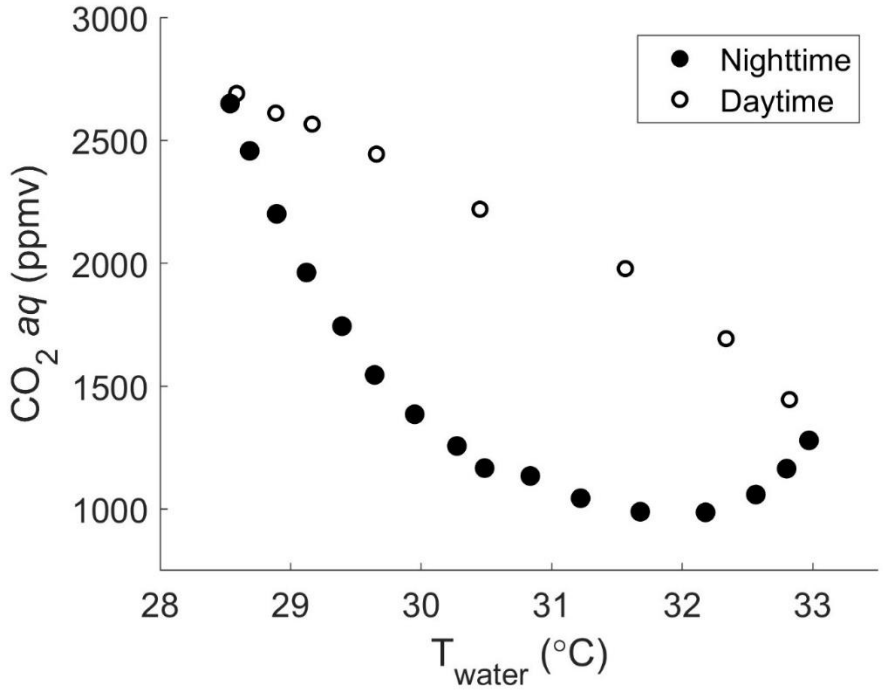

Figure S4.8. Hourly average water temperature in degrees Celsius versus hourly average dissolved CO_2 concentration at the tidal mangrove, US-EvM. "Daytime" represents measurements made from 8 am – 3 pm, shown as white circles. "Nighttime" is all other hours, black circles.

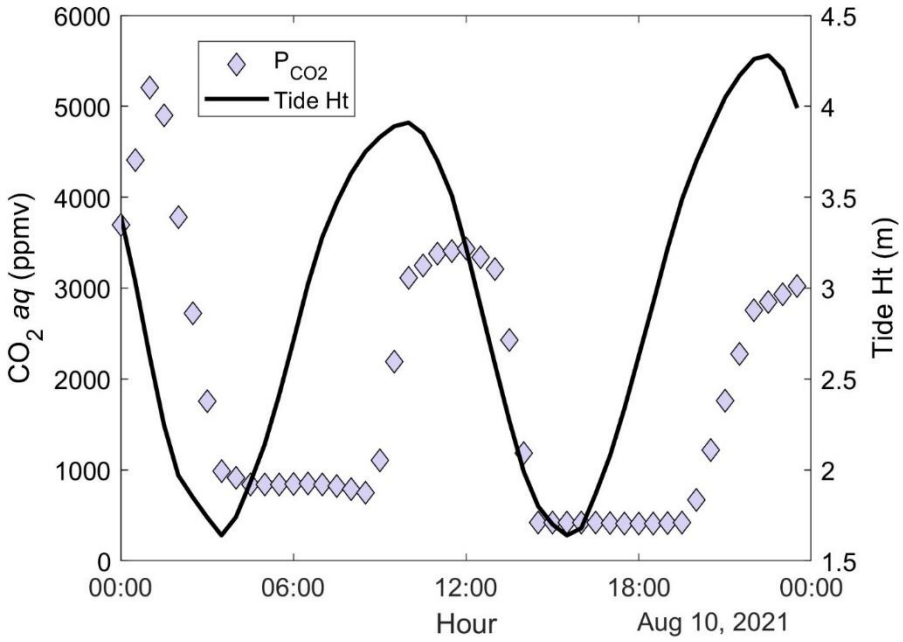

Figure S4.9. P_{CO2} (purple diamonds) and tide height (black line) at tidal wetland, US-GCE on August 10th, 2021.

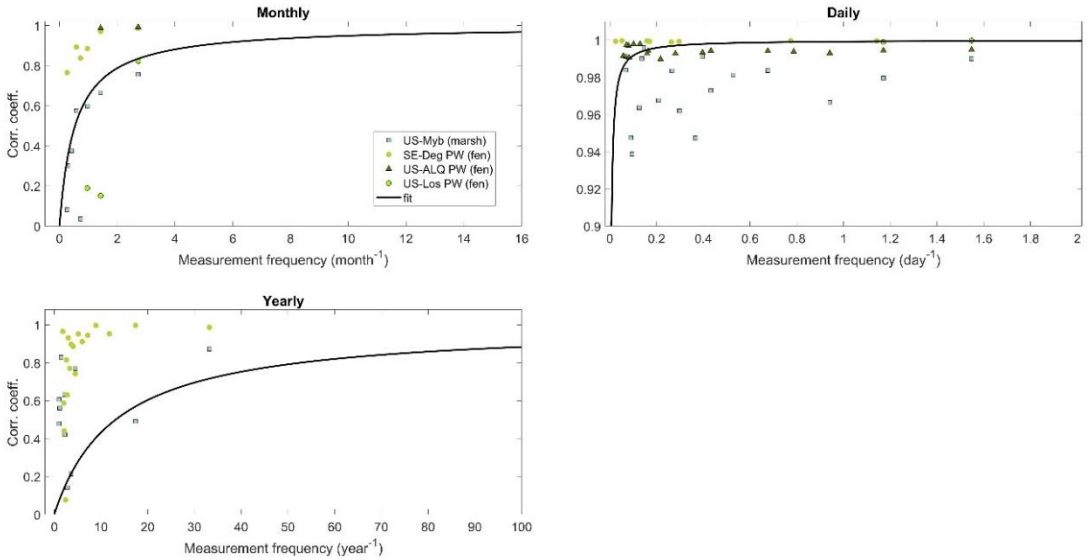

Figure S4.10. Optimal P_{CO2} measurement frequencies when comparing (A) Monthly averages of daily resolution data, (B) Daily averages of half-hourly resolution data, and (C) Yearly averages of daily resolution data.

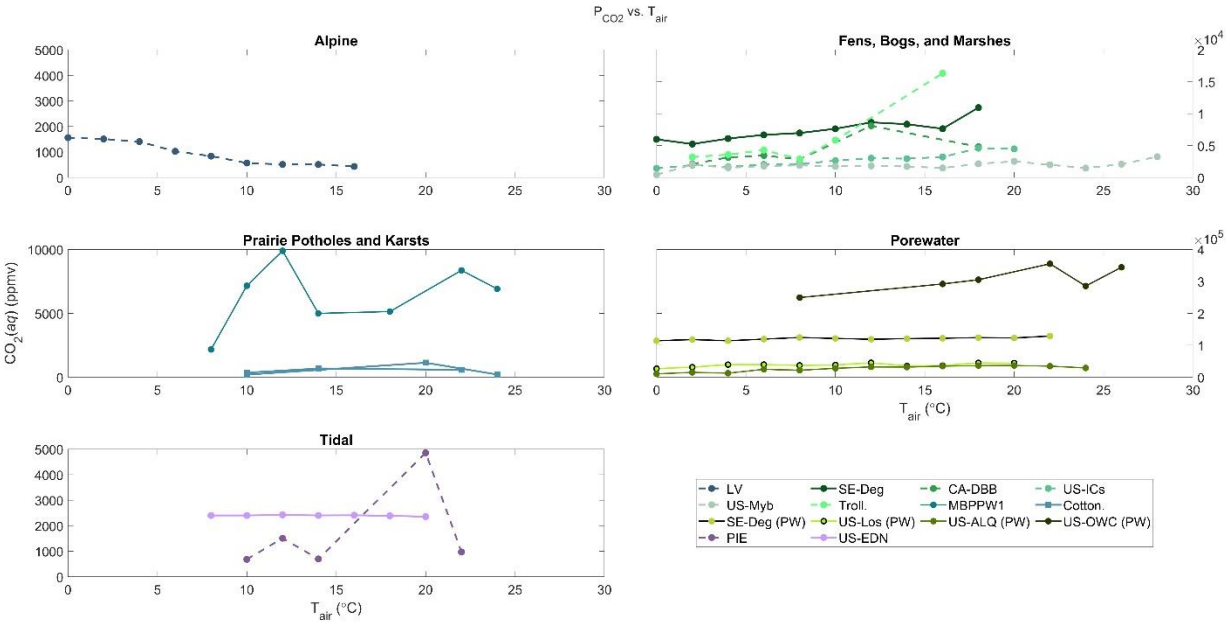

Figure S4.11. Daily average P_{CO2} versus T_{air} in (A) an alpine wetland, (B) fens, bogs, and marshes, (C) prairie potholes and karsts, (D) porewater, and (E) a tidal wetland. P_{CO2} was bin-averaged every 2°C of T_{air}. The x-axis shows the maximum T_{air} of each bin. Only sites with a temperature range greater than 10°C during the study period were included. P_{CO2} measurements made when T_{air} was below 0°C were not included.

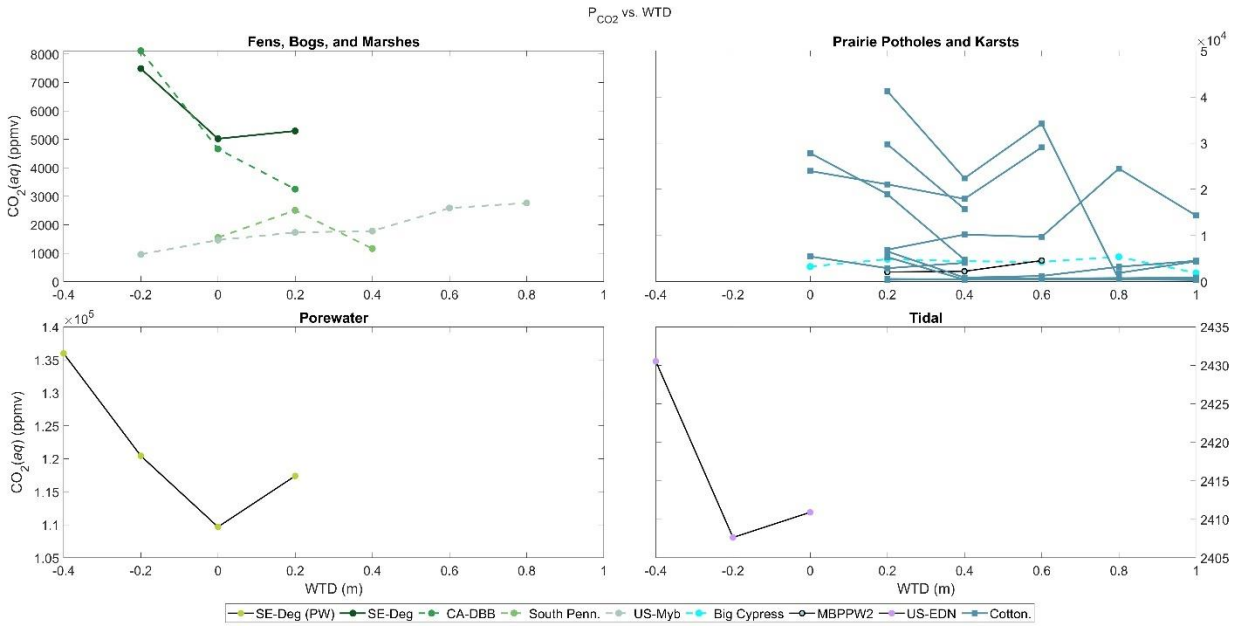

Figure S4.12. Daily average P_{CO2} versus relative water table depth (WTD) in (A) fens, bogs, and marshes, (B) prairie potholes or karsts, (C) porewater, and (D) a tidal wetland. P_{CO2} was bin-averaged every 0.2 m of relative WTD. Relative WTD refers to water table depth from a specific location for each wetland (e.g., water, soil, or buoy surface).

Table S4.2. Site instrumentation and references of studies utilizing or describing relevant data. IRGA stands for Infrared Gas Analyzer.

Site	**P_{CO2}**	**NEE**	**GPP**
Loch Vale	CO2 probe (Vaisala GMP-222)		
		Light chamber	
			Dark & light chambers
US-GCE	K30 CO2 sensor		
		Flux tower	

US-EvM	K30 CO2 sensor		
		Flux tower	
Big Cypress	Manual sampling and GC-FID?		
SE-Deg	(Porewater) CO2 probe (Vaisala CARBOCAP GMP221)		
	(Surface water) manual sampling and GC-FID		
		Flux tower	
APEX	Manual sampling, Continuous flow IRMS		
		sonic anemometer (CSAT-3; Campbell Scientific Instruments, Logan, Utah, USA) and open-path IRGA (EC-150; Campbell Scientific Instruments, Logan, Utah, USA).	
South Penn.	Manual sampling and GC-FID	None	None
CA-DBB	Manual sampling and GC-FID		
		Flux tower	
US-ICs	Manual sampling and GC-FID		

		IRGA (LI-7500A) and sonic anemometer (CSAT-3)	
YKD 1&2	eosGP IRGAs for Automated sampling; Manual sampling and GC-FID		
		Flux tower	
Cotton.	Manual sampling and GC-FID		
US-Myb	CO2 probe (EosGP)		
		open path IRGA (LI-7500; Li-COR Biosciences, NE, USA) and sonic anemometer	
US-ALQ	(Porewater) CO2 probe (Vaisala GMP-222)		
	(Surface water) CO2 probe (Vaisala GMM-222)		
		sonic anemometer (Campbell Scientific, Inc., Logan, 188 UT, CSAT-3), open path infrared gas analyzer	
US-Los	(Porewater) CO2 probe (Vaisala GMP-222)		
		sonic anemometer (Campbell Scientific, Inc., Logan, 188 UT, CSAT-3), open path infrared gas analyzer	
US-HB1	???		

		Integrated CO2 and H2O Open-Path Gas Analyzer and 3-D Sonic Anemometer (IRGASON)	
US-OWC	in-situ porewater dialysis sampler (peepers)		
		open-path IRGA (LI-7500, LI-COR Biosciences, Lincoln, NE) and ultrasonic anemometer (CSAT3, Campbell Sci.)	
US-EDN		open path IRGA (LI-7500RS, LI-COR, Lincoln, NE, USA) and sonic anemometer (Windmaster Pro, Gill Instruments Ltd., Lymington, Hampshire, UK)	

Table S4.3. Köppen climate classifications according to code used in Figure 4.2 (map).

Code	Description
Af	Tropical rainforest climate
Am	Tropical monsoon climate
As	Tropical dry savanna climate
Aw	Tropical savanna, wet
BSh	Hot semi-arid (steppe) climate
BSk	Cold semi-arid (steppe) climate
BWh	Hot deserts climate
BWk	Cold desert climate
Cfa	Humid subtropical climate
Cfb	Temperate oceanic climate
Cfc	Subpolar oceanic climate
Csa	Hot-summer Mediterranean climate
Csb	Warm-summer Mediterranean climate
Csc	Cool-summer Mediterranean climate
Cwa	Monsoon-influenced humid subtropical climate
Cwb	Subtropical highland climate or temperate oceanic climate with dry winters
Cwc	Cold subtropical highland climate or subpolar oceanic climate with dry winters
Dfa	Hot-summer humid continental climate
Dfb	Warm-summer humid continental climate
Dfc	Subarctic climate
Dfd	Extremely cold subarctic climate
Dsa	Hot, dry-summer continental climate

Dsb	Warm, dry-summer continental climate
Dsc	Dry-summer subarctic climate
Dwa	Monsoon-influenced hot-summer humid continental climate
Dwb	Monsoon-influenced warm-summer humid continental climate
Dwc	Monsoon-influenced subarctic climate
Dwd	Monsoon-influenced extremely cold subarctic climate
EF	Ice cap climate
ET	Tundra

Table S4.4. Cumulative annual GPP (gC m^{-2} yr^{-1}). Estimated from monthly average GPP during the study period at each site.

Site	Loch Vale (alpine)	MBPPW1 (prairie pothole)	MBPPW2 (prairie pothole)	SE-Deg (fen)	CA-DBB (bog)	Troll. (fen)	US-Myb (marsh)	US-Los (fen)	US-ALQ (fen)
GPP	794 ± 39	804 ± 33	558 ± 25	251 ± 8	410 ± 10	274 ± 9	1,685 ± 37	767 ± 25	899 ± 22

4.10.1 Further Site Descriptions and Instrumentation

4.10.1.1 Tidal

Georgia Coastal Ecosystems Long Term Ecological Research (GCE-LTER) flux tower (US-GCE) stands in a mesotidal salt marsh dominated by spartina alterniflora. Estuarine P_{CO2} at Sapelo Island has been well-studied, and has notable relationships with tidal direction, water temperature, and tide height (Wang & Cai, 2004; Jiang, Cai, and Wang 2008), but studies on flooded marsh waters at the same location are less common (Turner et al., 2022).

In comparison, the Everglades Saltwater Intrusion Marsh flux tower (US-EvM) is in a microtidal mangrove shifting from a freshwater emergent ecosystem to marine scrub and shrub as sawgrass dies off and red mangrove coverage increases. Below a sensitive periphyton mat sits a thin layer of marl soil. This calcitic mud is a product of the periphyton formed by the oxidation of various biological materials in dissolved calcium-carbonate-rich water. Underlying limestone bedrock promotes active carbonate sedimentation in the Everglades. Although

former studies at this site are limited, research on other freshwater marshes in the Everglades have determined that marsh productivity and overall C sink are partially influenced by periphyton mats and the duration of annual flooding (shorter-hydroperiod sites can have higher C sinks). Water table does not influence CO_2 emissions in all Everglades wetlands, especially those where plants are intolerant of prolonged submergence (Jimenez et al., 2012). Research on seagrass ecosystems of the Florida Keys suggests that the marine origin of air reaching central Florida Bay, shallow water depth, and intense solar heating contributes to water-temperature controlled CO_2 flux and unique diel fluctuations in carbonate chemistry (Van Dam et al., 2021).

North Inlet Crab Haul Creek flux tower (US-HB1) captures fluxes over a tidal salt marsh in the North Inlet-Winyah Bay National Estuarine Research Reserve. The marsh is dominated by *Spartina alterniflora* and tide height can range 1.4 m on average, fully exposing the marsh surface at low tide. Further information on site characteristics and instrumentation can be found in Forsythe et al. (2020b).

The flux tower at Eden Landing Ecological Reserve (US-EDN) captures the exchange of gases over former industrial salt evaporation ponds where tidal action was restored in 2008 (Shahan et al., 2022). Marsh vegetation includes *Salicornia pacifica* and *Spartina foliosa*, but the majority of the landscape is bare mudflat.

4.10.1.2 Alpine

Loch Vale (LV) is an alpine watershed in Rocky Mountain National Park. Andrews Creek begins at Andrews Glacier and drains the northern sub-basin of the watershed, including a wet meadow immediately to the south of the measurement location dominated by sedges *Carex aquatilis* and *Eleocharis quinqueflora* (Wickland et al., 2001). The subalpine meadow only makes up 1% of the watershed, which is dominated by bare rock and is typically snow-covered from November to as late as June. Snowmelt took place from April-June of 1996. Snow cover began again in November of 1996. An ice layer 10 cm thick covered the wetland surface and snow accumulated on top, reaching a maximum snow depth of 3 m.

Peak stream discharge at the site typically co-occurs with snowmelt, in April or May, which also flushes out solutes (Podzorski, 2018). However, solute concentrations related to weathering will spike prior to snowmelt, potentially due to the release of organic acids from the snowpack. A former study of stream P_{CO2} at Andrews Creek found that it reached a maximum between April and May, when snow had the greatest depth, then quickly decreased as the snowpack melted (Clow et al., 2021b). CO_2 entering the stream through groundwater and soil accumulates under the snow in winter months until equilibrium is achieved, and diffusive transport of gasses through the snowpack begins. Starting around May and the beginning of June, holes in the melting snowpack allow CO_2 to escape from the stream to the atmosphere. Snowmelt water is CO_2-poor and further decreases stream P_{CO2}. Andrews Creek demonstrated more severe changes in P_{CO2} than the downstream location, Big Thompson.

4.10.1.3 Prairie Potholes and Karsts

Big Cypress National Preserve (Big Cypress) is a 2,950 km^2 freshwater swamp featuring seasonally flooded karst wetlands, also referred to as cypress domes, which are hydrologically

disconnected from surrounding uplands until water level reaches a critical threshold and spills over the edges of the dome. A previous study at the site analyzed CH_4 concentrations in sediment, ebullition, porewater, and surface water and described the site in further detail (Ward et al., 2020).

MBPPW1 & 2 are geographically isolated freshwater marshes in the Prairie Pothole Region of Canada. MMPW1 was embedded in perennial cover used for grazing cattle. This site was completely covered by emergent vegetation consisting almost entirely of *Schoenoplectus tabernaemontani*, with a few small patches of *Typha spp*. MBPPW2 had large open-water areas with submersed macrophyte beds surrounded by a dense emergent vegetation fringe dominated by Typha spp. MBPPW2 was a net CO_2 source and had moderate CH_4 emissions while MBPPW1 was a net CO_2 sink and emitted a negligible amount of CH_4 from summer 2021 to summer 2022. Nutrient concentrations are suspected to cause differences in CH_4 fluxes at both sites. Soil temperature also drives CH_4 emissions at MBPPW2.

Cottonwood Lake Study Area (Cotton.) covers 0.89 km^2 of land in Stutsman County, North Dakota, USA. The site includes several prairie potholes. North American Prairie Potholes function similar to bogs in that water is sourced mainly by precipitation and snowmelt or other forms of runoff. High regional evapotranspiration rates lead to frequent drying of smaller prairie potholes (Hayashi et al., 2016).

4.10.1.4 Bogs, Fens, and Marshes

Lost Creek flux tower (US-Los) is in a riverine shrub fen located 29 km from Allequash Creek Site flux tower (US-ALQ). US-ALQ is a riverine sedge fen with comparatively more canopy sheltering than US-Los. Both sites have similar daily average NEE, GPP, and ecosystem respiration (Reco) throughout years with co-occurring data collection, with some differences in seasonality. Both sites were part of the Chequamegon Heterogenous Ecosystem Energy-balance Study Enabled by a High-density Extensive Array of Detectors in 2019 (CHEESEHEAD19) and more information can be found about each site in Desai et al. (2022).

Delta Burns Bog flux tower (CA-DBB) is in a rewetted raised bog near Vancouver, Canada dominated by sedges and *Sphagnum spp*. Peat was harvested in the bog from 1957-1963. Restoration involving ditch blocking to rewet the landscape began in 2001. Previously, CH_4 and CO_2 flux at the site were found to be driven by photosynthetically active radiation and 5 cm soil temperature (Lee et al., 2017). Flux tower instrumentation and a more detailed description of this site can be found in D'Acunha et al. (2019).

Degerö Stormyr flux tower (SE-Deg) is a nutrient-poor fen situated on a plateau separated from the Umeälven and Vindelälven river valleys in Vindeln, Sweden. Runoff from surrounding forests flows into the site and out through a stream on the other side, creating bog-like conditions. The site is dominated by sedges with some tree cover. Recent research highlights the loss of CO_2 from deep porewater (2 m) at SE-Deg through rapid diffusion in fall months (Campeau et al., 2021a). Although growing season porewater CO_2 increased with depth, this gradient weakened or totally collapsed in fall, when the porewater temperature profile was only weakly stratified. A more thorough site description is available in Leach et al. (2016), and instrumentation is described in Sagerfors et al. (2008).

Similarly, Trollberget rewetted peatland site (Troll.) is a formerly drained peatland located in Trollberget Experimental Area of Krycklan in Sweden (Laudon et al. 2021). It was emptied in the 1920s using ditches and was rewetted in November 2020. Since then, it has been the subject of studies on nutrient availability, plant productivity, and other peat properties (Skogssällskapet, 2020; Casselgård, 2020).

The Izaviknek-Kingaglia uplands of the Yukon-Kuskokwim Delta (YKD) are made up of peat plateaus, lakes, fens, and streams, overlying discontinuous permafrost (Frost et al., 2020). Vegetation includes a mixture of lichen, low-lying shrubs, *Sphagnum spp.* and various graminoids. Upland peat plateau ponds at the site are minimally vegetated. Wildfires, the most recent of which occurred in 2015, caused significantly lower surface water CO_2 concentrations in burned fen ponds compared to unburned fen ponds in the YKD but caused no notable differences in plateau ponds or fen channels (Zolkos et al., 2022). CO_2 concentrations tended to be highest in fen channels and plateau ponds compared to other environments. Porewater featured higher CO_2 concentrations than surface water. Surface water chemistry was more influenced by environmental conditions, and landscape type, year of sample collection, and water sample type (porewater vs. surface water) were important factors in determining geochemistry and hydrochemistry. U-star filtering was not performed on data from YKD1&2 or US-OWC due to a lack of sufficient data.

The Imnavait Creek Watershed Wet Sedge Tundra flux tower (US-ICs) drains water from the Brooks Mountain Range to the Arctic Ocean. When warmer falls delay the timing of annual soil freeze, the site loses CO_2 which has accounted for approximately 4% of total soil C stocks in the past (Euskirchen et al., 2017). Soil CO_2 at Imnavait Creek fen and the nearby Toolik Field Station increased with depth during growing season and was lower in denser, moister, and less wind-exposed tussocks (i.e., high points) than swales (i.e., low points) from June 2017 to September 2019 (Pedron et al., 2022). Topsoil CO_2 concentrations increased from fall to late winter, which suggested CO_2 buildup under the snowpack, and lower pore space volume and conductivity. Winter soil CO_2 concentrations were higher in tussocks and contrary to during the growing season, CO_2 decreased with depth. Spring season featured lower, more uniform CO_2 concentrations potentially due to the release of CO_2 with snowmelt (i.e., ventilation) in addition to other factors. A more thorough description of the site and instrumentation is available in Euskirchen et al. (2017).

Mayberry Wetland (US-Myb) is an impounded freshwater marsh which was restored in 2010 from pepperweed and annual grassland pasture to a patchwork of deep and shallow open water with occasional *Typha spp.* and *Schoenoplectus acutus*. The site is owned by Mayberry Farms but is managed by the California Department of Water Resources and Ducks Unlimited. Mayberry has shown large interannual variability in annual cumulative NEE fluxes and a slower vegetation expansion rate and lower nutrient availability than other restored wetlands in the Sacramento-San Joaquin Delta (Valach et al., 2021). Some years from 2010–2018 demonstrated near C-neutrality (neither a strong C sink nor a C source) at Mayberry but were likely the result of disturbance events.

Four upland peatlands were sampled in the south Pennines, UK, nicknamed Stalybridge, Holcombe Moor, Bleaklow, and Featherbed Moss. All sites are dominated by cottongrass (*Eriophorum vaginatum* and *E. angustifolium*) and are used for rough sheep grazing. Peatland ponds sampled within each site have all been created via bunding or damming of gullies in the

last two years as part of peatland restoration programs in the area. Peatland pond volume varied from small (volume <1m^3) to medium (1-10m^3) or large (>10m^3). We have categorized it as a bog for the purpose of this study.

4.10.1.5 Porewater

Bonanza Creek Rich Fen (US-BZF) is a boreal rich fen peatland situated in the Tanana Flats of inland Alaska. Neighboring wetlands have near-surface permafrost, but US-BZF does not. P_{CO2} was measured approximately once a month from May to August 2016 at a control plot as part of the APEX experiment located 0.05 km southwest of the tower.

Old Woman Creek flux tower (US-OWC) is situated in a permanently flooded natural freshwater estuary of Lake Erie, the shallowest of the Great Lakes. A majority (66%) of the Old Woman Creek watershed is agricultural land, which partially contributes to increased sediment and nutrients downstream after storms. The estuary is connected to the lake depending on stream flow and lake wave action, otherwise a barrier beach prevents water flow in or out, contributing to bog-like surface water conditions. Dominant vegetation surrounding the tower is *Nymphea odorata, Nelumbo lutea,* and *Typha spp*. All other sites with available porewater CO_2 data are described above. For conversion of porewater concentration (mM) to ppm CO_2 at US-OWC, we used the ideal gas law at standard temperature and pressure (0°C, 1013 hPa).

4.10.1.6 Statistical analysis

Daily average P_{CO2} was used for calculating monthly averages, plotting against WTD and T_{air}, and in signal analysis to eliminate the known, short-term negative influence of temperature on dissolved CO_2, and to reduce noise due to fluctuations in half-hourly or hourly data due to the diel cycle.

In seasonal cycle plots, GPP and P_{CO2} were averaged together each month and across multiple years (for multi-year datasets) and plotted according to timestamp on the last measurement of each month. This ensures that at sites where large data gaps existed, the seasonal cycles were still representative of the time periods captured (rather than assuming monthly averages equally represented all days in a month). Seasonal and diel cycle plots demonstrated time periods with overlapping P_{CO2} and GPP measurements from each site unless concurrent data was not available or large data gaps obscured the seasonal or diel cycles, in which case the longer time series of one of the variables (at similar times of year as the other variable, if possible) was used. Due to changes in the timing of the tides at some tidal wetlands from one day to the next, only a single day of data was shown for some sites in the diel P_{CO2} plot.

5 Conclusion

5.1 Overview

This dissertation began by introducing wetland C cycling (i.e., where wetland C begins and ends, its various forms) and why it is studied. The lag time between photosynthetic rates and soil respiration observed in isotopic tracer studies led to the hypothesis that wetland C can be traced *post hoc* with information on gas exchange. The introduction to this dissertation further postulated that because photosynthesis plays a role in the time between C uptake and release, information on lagged relationships driven by plants and their photosynthetic rates might improve lateral and vertical flux estimations, or eventually, the entire wetland C sink.

Chapter two investigated drivers of CH_4 flux from two adjacent fen wetlands in northern Wisconsin. Lag analysis showed that lower CO_2 uptake by plants (GPP) was correlated with lower subsequent CH_4 emissions in an extremely wet year, likely due to substrate limitation for methanogens. T_{air} also had an influence on CH_4 emissions and was removed to isolate the impact of GPP.

In chapter three, the ability of a recently developed low-cost P_{CO2} platform to estimate tidal effects in coastal wetlands was tested in a coastal salt marsh. P_{CO2} data was combined with tide gage data and assessed with Granger causality to verify known drivers of P_{CO2} concentrations, such as T_{air} and WTD. Results demonstrated that the CO2-LAMP can be used in wetland settings and observations can be combined with tide gage data to estimate lateral P_{CO2} loss. Granger causality testing revealed known drivers of P_{CO2}, including tide height and salinity. Lateral P_{CO2} export estimations changed with tide gage location and sensor accuracy.

Finally, in chapter four P_{CO2} was synthesized from 22 Northern Hemisphere wetlands to determine whether photosynthetic rates had a similar influence on surface and porewater CO_2 as with GPP and CH_4 flux. Wetland type had an impact on surface water P_{CO2} concentrations on the daily scale, but not on annual averages. GPP also did not have a consistent influence on P_{CO2} across sites.

Together, these findings indicated that photosynthetic rates influence yearly CH_4 fluxes in wetlands, but not P_{CO2}. Chapter 2 proved that wetland photosynthetic rates influence ecosystem-scale CH_4 emissions, as was initially expected based on countless studies of the lagged influence of wetland GPP on FCH_4. Plants control substrate availability for methanogens, resulting in a delay between photosynthetic CO_2 uptake and methanogenic production of soil CH_4. However, the next two chapters provided evidence that water chemistry (e.g., P_{CO2}) can be controlled by completely different factors than what drives CH_4 production. For example, P_{CO2} in floodwaters of a salt marsh along the East Coast of the United States fluctuated with tide height and direction in Chapter 3. Similarly, there was not a consistent relationship between daily average P_{CO2} and GPP in Chapter 4. Daily average porewater and surface water P_{CO2} in wetlands from across the Northern Hemisphere were more strongly related to wetland type and hydraulic residence time, suggesting that hydrology may have a stronger control over P_{CO2} than factors related to vegetation.

Contrary to the initial hypothesis, it is unlikely that photosynthetic rates can be used to track wetland C cycling. Although there was physical reasoning for a connection between lateral and vertical fluxes in wetlands, there were complex relationships between environmental drivers, changing C dynamics across daily and seasonal scales, and site-specific differences. For

instance, tidal marshes can export large amounts of C despite lower daily average P_{CO2} concentrations than bogs and prairie potholes/karsts because of strong lateral flow. This results in tidal wetlands losing a larger fraction of the net ecosystem C balance compared to inland wetlands (Bogard et al., 2020). Alpine wetlands might have large lateral CO_2 loss due to weathering, but after seasonal snowmelt, the source of that CO_2 and surface water flow is depleted and the hydraulic residence time is much higher. Each wetland is unique, and relationships between environmental factors observed at some wetlands should not be extrapolated across all wetlands.

5.2 Categorizing lateral exports by wetland type can simplify wetland C budget

As the CO_2 concentration of our atmosphere continues to rise, the urgency of quantifying net ecosystem C balances increases. In wetlands, this demand has translated into a desire to calculate C leaving the wetland through surface water and CH_4 emissions stimulated by higher water levels, with the goal of reducing C loss and maximizing natural C storage. As stated in Novick (2022), one of the essential criteria of successful nature-based climate solutions are to account for leakage so that improvements in one area (e.g., C uptake) are not negated by deterioration in another area (e.g., dissolved CO_2 in surface water runoff). One way to monitor this is through advanced C cycle measurement tools, specifically at the forest or farm level. The report states, "…more information is required regarding potentially significant leakage through lateral transport of dissolved and particulate carbon [Abril & Borges, 2019; Bogard et al. (2020); Arias-Ortiz et al. (2021)]" (Novick (2022)). Tracking lateral loss of dissolved

CO_2 is an ambition of the federal government, the scientific community, and investors of the C market.

Given that wetland GPP does not have a consistent influence on P_{CO2} in surface or porewater, there is no relationship which could be modeled using eddy covariance or chamber-based flux data to estimate wetland lateral C export and improve our understanding and preparation for the future climate. Still, the findings presented here can help make measuring surface and porewater P_{CO2} concentrations and lateral export more efficient. Results presented in the multi-site synthesis of Chapter 4 showed that P_{CO2} across wetland types on the yearly scale is similar. A singular estimate of P_{CO2} concentrations in surface and porewater could therefore be used in models operating at a yearly resolution. P_{CO2} on the daily basis was correlated with GPP and could be ranked roughly according to wetland type and hydrology. Additionally, although continuous measurements are useful for signal and causal analyses, P_{CO2} measurements do not need to be continuous to accurately estimate daily, monthly, or yearly averages.

Applying these findings to the layout of future studies can help simplify estimating wetland C budgets. As of the writing of this document, the most recent version of the community land model (CLM5) does not include wetlands as a separate land unit but instead utilizes surface water storage as a proxy for wetland coverage (Lawrence et al., 2019). Recent attempts have been made to incorporate coastal wetlands into terrestrial models such as the Energy Exascale Earth System model (E3SM) and have succeeded in predicting responses of net primary productivity (NPP) to elevated CO_2 and temperature (O'Meara et al., 2021). Causal relationships have also been implemented in machine learning algorithms and frameworks to

improve forecasting of wetland gas emissions (Yuan et al., 2022) or assess complex multi-driver relationships in other ecosystem types (Suzuki et al., 2022). Relationships presented in earlier chapters, such as that of GPP and FCH_4, tide height and P_{CO2}, or T_{air} and P_{CO2}, can also inform causality-enabled machine learning models to anticipate wetland gas emissions under future warming conditions, given their ability to handle complex, lagged, nonlinear relationships.

5.3 Reducing C loss with water table control

Restoring water tables of flooded or drained degraded wetlands to surface level could reduce anthropogenic volumetric CO_2 emissions by as much as 10% (Zou et al., 2022). Wetland restoration can be as simple as clearing debris out of culverts, installing new ones, or digging trenches to mimic historic surface water flow paths. Results can be immediate and noticeable and hasten soil C and N storage which may otherwise take 60 years or more to naturally accumulate (Cormier et al., 2021). Similarly, removing old dikes from coastal estuaries can restore tidal connectivity and improve allochthonous C, organic matter, and sediment elevation with limited methane emissions. The resulting return of invertebrates also supports young salmon which prey on them (Woo et al., 2021).

Despite the insights provided by these studies and many others, the relationship between water table height and CH_4 emissions is not straightforward. CH_4 emissions begin to decline when water levels supersede a site-specific critical inundation level (Calabrese et al., 2021), which was potentially reached in a year with record-high precipitation in northern Wisconsin and resulted in lower CH_4 emissions than the following, drier year as detailed in Chapter 2. Studies in the years following have further confirmed these suspicions about wetland FCH_4 limitation, noting an exponential increase in wetland FCH4 with rising water level and a peak in

methane emissions after 20 days of flooding (i.e., the water level is at the surface), followed by a decrease in FCH_4 (Sha et al., 2023). Analyzing the lagged CH_4 flux response to GPP and the lagged response in GPP to changes in WTD established that methanogens were limited by less plant-derived substrates even when anaerobic conditions were otherwise ideal for methanogenesis. This relationship suggests that consistently high water table heights might reduce wetland CH_4 flux at the cost of plant productivity and potentially contribute to negative consequences for vegetation in the longer term. Periodic water level fluctuations may be a better way to manage wetland gas emissions, as they more closely mimic natural hydrological conditions.

Rewetting wetlands for climate mitigation is obviously not as simple as increasing water levels. Other factors can influence the ecosystem C budget after rewetting, including whether rewetting is active or passive (Nyberg et al., 2022), and whether the wet period takes place earlier or later in the season, which may result in lower or higher emissions, respectively (Euskirchen et al., 2020). Incorporating these findings into environmental management might involve rewetting wetlands by installing culverts with adjustable valves and more closely managing water levels afterwards, or even curating environmental management plans based on site-specific hydrology and P_{CO2} concentrations. Wetlands may benefit from (1) higher water levels in the spring, (2) short-term but larger increases in water table level followed by drawdowns to help protect vulnerable plant life and provide organic substrate to soil microbes, and (3) adjusting the maximum water table height to match the site-specific critical inundation level.

Manipulating wetland water levels to reduce methane emissions could stress ecosystems already undergoing changes due to climate warming, such as reduced soil water, permafrost thaw, elevated soil DOC, and increased ecosystem respiration (Zhang et al., 2023; Walvoord & Striegl, 2007). Existing stressors are even higher in coastal regions, where sea level rise and more frequent storms combine to cause the widespread loss or conversion of both saltwater and freshwater wetlands (Herbert et al, 2015; White et al., 2022).

Combing through existing literature for past data on DIC, DOC, or discharge and linking that with more recent measurements of vertical gas exchange from eddy covariance or chamber flux data collected at those same locations could be one solution to approximating lateral C export without the time required for designing and carrying out long term monitoring or ecosystem-level experiments. Although studies that combine measurements from throughout time to estimate lateral loss of wetland C will not provide the high level of certainty from more intentional research experiments with concurrent data, they still provide a foundation for further study. In Chapter Four, this was exemplified by early measurements of gas exchange in a fen wetland of the Loch Vale watershed in the Rocky Mountain Range and more recent measurements of dissolved CO_2 taken at the same location. Comparing these two datasets from different studies revealed that P_{CO2} at the site likely peaks prior to maximum monthly CO_2 uptake by vegetation. This is a unique observation compared to many other wetland sites in the study where P_{CO2} concentrations peaked much later in the year. Future studies can then focus more on wetland carbon cycling during snowmelt and in later months when primary productivity reaches its peak. Data combing can also lead to better inventories of typical

wetland DIC or studies of how wetland DIC concentrations and seasonal cycles have changed over time.

5.4 Study limitations

5.4.1 Technical and physical issues

Gas and water vapor passed through the gas-permeable membrane and eventually deteriorated the low-cost, waterproof CO2-LAMP sensor platforms which collected some of the data presented in Chapters 3 & 4. Other, unknown technical issues caused the breakdown of the first Smart Rock sensor, which was replaced by the OPEnS lab. The sensors were replaced, but due to the nature of data collection, the technical difficulties resulted in discontinuous data and limited data analysis.

The harsh environments of the coastal saline and saltwater intrusion marshes where the sensors were installed could have had an impact on their performance, as well as damage during travel or my own soldering abilities. For instance, the tidal regime at US-GCE likely jostled wires and other mechanical components, leading to frequent error codes and a need for more regular maintenance. Although the maximum T_{air} during the time of study for all sensors did not surpass the optimal temperature ranges for either the Arduino Uno or K30 CO_2 sensor, and the maximum operating temperature for the other sensor components (e.g., latching relay) is unknown, temperatures could have built up inside the sensor housing. Other environmental conditions could also have contributed to the lifespan of the sensors.

5.4.2 Time management

This research was also limited by my inexperience with project management and graduation deadline. Time spent on building sensors and collecting data was further limited by funding and deadlines imposed by individual research grants. This project would have benefited from a larger budget and a longer timeframe with fewer but more purposeful research objectives. For instance, data collected in Sapelo Island, USA did not reflect the duration of study due to technical and time management issues. Allocating more time to repair and maintain sensors while on the island might have produced higher quality, longer-duration data. More frequent trips to the island would have also exposed technical issues earlier and allowed for quicker response times to those issues, resulting in better data quality and more thorough analysis.

5.4.3 Finding collaborators and open data

One of the most evident limitations to data analysis and interpretation of results was the number of sites with adequate data. The number of sites included in the synthesis of Chapter 4 was limited by a few factors; data searchability, accessibility (i.e., open source or quickly provided by author upon request), and compatibility with study requirements (i.e., direct measurements of GPP, NEE, and P_{CO2} near a wetland; preferable concurrent and continuous). Inaccessible (e.g., behind a paywall or not open) data and non-digitized publications restricted the potential broad range of site coverage in terms of both year of study and location. Sites included in Chapter 4 had a range of data collection methods, which differed in both frequency and technique. However, all methods used produced direct measurements of GPP, NEE, or P_{CO2}.

5.5 Future research

Agriculture is the largest global anthropogenic CH_4 source, with 80% of those emissions coming from livestock and 20% from land-based agriculture. Global FCH_4 from agriculture must be reduced by 24-47% by midcentury, accompanied by net zero CO_2 emissions, to limit warming to 1.5°C (Reisinger et al., 2021). Some countries already have plans to reduce agricultural FCH_4 or have goals to reduce livestock contributions starting in 2050. If livestock CH_4 emissions are not reduced, global warming will not be limited to 1.5°C unless the remaining C budget shrinks by approximately one-fourth.

Methane emissions reduction efforts should refocus on agriculture rather than wetland water table manipulation, considering their relative contributions to the climate crisis and their ability to be controlled without causing harm to the natural environment. Other ways to reduce livestock CH_4 emissions include bioenergy C capture and storage, CH_4 inhibitors, vaccines, low-emissions breeding, seaweed as feed, and more. The simplest solutions are dietary change, reduced food loss, and less waste.

The root causes of climate change must also be addressed to reduce ecosystem stressors such as increased rainfall, which will cause higher amounts of C leaching from terrestrial ecosystems (Öquist et al., 2014; Cui et al., 2023). There is a need to uncover new trends in the magnitude of terrestrial C leaching into temperate rivers, measure ecosystem gas emissions from tropical, high-latitude, and high-altitude regions, and collect more long-term time series measurements of ecosystem metabolism, gas emissions, and other ancillary variables (Battin et al., 2023). Merging data from low-cost sensors, government agencies, individual sites, and satellites will provide more information on ecosystem processes, responses

to flow extremes, wetland vegetation characterization, and more. Future research should also prioritize quantifying groundwater C contributions to wetlands and C export from coastal wetlands to the ocean by measuring changes at the catchment scale (Casas-Ruiz et al., 2023; Santos et al., 2021).

Researching climate impacts on wetland gas exchange can be a daunting task, yet it is necessary to properly design large-scale wetland management and restoration plans (Erwin, 2009). News coverage of certain environmental research topics can appear to highlight negative results with “doom and gloom” language despite articles using optimistic language and providing potential solutions in most cases (Johns & Jacquet, 2018). Positive research findings regarding modern-day wetlands do exist. For example, C sequestration and soil accretion in coastal systems appear to be adapting to accelerating relative sea level rise (Weston et al., 2023). In addition, land loss is slowing due to declining groundwater extraction in the Mississippi River Delta (Edmonds et al., 2023). Wetland restoration and protection are undoubtedly part of the global movement to address climate change, alongside investments into the carbon market and climate tech (Barrett, 2009).

Pessimistic defeatism is uncommon but attracts more media attention and leads to denial, despair, and paralyzing anxiety about climate crisis (Moser & Dilling, 2004). Investigation into anthropogenic influences on climate and ecosystem change must continue despite stress due to climate guilt, and scholars must continue to describe these effects in a neutral way. As experimentation on natural ecosystems continues, discoveries of wetland resiliency and adaptation will inspire and inform climate action (e.g., grassroots movements, behavioral

change) or provide crucial information on management techniques and goals for restoration and reforestation projects.

5.6 References

Abril, G. & Borges, A. V. Ideas and perspectives: carbon leaks from flooded land: do we need to replumb the inland water active pipe? *Biogeosciences* 16, 769-784 (2019).

Barrett, S. (2009). The coming global climate–technology revolution. *Journal of Economic Perspectives*, *23*(2), 53-75.

Battin, T. J., Lauerwald, R., Bernhardt, E. S., Bertuzzo, E., Gener, L. G., Hall Jr, R. O., ... & Regnier, P. (2023). River ecosystem metabolism and carbon biogeochemistry in a changing world. *Nature*, *613*(7944), 449-459.

Bogard, M. J., Bergamaschi, B. A., Butman, D. E., Anderson, F.,Knox, S.H., & Windham-Myers, L. (2020). Hydrologic export is a major component of coastal wetland carbon budgets. Global Biogeochemical Cycles, 34, e2019GB006430. https://doi.org/ 10.1029/2019GB006430

Calabrese, S., Garcia, A., Wilmoth, J. L., Zhang, X., & Porporato, A. (2021). Critical inundation level for methane emissions from wetlands. *Environmental Research Letters*, *16*(4), 044038.

Casas-Ruiz, J. P., Bodmer, P., Bona, K. A., Butman, D., Couturier, M., Emilson, E. J., ... & Del Giorgio, P. A. (2023). Integrating terrestrial and aquatic ecosystems to constrain estimates of land-atmosphere carbon exchange. *Nature Communications*, *14*(1), 1571.

Cui, T., Li, Y., Yang, L., Nan, Y., Li, K., Tudaji, M., ... & Tian, F. (2023). Non-monotonic changes in Asian Water Towers' streamflow at increasing warming levels. *Nature Communications*, *14*(1), 1176.

Edmonds, D. A., Toby, S. C., Siverd, C. G., Twilley, R., Bentley, S. J., Hagen, S., & Xu, K. (2023). Land loss due to human-altered sediment budget in the Mississippi River Delta. *Nature Sustainability*, 1-8.

Erwin, K. L. (2009). Wetlands and global climate change: the role of wetland restoration in a changing world. *Wetlands Ecology and management*, *17*(1), 71-84.

Gaveau, D. L., Salim, M. A., Hergoualc'h, K., Locatelli, B., Sloan, S., Wooster, M., ... & Sheil, D. (2014). Major atmospheric emissions from peat fires in Southeast Asia during non-drought years: evidence from the 2013 Sumatran fires. *Scientific reports*, *4*(1), 1-7.

Herbert, E. R., Boon, P., Burgin, A. J., Neubauer, S. C., Franklin, R. B., Ardón, M., ... & Gell, P. (2015). A global perspective on wetland salinization: ecological consequences of a growing threat to freshwater wetlands. *Ecosphere*, *6*(10), 1-43.

Johns, L. N., & Jacquet, J. (2018). Doom and gloom versus optimism: An assessment of ocean-related US science journalism (2001-2015). *Global Environmental Change*, *50*, 142-148.

Lawrence, D. M., Fisher, R. A., Koven, C. D., Oleson, K. W., Swenson, S. C., Bonan, G., ... & Zeng, X. (2019). The Community Land Model version 5: Description of new features, benchmarking, and impact of forcing uncertainty. *Journal of Advances in Modeling Earth Systems*, *11*(12), 4245-4287.

Moser, S. C., & Dilling, L. (2004). Making climate hot. *Environment: Science and Policy for Sustainable Development*, *46*(10), 32-46.

Novick, K. (2022). The science needed for robust, scalable, and credible nature-based climate solutions in the United States: Full Report.

O'Meara, T. A., Thornton, P. E., Ricciuto, D. M., Noyce, G. L., Rich, R. L., & Megonigal, J. P. (2021). Considering coasts: Adapting terrestrial models to characterize coastal wetland ecosystems. *Ecological Modelling*, *450*, 109561.

Oquist, M. G., Bishop, K., Grelle, A., Klemedtsson, L., Kohler, S. J., Laudon, H., … & Nilsson, M. B. (2014). The full annual carbon balance of boreal forests is highly sensitive to precipitation. *Environmental Science & Technology Letters*, *1*(7), 315-319.

Reisinger, A., Clark, H., Cowie, A. L., Emmet-Booth, J., Gonzalez Fischer, C., Herrero, M., ... & Leahy, S. (2021). How necessary and feasible are reductions of methane emissions from livestock to support stringent temperature goals?. *Philosophical Transactions of the Royal Society A*, *379*(2210), 20200452.

Santos, I. R., Burdige, D. J., Jennerjahn, T. C., Bouillon, S., Cabral, A., Serrano, O., ... & Tamborski, J. J. (2021). The renaissance of Odum's outwelling hypothesis in'Blue Carbon'science. *Estuarine, Coastal and Shelf Science*, *255*, 107361.

Sha, C., Wang, Q., Wu, J., Hu, W., Shen, C., Zhang, B., & Wang, M. (2023). Regulation of Methane Emissions in a Constructed Wetland by Water Table Changes. *Sustainability*, *15*(2), 1536.

Suzuki, K., Matsuzaki, S. I. S., & Masuya, H. (2022). Decomposing predictability to identify dominant causal drivers in complex ecosystems. *bioRxiv*.

Walvoord, M. A., & Striegl, R. G. (2007). Increased groundwater to stream discharge from permafrost thawing in the Yukon River basin: Potential impacts on lateral export of carbon and nitrogen. *Geophysical Research Letters*, *34*(12).

Weston, N. B., Rodriguez, E., Donnelly, B., Solohin, E., Jezycki, K., Demberger, S., ... & Craft, C. B. (2023). Recent acceleration of wetland accretion and carbon accumulation along the US East Coast. *Earth's Future*, *11*(3), e2022EF003037.

Yuan, K., Zhu, Q., Li, F., Riley, W. J., Torn, M., Chu, H., ... & Jackson, R. (2022). Causality guided machine learning model on wetland CH4 emissions across global wetlands. *Agricultural and Forest Meteorology*, *324*, 109115.

Zhang, Y., Song, C., Wang, X., Chen, N., Ma, G., Zhang, H., ... & Sun, D. (2023). How climate warming and plant diversity affect carbon greenhouse gas emissions from boreal peatlands: Evidence from a mesocosm study. *Journal of Cleaner Production*, 136905.

Zou, J., Ziegler, A. D., Chen, D., McNicol, G., Ciais, P., Jiang, X., ... & Zeng, Z. (2022). Rewetting global wetlands effectively reduces major greenhouse gas emissions. *Nature Geoscience*, *15*(8), 627-632.